City Research Online

City, University of London Institutional Repository

Citation: Ning, Y. N. (1991). A study of optical fibre interferometric systems using multimode laser diode light sources. (Unpublished Doctoral thesis, City, University of London)

This is the accepted version of the paper.

This version of the publication may differ from the final published version.

Permanent repository link: https://openaccess.city.ac.uk/id/eprint/29242/

Link to published version:

Copyright: City Research Online aims to make research outputs of City, University of London available to a wider audience. Copyright and Moral Rights remain with the author(s) and/or copyright holders. URLs from City Research Online may be freely distributed and linked to.

Reuse: Copies of full items can be used for personal research or study, educational, or not-for-profit purposes without prior permission or charge. Provided that the authors, title and full bibliographic details are credited, a hyperlink and/or URL is given for the original metadata page and the content is not changed in any way.

City Research Online: http://openaccess.city.ac.uk/ publications@city.ac.uk

A Study of Optical Fibre Interferometric Systems Using Multimode Laser Diode Light Sources

Ya Nong Ning

A Thesis Submitted for the Degree of
Doctor of Philosophy

Measurement and Instrumentation Centre
Department of Electrical, Electronic
and Information Engineering

School of Engineering

City University

Northampton Square
London EC1V OHB

1991

To

My dear wife, Xilin and son, Yuzhu

and whom I love,

and who love me

Table of Contents

Acknowledgments

During the time of this work, I have sought help from a number of people inside and outside the University, all of whom have been very kind in offering their time and expertise. Foremost, I wish to express my sincere appreciation to **Dr. A.W. Palmer** and **Dr. K.T.V. Grattan** for their excellent supervision of this work and their ability to motivate and encourage at all times. In addition, I would like to thank them for their great efforts in helping me to solve different kinds of problems during the past three years.

In particular, I would like to thank **Dr. K.T.V. Grattan** for his invaluable efforts to encourage and help me to publish my research results, also, for his encouragement and arrangement for my presentation at the conference (OE/Fibre, 1990) in San Jose, CA, U.S.A. I am much indebted to **Dr B.T. Meggitt** for his critical discussion and valuable advice.

I am grateful for the financial support by the British Council and the State Educational Commission of China. Also I wish to acknowledge the support from the Department of Optic-electronic instrumentation, Chongqing University by the way of "reserving the post whilst studying".

Finally, I am obliged to Mrs. Linda Carr for her patience and time in typing my papers submitted for publishing. A debt of gratitude is also owed to all the technical staff, especially **Mr. Roger Valsler, Mr. Dave Jackson** and **Miss. Helen Shepherd** for their assistance throughout.

Declaration

The author grants power of discretion to the University Librarian to allow this thesis to be copied in whole or in part without further reference to him. This permission covers only single copies made for study purpose, subject to normal conditions of acknowledgment.

Abstract

Optical fibre sensing techniques are playing an increasingly important role in applications where precise and non-destructive measurements are required. Not only are traditional electronically based sensors being gradually replaced by their optical fibre analogues, but also the classical optical measuring devices, such as bulk optical interferometers, are being reconfigured as devices constructed from optical fibre and fibre components. On the other hand, the availability of different types of light sources with different spectral distributions, such as light emitting diodes, single mode and multimode laser diodes, opens up the possibility of widely use these sources for optical fibre sensor applications.

The main theme of this thesis is a series of investigations of the characteristics of the output from interferometric systems that use multimode laser diodes as their low coherence light sources. The multimode laser diode, developed recently in commercial quantities for use with the compact disc player, offer high light output levels in a small emitting area, which makes it the preferred choice for optical fibre sensor applications.

The discussions began with a general introduction to the thesis. In chapter 1 the principle of optical sensing by using an interferometer is introduced and an outline of the basic framework of this thesis can be seen. Based upon a new classification of the optical fibre sensing techniques, a general discussion and a review of interferometric systems using low coherence light sources are shown in chapters 3 and 4 respectively. By using a new electronic signal processing scheme, a common-mode bulk interferometer was replaced with its optical fibre analogue, which is described in chapter 5.

The main characteristics of the output intensity distribution from several types of interferometric systems which were illuminated by light from multimode laser diodes were intensively studied both theoretically and experimentally. The results of the investigation and the possible applications of using the schemes developed in this work are shown in the chapters 6 to 9. A general conclusion and suggestions for the future of the work are presented.

Chapter 1

Introduction to the thesis

Abstract

In this chapter, introductory material and an outline of the basic framework of this thesis are presented.

1.1. Introduction

Optical fibre sensing techniques (OFST) offer significant advantages in applications where precise and non-destructive measurements are required. In the past decade, optical fibre sensor systems have been the subject of extensive research activity, and a number of such systems have been developed and reported for different types of applications [1, 2]. As a result, optical fibre sensing techniques have become one of the fastest growing areas of technology, and have been used for almost every aspect of measurement in industry, medicine and domestic environment.

One of the most significant achievements of OFST is that they enable the classical optical interferometer to be reconfigured as a device constructed from optical fibres and optical fibre couplers [2]. Thus, the internal and external alignment problems of the classical optical bulk interferometer are efficiently eliminated in its optical fibre version. Furthermore, through the use of the optical fibre components, these interferometric systems are capable of providing considerable design versatility, permitting the flexible inter-connection of the various optical sub-assemblies and, also, preserving most of the useful properties of the optical fibre, such as physical flexibility and lightness, low material cost, good electrical insulation and chemical inertness.

1.2 . Interferometric optical fibre sensors

Of the numerous optical fibre sensing techniques which have been demonstrated, interferometric sensors have a high level of sensitivity and potentially a wide range of engineering applications. Since the working principle of an interferometric system is chiefly based upon the measurand-induced changes in the optical phase (or equivalently, frequency) or an optical path difference (OPD), a number of optical fibre interferometric systems have been constructed in a manner where the measurand is converted to an optical phase change, or, a change of the optical phase difference [2, 3].

An OFS system operates by measuring a relative optical wave delay along a fibre sensing area (intrinsic operation), or in a sensing tip (extrinsic operation). This optical delay may be changed by a measurand to a change in optical phase. The output from an optical fibre interferometer is therefore related to this optical phase difference and can be written as

$$I=I_O\,(1+\cos\phi) \qquad (1.1)$$

where I is output intensity, I_O is a constant, ϕ is an OPD induced by the measurand (a detailed discussion is given in chapter 2).

By using different types of signal recovery techniques, which are discussed later in section 4.3, a wide range of the optical fibre interferometric sensor systems have been developed [3, 4].

Amongst these systems, the fibre-based laser Doppler interferometric systems have been highly developed as an important technique for example for remote flow measurement [3], and non-contact vibration measurement [4]. Since these systems are developed for remote dynamic measurement, they are also known as "optical fibre laser velocimeters" or "optical fibre anemometers". The main optical schemes developed in this work relate to applications to these types of systems.

1.3. The optical fibre interferometric system using low coherence light sources

Amongst optical fibre interferometric systems, the common-mode configuration, in which the signal light beam and the reference beam travel along the same fibre, exhibits a unique property of the insensitivity to environmental perturbation. This is largely due to the fact that any extraneous phase fluctuation in the fibre is common to both beams, and therefore, as the signal beam interferes with the reference one, this unwanted phase fluctuation is cancelled out.

As mentioned above, an optical fibre common-mode system has a high potential for being used in the difficult environment, however, when it is used in flow measurement, it is hard to determine where the measurement is made, i.e., the geometry of the measurement volume is not easily determined or defined [5]. This problem is caused by the fact that when a high coherence light beam from the fibre probe penetrates into the flow, the back-scattered light, which may come from anywhere along the optical axis near fibre tip, will be collected by the fibre probe and interfere with the light reflected from its end face. Therefore, the geometry of the measurement volume where the interaction of the light beam with the flowing (scattering) particles occurs cannot be determined simply from the interference patten. Furthermore, the normal classical-type interferometers that use high coherence light sources have other problems which result from the optical characteristics of the high coherence light source. For example, these systems only have a limited unambiguous operating range, and their operating position will be lost when the interferometer system is switched off.

In order to overcome the problems induced by the use of a high coherence light source, a considerable effort has been made to develop a low coherence light source interferometric system, the so-called "white-light interferometer" [1, 6]. As a result, interferometers using different types of low coherence light sources have been investigated and a range of interferometers with different types of configurations have been developed [6, 7, 8, 9]. The main work presented in this thesis is a summary of these investigations, concentrating on the study of the characteristics of a multimode laser diode in several types of interferometer configurations for the optical fibre sensor applications.

1.4. The work reported in this thesis

The work presented in the thesis includes three different sections, which are: a review section (chapters 2 and 3), an initial study section (chapter 4) and a report of main research work undertaken (from chapter 5 to chapter 9).

In the review section, a new systematic classification of optical fibre sensor techniques (OFST) is proposed and presented (chapter 2) [10]. By using this classification scheme, a fuller overview of the current status of OFST may be seen. A review of interferometric systems using low coherence light sources [11] is given in chapter 3. In this review, research activity in this area is shown, and as a result the main part of the work shown this thesis may be outlined.

In the section detailing the main research activity of this thesis, initial work was started with an investigation of a new scheme for measuring the frequency and displacement of a vibrating object. The aim of that was to replace an optical bulk arrangement [12] with an common-mode optical fibre configuration. Such a scheme may be described as "a pseudo-quadrature recombination scheme" (the details can be seen in chapter 4) and represents an electronic analogue to an optical signal processing scheme [5]. Although this scheme appears extremely simple in this configuration and may be fabricated at low cost, by comparison to the one using optical signal processing, it does, however, provide less information than that of the latter, i.e., the direction of the motion can not be determined by using this scheme [13, 14].

In order to find a solution to the problem of determining the motion direction, an investigation of the characteristics of a new type of low coherence light sources - a multimode laser diode for use in optical interferometers - was carried out. In chapter 5, the characteristics of a multimode laser diode in a Michelson interferometer are presented [15, 16]. In chapter 6 and 7, those of a multimode laser diode in a coupled Fabry-Perot : Michelson interferometer [8] and a coupled dual Michelson interferometer [17] are shown, respectively. From the results of these studies, it can be seen that by employing a multimode laser diode as the light source in an interferometer, it is possible to solve some of the problems induced by the use of a high coherence light source. For instance, the geometry of the measurement volume may be determined by using the "white-light interferometer" scheme, or the "coherence length modulation" scheme (chapter 8) [18], and the direction of a motion can be determined by employing a heterodyne signal processing scheme in a coupled dual interferometer (chapter 9) [19].

This thesis concludes with a chapter (chapter 10) in which the main results of this work are summarized. The advantages, and the problems, of using a multimode laser diode as the light source in an optical interferometer are shown. The major developmental requirements needed for using the schemes developed in this work are indicated.

References:

[1] R,S. Medlock, "A review of modulation techniques for optical fibre sensors" Int. J. Opt. sen., 1, 27-48, 1986.

[2] D.A. Jackson "Monomode optical fibre interferometers for precision measurement" J. Phys. E, 18, 891-100, 1985.

[3] D.A. Jackson and J.D.C. Jones, "Extrinsic fibre-optic sensors for remote measurement: Part one", Optical and Laser Technology, 18, 243-52, 1986.

[4] G.E. Moss, L.R.Miller, R.L. forward, "Photo-noise-limited laser transducer for gravitational antenna", Appl. Opt. 10, 2495-7, 1971.

[5] D.A. Jackson and J.D.C. Jones, "Extrinsic fibre-optic sensors for remote measurement: Part two", Optical and Laser Technology, 18, 299-307, 1986.

[6] G.Beheim, K.Fritsch and N.Poorman, "Fibre-linked interferometric pressure sensor", Rev. Sci. Instrum. 58(9), 1655-9, 1987.

[7] Y.N. Ning, B.T. Meggitt, K.T.V. Grattan and A.W. Palmer, "Characteristics of laser diodes for interferometric use", Appl. Opt. 28, 3656-60, 1989.

[8] Y.N. Ning, K.T.V. Grattan, A.W. Palmer and B.T. Meggitt "Characteristics of multimode laser diode in a dual interferometer configuration", IEEE J. Lightwave Technology, 1773-8, 1990.

[9] S.A. Al-Chalabi, B. Culshaw, D.E.N. Davies,"Partially coherence sources in interferometric sensors", Proc. First Int. Conf. on OFS, 132-5, 1983.

[10] Y.N. Ning, K.T.V. Grattan, W.M. Wang and A.W. Palmer, "A systematic classification and identification of optical fibre sensors", Sensors and Actuators, 29, 21-36, 1991.

[11] Y.N. Ning, K.T.V. Grattan and A.W. Palmer, "Fibre-optic interferometric systems using low coherence light sources", Sensors and Actuators, 30, 181-192, 1992.

[12] M. Corke, J.D.C. Jones, A.D. Kersey and D.A. Jackson "Dual Fabry-Perot interferometers implemented in parallel on a single monomode optical fibre", OFC/OFS' 85, San Diego, Califorrnia, USA. Technical Digest 128, 1985.

[13] Y.N. Ning, B.T. Meggitt, K.T.V. Grattan, and A.W. Palmer "An all fibre low cost rangefinder for small detection measurement", Proceedings, SPIE 1043, 284-90, 1989.

[14] Y.N. Ning, K.T.V. Grattan, A.W. Palmer and B.T. Meggitt "A novel detection scheme for vibration monitoring using optical techniques", t Optics and lasers in Engineering, 15, 115-126, 1991.

[15] K.T.V. Grattan, B.T. Meggitt, Y.N. Ning and A.W. Palmer "Application of multimode semiconductor laser diode to fibre optic interferometric sensors", Proceeding of "Captures '89", Conf. Proc. Pub - CIAME, Paris, 484-91, 1989.

[16] K.T.V. Grattan, A.W. Palmer, Y.N. Ning and B.T. Meggitt "Interferometric sensors - extension of range using low coherence light from laser diode"' (EFOC/LAN 1989) Conf. Proc. Information Gatekeepers, Boston, 375-380, 1989.

[17] Y.N. Ning, K.T.V. Grattan, A.W. Palmer and B.T. Meggitt "Coherence length modulation of a multimode laser diode in a dual Michelson interferometer configuration", Appl. Opt. 31, 1322-7, 1992.

[18] B.T. Meggitt, Y.N. Ning, K.T.V. Grattan, A.W. Palmer and W.J. Boyle "Fibre optic anemometer using an optical delay cavity technique", Eighth Int. Conf. on Fibre optics and opto-electronics, London, 1990, SPIE 1314, 321-9, 1990.

[19] Y.N. Ning, K.T.V. Grattan, A.W. Palmer, B.T. Meggitt and K. Weir, "A novel optical heterodyne vibration sensor scheme preserving directional information and using a short coherence length source" Optics Communications, 85, 10-16, 1991.

Chapter 2

The review of optical fibre sensing techniques based on a new systematic classification

Abstract:

In this chapter, a new kind of classification for optical fibre sensors has been introduced. Optical fibre sensors are classified according to the type of fibre used, the light sources and the modulation schemes respectively on which they are based. Each of these categories is further sub-sectioned into several divisions and illustrations from systems developed and reported in the literature are given, with various sensor designs represented according to these criteria.

2.1. Introduction

Various optical fibre sensor techniques have been discussed and reviewed by a number of authors [1, 2, 3, 4, 5] during the last ten years, during which time the recent explosive growth in the number of papers published in the field has been observed. A general framework for the classification and categorisation of such sensor techniques can be seen from a number of different points of view.

However, the classification rules used to frame the various optical fibre sensor techniques differ substantially from one author to another. This is largely due to the different fields in which they are interested, the nature of the grouping of sensors that they use, and indeed the intended readership of the paper. For instance, Jackson et al [1] and Jones [2] have classified sensors according to the use of a coherent or incoherent optical measurement technique approach. Other reviews have been made on the basis of different measurands or the use of modulation techniques. Examples are the use of the optical fibre sensor (OFS) for temperature measurement by Glenn [4], the use of the optical fibre for chemical measurement by Harmer [5], and the use of the optical fibre for biomedical applications by Katzir [6]. Further work has relied upon the basis of intensity modulation by Medlock [7], as well as, for example, by Grattan, a focusing upon new developments and trends [8].

Although a basic classification of optical fibre sensors, as merely "intrinsic" or "extrinsic" has been introduced in a number of publications [1, 2, 3], it is somewhat over-simplified for OFS techniques, because such a classification neither gives a overview of the sensor itself nor detailed information about the range of activity in the OFS techniques area.

In order to develop a fuller overview of the variety of OFS devices under study today, it is worthwhile to introduce a new classification of these techniques. By examining the structure of a typical optical fibre sensor, it may be seen as logical to classify OFS techniques according to three basic and separate criteria:

(a) source of illumination used
(b) type of fibre employed and
(c) optical modulation scheme employed

Such a classification springs almost instinctively from the nature of the term optical fibre sensor - the optical source, coupled to a transmitting fibre to allow the light to undergo transaction or modulation in the sensor process.

2.2. Classification in Cartesian geometry representation

If a Cartesian co-ordinate representation is used to group these three "variables", a spatial framework for the classification process can be employed and different types of sensor can then be fitted to such a representation, to illustrate their comparative features.

Such a classification for generalised sensors, whether electrical, mechanical, or otherwise has been discussed by Middlehoek [9], and Finkelstein [10], but herein it is applied in a rather different way to one specific class of sensor, rather than to the general family of all sensors.

2.2.1. Source of illumination used

The x-axis of the geometrical space is used to represent light sources which then may be characterised by their spectral distribution, as shown in Figure 2.1. There are at least five common and convenient classifications of light sources that have been reported for use in various types of OFS:

(i) single-mode laser source (e.g. single-mode He-Ne laser, single mode laser diode)

(ii) two-mode or "a few-mode" light sources (e.g. lasers with various cavity configurations)

(iii) the N-mode light source (N>>2 e.g. the multimode gas lasers , or multimode laser diodes)

(iv) narrow-band continuous spectrum light source (e.g. the light emitting diode (LED) or the superluminescent LED)

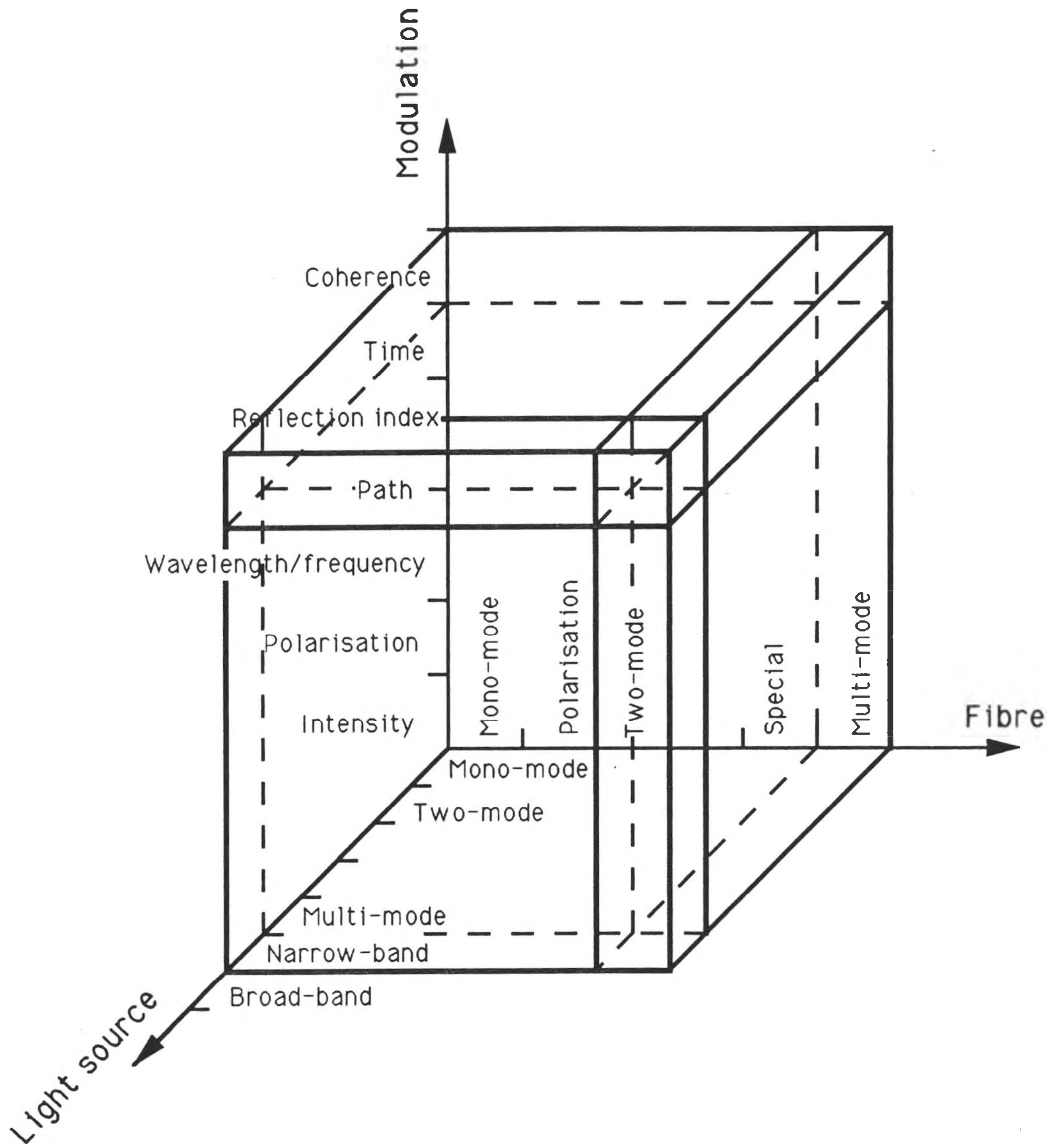

Figure 2.1. *The schematic classification in a 3-D Carthusian coordinate scheme.*

(v) the broad-band continuous spectrum light source (e.g. the tungsten lamp, the mercury lamp, the continuous output xenon lamp).

2.2.2. Type of fibre employed

On the y-axis of the geometrical space, the various fibres that may be employed are classified by their mode - propagation characteristics. The number of modes transmitted and the polarization-related characteristics can be used, on the basis of a division of fibre types into at least five groups, as shown in Figure 2.1.

(i) monomode fibre
(ii) polarization - maintaining fibre
(iii) two - mode fibre
(iv) multimode fibre
(v) specialized fibres e.g. doped fibres, liquid-core fibres etc.

2.2.3. Optical modulation/sensor techniques

On the z-axis of the space, as shown in Figure 2.1, is illustrated a characteristic of the OFS based on the parameters of the interaction electric field, E, given by $E=E_0 \exp[j(\omega t+2\pi nL/\lambda)]$, where E_0 is the amplitude, ω the optical frequency, n the refractive index of the medium, L the optical path and λ the wavelength. The modulation of the field can be categorized into at least seven groups:

(i) intensity modulation
(ii) polarization modulation
(iii) wavelength/frequency modulation
(iv) path modulation
(v) refractive index modulation
(vi) time modulation , and
(vii) coherence length modulation,

The modulation types (iii) to (vi) are also termed as "phase modulations" because their variation will cause a change of the phase of the light propagating in the optical fibre. It should be pointed out that the phase of an optical wave is defined with respect to a particular reference and thus a useful phase modulation for sensing can only be achieved, in practice, for a light source with fixed and known initial phase conditions. The random variation in the initial phase over a period of time (the detector response-time) will result in a degeneration of the interference output in an interferometer, i.e., the fringe visibility k, which is defined as $(I_{max}-I_{min})/(I_{max}+I_{min})$, will reduce to zero, and thus will make the detection of the phase modulation particularly difficult. In other words, a phase modulation sensor can only effectively be operated with the two optical path differences inside the coherence length of the optical source.

By using this classification system, as illustrated in Figure 2.1, the many OFS techniques described can more readily be surveyed and examined, and their relationship one to another be seen. What is more, such a representation can more clearly indicate those areas where sensor schemes have already been proposed and/or exploited and its examination may show both areas of inactivity or those that are underdeveloped and point to new techniques which further could be exploited, as the technology to achieve them matures.

It should be noticed that an OFS can employ more than one type of light source, modulation technique, or fibre at any one time. Such types of OFS can then be represented by more than one "cubic unit" in the geometrical space in Figure 2.1. If an OFS "family" is represented by a number of different "cubic units", such a family may be of a multiplexed type [11], while if the same cubic unit represents a number of types of OFS, this may be a distributed type of OFS [12].

2.3. light source - optical characteristics of the OFS family

Light sources can be classified according, for example, to their spectral or coherence characteristics into at least five groups. Table 2.1 shows the spectral distribution, coherence length and intensity/wavelength relationship for a number of such sources. The coherence characteristic of a light source is a measure of the extent to which a phase relationship is maintained both across the beam (spatial coherence) and along the beam (temporal coherence). In an OFS, the spatial coherence of the light wave is

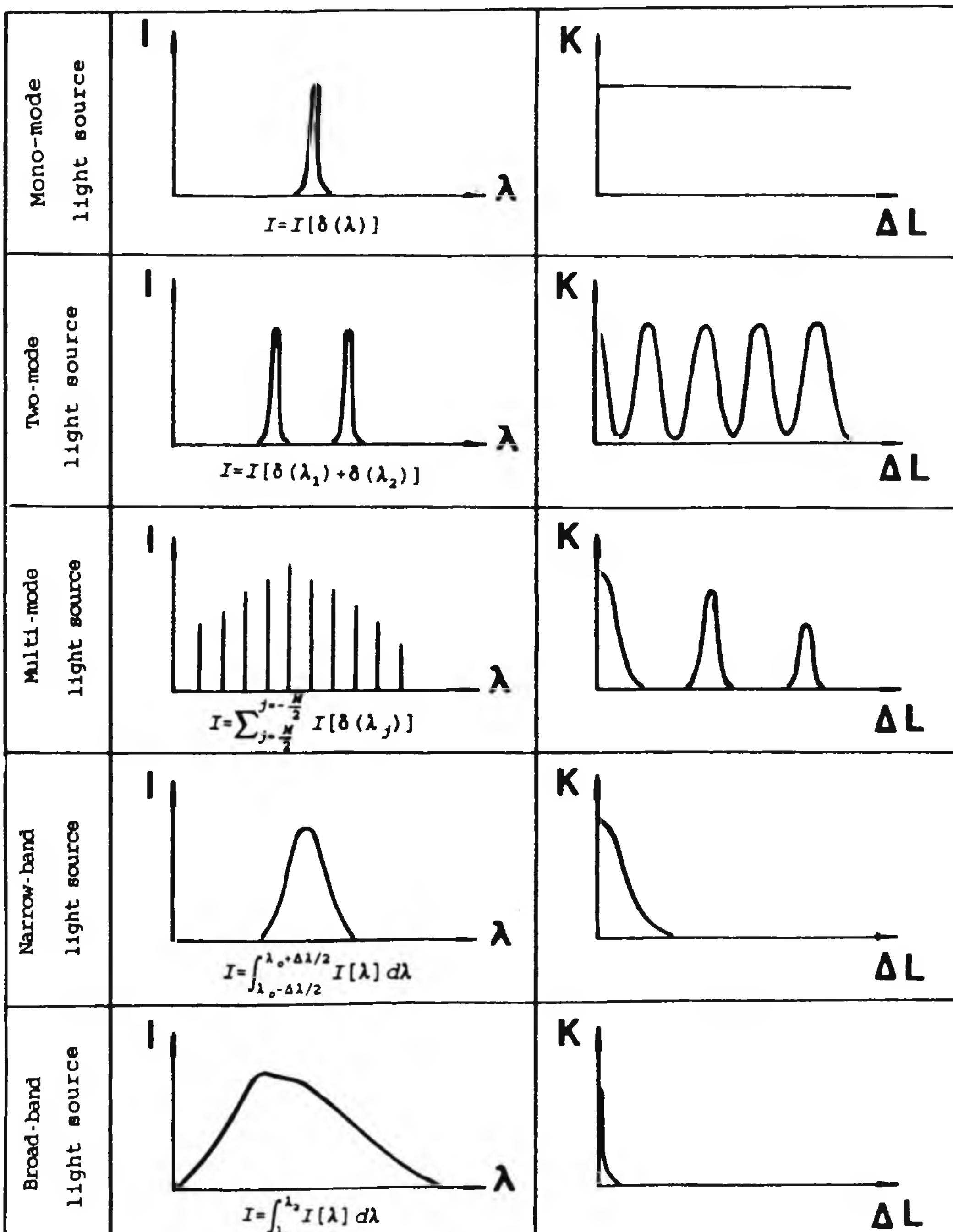

Table 2.1. *The spectral distribution [$I(\lambda)$] coherence length ($k \sim L$) and intensity expression for five groups of light sources (I: intensity, λ: wavelength, k: fringe visibility, L: optical path difference).*

often not particularly important because of the small cross-sectional area of the fibre core, but as a contrast, the temporal coherence of the optical radiation is often extensively considered in selecting the appropriate light source for a particular sensor. In a multimode fibre, the spatial coherence of the modes is lost, whilst in a single mode fibre it is, by definition, preserved. A useful indicator of the temporal coherence is the coherence length of the source or the resulting fringe visibility of interference fringe in a detection interferometer, the relationship between the coherence length and the spectral width of the light source being written as [13]:

$$L_C = \frac{\lambda^2}{\Delta\lambda} \qquad (2.1)$$

Where L_C is the coherence length, λ is the wavelength of light and $\Delta\lambda$ is the spectral width of light source.

2.3.1. Monomode light sources

Many types of single mode laser or laser diode belong to this group of sources. Because their bandwidth is very narrow, their coherence lengths are usually very long compared to the optical path inside of the OFS itself. For a suitably chosen He-Ne gas laser, the coherence length is of the order of a few hundred meters, for example, and a typical spectral width for a single longitudinal mode in such a laser is about 1 MHz, which corresponds to a coherence length of the order of a few hundred meters [13]. For a typical laser diode such as that used in a 'CD' - player, a very short coherence length is desired and used, to avoid phase sensitive effects in the reading of data from the optical disc. The spectral width can be reduced to ~100 MHz, resulting in L_C having a value up to a few metres [14].

2.3.2. Two-mode light sources

Such light sources can be produced relatively easily for use in an OFS by for example, driving a single-mode laser diode at two different values of currents through use of a square wave modulation [15], or, by combining two or more single-mode lasers which have different wavelengths [16] or by the use of bandpass filters to obtain a several wavelengths from an LED [17]. The coherence length obtained in each of these cases is, however, much less than that of single-mode laser. Obviously, in the latter two cases, the coherence lengths of the wavelengths generated will be independent of each other, and equivalent to those obtained from separate sources. However, the fringe visibility in a detection interferometer changes periodically with the change of the optical path difference, as shown in Table 2.1.

2.3.3. N-mode (multimode) light sources

This group of light sources covers a wide range of multimode solid state (doped insulator), liquid or gas lasers or the semiconductor laser diode. For instance, the He-Ne gas laser with a cavity length of 0.5 m has a mode separation of 4×10^{-4} nm and the width of the lasing transition at 633 nm is typically about 2×10^{-2} nm, with the number of the longitudinal modes in the laser output being of the order of 4 or 5 [13].

When a single mode laser diode is powered by a drive current under the threshold for laser action [18], it may conveniently be used as a N-mode light source as well as the coherence characteristics deteriorate severely under these circumstances. The coherence characteristics of this type of light source are not easily described because the interference effects of multimode light are much more complex than those of light from a monomode laser. Thus interference fringes will appear in some spatial regions but not in others. This is due to the superposition of the fringes which are generated by each longitudinal mode of the device [19]. As a result of this superposition, those interference regions will occur periodically along the optical path difference. The concept of a "coherence region" has been introduced in some papers to explain this and therein, [19], the coherence characteristics of these sources have been discussed in greater detail [19, 20].

The laser diode is revolutionizing the potential for OFS devices and in summary the devices range from low coherence length, simple structures with a width of the lasing transition of 2-5 nm, available at prices from a few tens of dollars (depending upon power delivered) through distributed feedback lasers with sub-nanometer linewidths and available at a price that rules them out of most OFS applications to quantum well devices with the linewidth performance of a He-Ne laser.

Other laser devices may be employed in OFS use, e.g. the Ar ion laser or the He-Cd laser. Both these devices are expensive, physically quite large and require power supplies which use a considerable level of electrical input, but they do provide a continuous (and thus capable of modulation) output in the blue or ultra violet part of the spectrum. This is a region where LEDs or laser diodes are very weak and for such sensors as those employing luminescence, where excitation at short wavelengths is preferable, they are a useful source. In addition early work on distributed sensors employed these sources, due to their high power (several watts being routinely available), and favourable non-linear scattering characteristics. The coherence length of a typical Ar ion laser may be quite long, comparable to that of the He-Ne laser.

2.3.4. Narrow-band continuous spectral light sources

This type of light sources have been widely used for many different kinds of OFS. The ordinary light emitting diode (LED) or super-radiant diode (SRD) are examples of this group with importance for OFS use. Illustrated schematically in Table 2.1, the width of their output spectrum is about 20-80 nm [21], and as a consequence their coherence length is of the order of 50 μm or less [22]. In addition, discharge lamps can produce a series of spectral lines of varying widths, distributed across the spectrum according to the energy levels present within the gas itself. The low-pressure mercury lamp, for example, gives a series of lines from the UV into the visible spectrum, with however, some difficulty in coupling the divergent output from such a device into an optical fibre. This is a significant problem for all lamp sources, although output optical powers may be such that efficient coupling, whilst preferable, is not essential. A range of low pressure gas discharge lamps exist, yielding specific special lines over a wide range of the spectrum. However, there are often problems with the bulk of the lamp and power supply in OFS applications, and the need for lamp cooling. Invariably, in cases where the lamp is inefficient or delivering low optical power at the wavelength of interest, good optical coupling via a carefully chosen lens combination is required. This usually will increase the physical bulk of the source and may limit the application to OFS devices.

2.3.5. Broad-band continuous spectrum light sources

This group of light sources is well suited to a number of optical fibre sensor applications, particularly those requiring excitation at wavelengths of less than ~500 nm, and especially in the ultra violet part of the spectrum (λ < 350 nm) where solid state sources are largely unavailable and the use of lasers is uneconomic. Additionally these sources can offer a wide wavelength spread which is useful for sensors using wavelength - encoding techniques. Modulation of the light can be achieved using simple "chopper" techniques (limited to ~few kHz) or using an electro-optic approach but these are usually very inefficient with such sources. As an example, the millimetre-sized tungsten-halogen incandescent lamp is available [23], the optical output being in the spectral range from wavelengths in the near UV and in the visible from about 400 nm upwards, into the infra red part of the spectrum, where substantial power can be obtained. Discharge lamps such as the xenon lamp or mercury lamp (at low or high pressure) are widely employed for emission on either discrete spectral lines or as a broad band over the region from the vacuum ultra violet to longer wavelengths.

The coherence lengthes of this group of light sources are usually very short, e.g. the coherence length of a typical white light source is only 3 or 4 wavelengths. Details of such sources are discussed in a number of familiar reference texts [14], as their use in conventional analytical instrumentation has been familiar for many years. However, their mechanical instability and physical bulk makes them unsuitable for many OFS applications, in addition to which such lamps are often inexpensive but yield a substantial percentage of their power output as heat.

2.4. Fibre-structure characteristics of the OFS

Current OFS technology has arisen largely on the basis of optical components and especially optical fibres made available as a result of the explosive growth in their use for communications purposes. Whilst the technology for producing ultra-low-loss monomode fibres has been developed in recent years to a highly sophisticated level, this same technology is also applicable to the production of fibres for sensor purposes, where, however, other fibre characteristics are needed. Thus the OFS development market is fortunate in being able to call upon relatively cheap and readily available technology to produce fibres with specific characteristics to suit sensing purposes. Whilst fibres produced for communications purposes are preferred to have as low a sensitivity as possible to external effects, even ordinary silica fibres are used in many distributed sensor applications, due to their sensitivity to temperature, for example through changes in non-linear scattering processes. As these OFS techniques have developed rapidly, different types of fibre have been manufactured and the number of these types will continue to increase to meet new and special applications. The fibres considered here are characterised by the nature of their structure (such as, the core radius, numerical aperture (NA), polarization performance), and other considerations.

The numerical aperture (NA) is given by:

$$NA = Sin\theta_m = (n_1^2 - n_2^2)^{1/2} \tag{2.2}$$

Where n_1, n_2 are the refractive indices of the core and cladding respectively, and θ_m is the maximum angle of incidence to retain guiding of light, as shown in Figure 2.2.

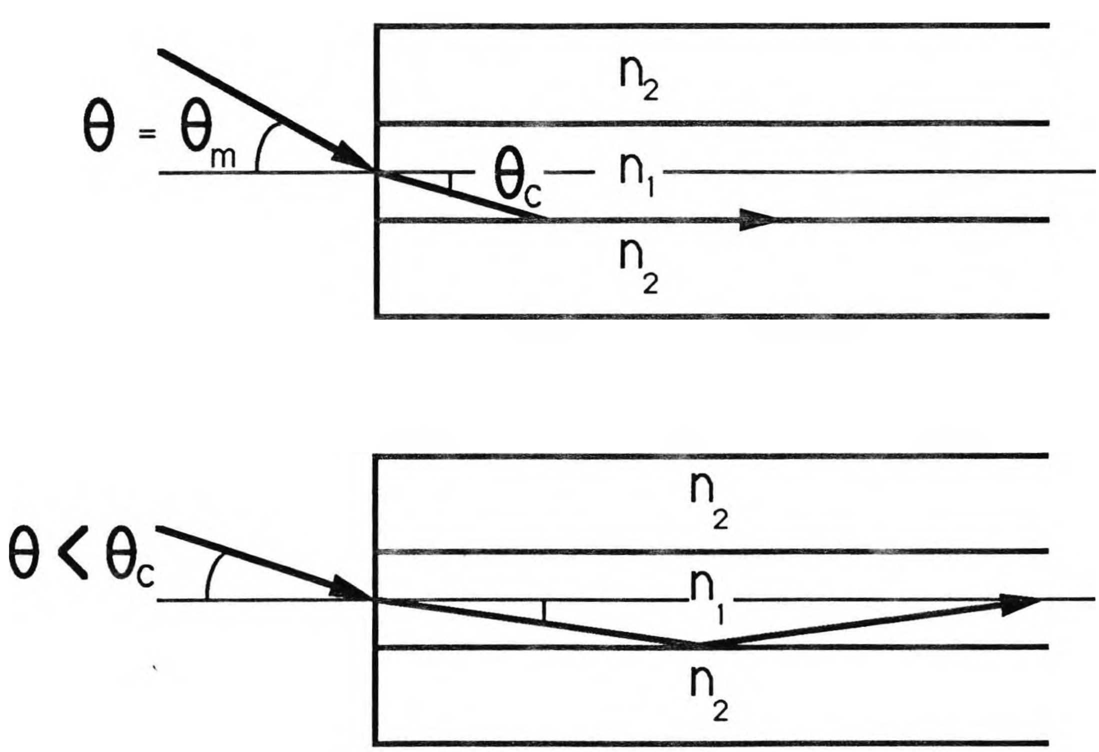

Figure 2.2. *Propagation of light beam in fibre.*

2.4.1. Monomode fibre

Monomode optical fibre is widely used in optical fibre sensors based on phase modulation to encode the measurand. The main characteristic of a fibre is determined by its Vebert Number (V), which is defined as $V = (2\pi a/\lambda)\,(n_1^2 - n_2^2)^{1/2}$, where a is the fibre core diameter, λ is the wavelength of light guided in the fibre, and n_1 and n_2 are the refractive indices of fibre core and the outer cladding respectively. The Vebert number of monomode fibres is normally less than 2.405. A typical monomode fibre designed to operate at a wavelength of 633 nm has a value of NA of about 0.10 [24], a core radius of a few micrometers, with a cladding radius of between 40 to 60 μm [21]. In an ideal fibre which is perfectly circular, when a linear state is lunched into it, two orthogonal polarization states can be generated and the polarization state of the guided wave (the HE_{11} mode) propagates along the fibre unchanged. Unfortunately, in a practical fibre, such ideal conditions do not exist. As a result of its dominant intrinsic and any additional extrinsic birefringence, the guided waves at two orthogonal polarization states will have a phase difference developed between them after propagating a certain distance along the fibre. The distance over which a phase difference of 2π occurs is called the beat length (L_b), which can be written as:

$$L_b = \frac{\lambda}{n_x - n_y} \tag{2.3}$$

where n_x, n_y are the effective refractive indices with x and y being the axes of a non-circularly symmetric fibre core, and λ is the free space wavelength. Typical single-mode fibres have a beat length, L_b, in the centimetre region, dependent upon physical characteristics [13]. Thus this kind of fibre can only be used where the polarization state can be neglected in the sensing operation.

2.4.2. Polarization-maintaining fibre

Many optical fibre sensors rely upon the use of polarization effects, and the maintenance of the state of polarization of light propagating in fibre is important. In order to overcome the problem of a variable state of polarization in a monomode fibre, considerable effort has been expended to develop polarization - maintaining fibre. This characteristic is induced during the manufacturing process, by inducing stresses in the material itself.

There are two main categories of polarization maintaining fibre (PMF) available - linear polarization-maintaining fibre (LPMF), and circular polarzation - maintaining fibre (CPMF). In the former category, only one of two orthogonal polarizations states (HE_x or HE_y) can be maintained at the output of the fibre whilst, in the CPMF, a round fibre is twisted to produce a difference between the propagation constants of the clockwise and counter-clockwise circularly polarised HE_{11} mode. Table 2.2 shows in more detail the classification of PMF and the subject is discussed in greater detail by, for example, Okoshi [25].

2.4.3. The two-mode fibre

Fibre allowing the propagation of only a few modes represents a new kind of fibre, recently developed, which can provide a number of independent transmission channels in a single strand fibre. A number of investigations have been carried out to understand better the modal and the polarization characteristics of these fibres [26, 27]. Although the multichannel capacity of few-mode fibre has not yet been fully exploited, due to mode-control problems, two mode fibre has been used in several types of OFS [28, 29]. It is usual to derive the two modes which are excited from a single source to ensure a known coherence relationship between them. It is very difficult to excite and maintain two modes independently. The two-mode fibre, with a V-number between 2.4 and 3.8 can guide two spatial modes, the LP_{10} and LP_{11} modes [30]. The polarization and intensity distribution for a highly elliptical core, two-mode fibre (operated with LP_{10} and LP_{11}) can be kept unchanging over a wavelength range between 488 nm and 633 nm [31].

2.4.4. Multimode fibre

Multimode optical fibre, with a V number significantly greater than 2.4, has much larger core sizes and sometimes also much larger refractive index differences between core and cladding. The number of modes (M) guided by the fibre is determined from the V number and is given by $4V^2/\pi$. The core diameter of a multimode fibre is usually larger than 50 µm, which means it has more than 100 times the core cross - sectional area of a

- Linear-polarization maintaining fibres (LPM fibres)
  - Truely single polarization fibres (Differential attenuation fibres)
    - Geometical type
      - (1) Side-pit
      - (2) side-tunnel
    - Stress type
      - (1) Bow-tie
      - (2) Flattened depressed -cladding
  - Linearly birefringent fibres
    - Geometical type
      - (1) Elliptical-core
      - (2) Dumbbell-core
      - (3) Side-pit
      - (4) Side-tunnel
    - Stress type
      - (1) Elliptical-cladding
      - (2) Elliptical-jacket
      - (3) Pandn
      - (4) Four-section
      - (5) Bow-tie
- Circular Polarization maintaining fibres (CPM fibres) — — Cricular birefringent fibres — — — — — Stress type — — -Twisted round fibre

Table 2.2 *Classification of various polarization-maintaining optical fibres. (Ref. 25)* monomode fibre. This factor is also reflected in the material costs and thus in the price of the fibre itself. This is especially significant for long lengths or specialized fibres. A large index difference between core and cladding yields a large numerical aperture but may be difficult to fabricate. As a result of the larger core area and a large value of NA, multimode fibre presents a greater launching efficiency than monomode fibre from an optical source.

Multimode fibres are often used in an OFS, in applications where high light intensities are required, particularly in those that employ intensity - modulation techniques. There is flexibility to use a wide variety of optical sources, with suitable coupling optics. In many cases, light signals can be launched into fibres with reasonable efficiency and often incoherent sources show a high degree of optical power over a usable spectral band, so inefficient coupling still results in adequate light levels in the optical fibre for many sensor purposes. Multimode fibre sensors based on coherence modulation in an OFS have been produced [22, 32].

2.4.5. Specialized fibres

A number of types of special fibres have been made for particular usage in the field of optical fibre sensors, and are designed with only limited applicability in optical fibre communications systems. However, the use of fibre lasers as optical sources and subsequent laser amplifiers as part of an optical communication systems may bring some specialist fibres into the communication field. The difference between these and other kinds of fibre lies mainly in the modified shape of the fibre core or the material from which it is made. As the varied techniques used in OFS are developing steadily, the number of special fibres in use are continuing to increase. However, only a few of the wide variety of specialist fibres are considered below, to illustrate the broad nature of field.

2.4.5.1. D-shaped fibre

When light is guided along a fibre with "D"- shape core,the result is the exposure of the evanescent field near the core of fibre. As most of its cladding on one side of the fibre is removed, the thickness of the material which is left is very small (as shown in Figure 2.3.), and light modulation can be achieved in the evanescent field near the core. The techniques for manufacturing D-shaped fibre are described by Millar et al [33] and Dyott et al [34] respectively. One of the main potential uses of the single mode D shaped fibre is for polarization - holding directional couplers, where the process of coupling the guiding region, either through etching or by fusion, should be greatly simplified [35].

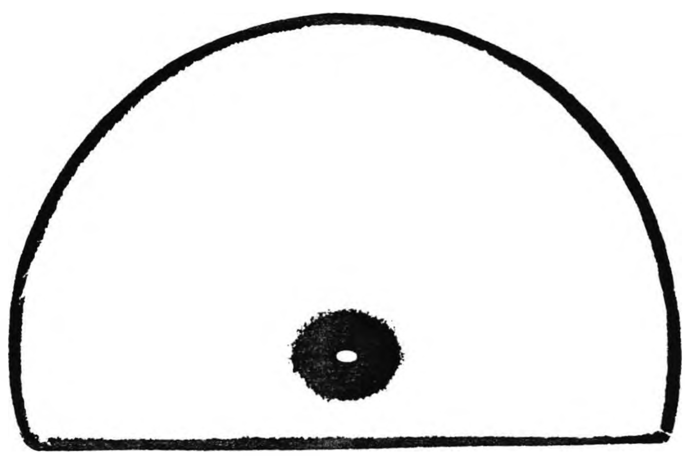

Figure 2.3. *The cross section of a D-shaped fibre*

2.4.5.2. Hollow-section Fibre

Hollow-section fibres are the result of a further development of the D-shape fibre. They may be produced by making a single longitudinal aperture at a fixed distance from fibre core. Figure 2.4 shows such an acrylate-coated metal-glass fibre, with a numerical aperture of about 0.16, the "cut-off wavelength" for transmission is about 1.25 μm, and the distance between the core and hollow section is about 3 μm. The polarization performance of such fibres is good, for example, the extinction ratio of a 5 cm length of the polarizing fibre is about 40 dB over spectral region from 1300 to 1600 nm [36], which is useful in sensor applications.

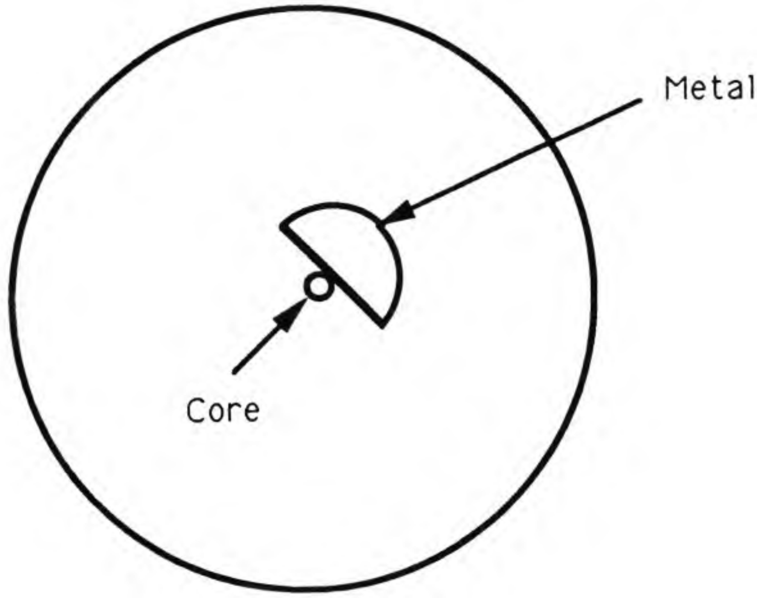

Figure 2.4. *Schematic diagram of a composite metal-glass polariser.*

2.4.5.3. Fibre doped with rare earths

As an alternative to modifying the shape of the optical fibre, by modifying the materials from which the fibre is normally fabricated (pure silica) or adding additional materials, new kinds of specialized fibre have been developed. Fibres doped with rare earths have a number of special properties, due to the introduction of these ions e.g. Nd, Eu, Dy, into the light guiding regions of the fibre. Those properties are exploited to construct different "in-fibre" sensor devices, to improve the measurement region of the OFS, or even to form new kinds of devices such as fibre lasers, fibre amplifiers, a fibre with an increased Verdet number or a fibre showing an increased Kerr effect and nonlinear optical coefficients. [37]. An important application has been the distributed temperature sensor with the rare earth doped fibre which has been developed recently. The sensitivity reported for it is better than 1°C, over a temperature region from -200 to +100°C and higher, with a spatial resolution being 3.5 m [38].

2.4.5.4. Liquid core fibre

Liquids have been used as the core material for fibres where special characteristics of the liquid material have been required for a specific sensor purpose. Thus the refractive index or scattering properties of the core material may be tailored to a particular application through the use of a specially chosen liquid. An important early example is in the work of Hartog [39] where a fibre filled with an organic liquid with significant scattering properties was used as the basis of an early distributed temperature sensor. However, problems exist in the fabrication of long lengths of such fibre and the possible hazards from the spillage of the core material. Additionally,such fibres are expensive to fabricate, and not widely acceptable in industrial installations.

2.5. Sensor - modulation techniques

The modulation techniques employed in optical fibre sensors vary widely in their measurand function, performance and position in the sensor system itself. The basic techniques considered here, however, are those in which the light itself is modulated. This process may conveniently be categorised into seven groups, according to the parameters of the electric field or the optical radiation varied. More than one type of modulation technique may be employed in one sensor, for example, path length modulation is often associated with the refractive index modulation, and this is still a dominant mechanism in many optical fibre sensors.

2.5.1. Intensity modulation

Intensity modulation techniques, employed widely in the earliest types of OFS, show the virtues of simplicity, reliability and achievability at low cost. The variation of the light intensity at the probe itself indicates the encoded change of an applied measurand, such as temperature, pressure [40], acceleration [41], or "on/off" state in a simple switch [42]. Various schemes to produce this type of intensity modulation have been produced, classified as, for example, [7]: fibre displacement; shutter modulation; reflective schemes; fibre loss; evanescent field coupling; absorption; light scattering; digital encoding and electro-optic modulation, amongst others. However, a basic drawback is the lack of an accurate reference signal in many cases, although several internal referencing schemes [43, 44] have been proposed. This intensity-based approach is not widely used in modern types of OFS, except for simple switches, although such devices tend to be comparatively inexpensive.

2.5.2. Polarization modulation

Polarization modulation is another interesting and very valuable technique for measurand encoding and signal recovery in many types of optical fibre sensor. The basic principle of operation is that the relevant physical quantity to be measured is transduced into a polarization change through an appropriate interactive effect e.g. the electro- or elasto-optic effect. The measured field can be inside the fibre (intrinsic sensor) or outside the fibre (extrinsic sensor) or even both situations may apply in one system. Historically, these were some of the first modulation schemes to be developed, and numbers of new sensors based on polarization modulation have been developed in the last few years. These are, in particular, sensors for measuring temperature, stress, current, and magnetic field, amongst others, which have been reported in detail in the literature [45].

2.5.3. Wavelength modulation/encoding

Wavelength modulation/encoding techniques are very valuable as a means by which a non-intensity dependent measurement may be made using optical fibres. Wavelength division multiplexing (WDM) has been discussed by a number of authors [46, 47] and relies on the encoding of the measurand information in terms of a specific wavelength of light received from the transducer. This frequently means, in a real sensor, the use of a broad - band spectrum optical source with the transducer acting as a wavelength-encoder, depending on its perturbation by an external parameter. Several displacement/rotation transducers have recently been developed [48, 49], primarily for testing in the aerospace environment, using gratings or filters which are mechanically rotated or moved in a linear fashion to yield the appropriate output.

There are two further kinds of wavelength modulation in common use in interferometric sensors. The first is the so-called "frequency modulated continuous wave" technique (FMCW) [50, 51, 52]. In the case of FMCW, a monomode laser diode in an unbalanced interferometer is driven with a linear ramping current. Since the wavelength (frequency) of the output is a function of the variation of the drive current. The variation of wavelength in the light source causes a phase difference in the output of the interferometer. Therefore the intensity received from the interferometer will yield the information on the optical path difference in the interferometer, and thus the information on the measurand. for the second example of the wavelength modulation, The modulation does not achieved by modulating the light source, but instead, it is achieved either by the Doppler frequency shifting from a moving body or by using a frequency modulator such as a Bragg cell in the experimental optical arrangement. In recent years, a considerable amount of effort has been expended in the development of such optical fibre systems [54, 55, 56], and they have become established as important techniques for the fluid flow measurement, surface velocity measurement [57, 58], and medical measurement applications [59].

2.5.4. Path modulation

This modulation is one of the most commonly-used modulation schemes in optical fibre sensors, usually of the interferometric type. The change of optical path difference may be caused by a physical displacement or measurands which can be converted to a displacement variation in an interferometer. When an interferometer is operated in a "zero path length difference" mode, and the linear displacement range is less than $\lambda/4$, corresponding to a value of <200 nm for a typical laser light source. However, when the displacement is greater than $\lambda/2$, the fringes will appear periodically, each fringe representing a λ change in optical path difference, corresponding to a change of 2π rad. By counting the number of the fringes, the displacement change can be calculated from the simple equation:

$$\Delta L = N\lambda/2 \tag{2.4}$$

where ΔL is the change of the displacement, N is the number of fringes counted and λ is wavelength of the light source. A number of parameters can be converted so as to produce a displacement and thus be amenable to measurement by this sensitive technique. As a result, a very wide range of sensors based on optical path modulation has been developed. The measurands vary from distance [60], to vibration [61], to those associated with a change of displacement, such as pressure [62].

2.5.5. Index modulation

Modulation of the material refractive index and its use for measurement purposes can be achieved both inside and outside the optical fibre in sensor use. In the first case, measurands such as temperature or pressure may be used to vary the index difference between the core and the cladding of a fibre, and thus the amount of light "leaking" from core to cladding causes a change in the output light intensity observed. In the second case, an external sensor element may be employed, for instance, by using a Lithium Niobate crystal, $LiNbo_3$, as a temperature sensor. The refractive index of such a sensor element is modulated by the measurand, and therefore the optical path within the material is changed. When an interferometer with a monomode light source is employed to determine this in an optical fibre sensor, the change of optical path difference can be used to vary the phase difference of the radiation in the interferometer and thus the output intensity observed. The fractional change in optical path length in a silica fibre is given by $dn/dT = 10^{-5}K^{-1}$ [4], the phase shift by $(2\pi nL/\lambda)$, which is approximately 1 rad K^{-1} cm^{-1} for a wavelength of 633 nm, the wavelength of the He-Ne laser. Other glasses less commonly used for optical fibres will show different characteristics. An approach using index modulation outside an optical fibre has been reported by Scheggi et al [63] in a sensor application.

2.5.6. Time modulation

With the use of coherent light sources, a temporal modulation can be transduced into a path length modulation through the use of the relationship:

$$\Delta L = c\, \Delta t \tag{2.5}$$

where ΔL is the optical path length transversed by light during a period of time Δt, and c is the speed of light. Therefore time modulation can be considered to be equivalent to a path length modulation under these circumstances.

With the use of an incoherent light source, time modulation, also known as rate modulation, is the form of modulation achieved using a low frequency applied to the light intensity or to produce pulses of known temporal duration. Information conveyed in the time domain can be highly dependent on the measurand using the correct sensor encoding. For example, the rate information from a rotating object such as a turbine, or in a vortex-shedding flowmeter or from a rotating shaft, can be delivered to an optical detector by optical fibre links to detect the optical radiation containing the information signal. The detected signal then can be converted into a digital signal.

A number of OFS techniques have been developed, based on time modulation, such as a quartz resonator hybrid OFS for displacement measurement [64] and pressure [65] and temperature sensors [66] based on fluorescent time decay. By the use of correlation techniques, the rotation of a shaft can be monitored directly from the light scattered by the shaft [61]. In such an application the signal received due to the reflection from the shaft is subjected to autocorrelation, and the rotation rate can be then calculated. Agreement to within a few percent with a mechanical device was observed in recent work [61].

2.5.7. Coherence length modulation

"Coherence length" is a term used as a measure of the temporal coherence of a light source. The "coherence region" of an interferometer output is the region where phase modulation can be achieved. For example in a Michelson interferometer, this is less than twice the "coherence length". The term of "coherence length modulation" used here represents the modulation of the so-called "white-light interferometer" scheme.

When the optical path difference (OPD) in a interferometer is less than the coherence length of the light source employed, the fringe visibility [1] of the output obtained is in the region between 1 to 0, and phase modulation can be achieved. However, when the OPD is greater than the coherence length the fringe visibility is zero, and the phase modulation becomes undetectable. In this latter case, the coherence length modulation technique can be used to "shift" an unbalanced interferometer into a "balanced" or a "near balance" region [22, 60]. The basic function of this modulation is to compensate the large OPD which is observed, in order to shift the coherence region from its original position to where the phase modulation can be achieved.

When coherence length modulation is introduced, it is necessary that a second detector interferometer is employed. The OPDs of the two interferometers are set to be larger than the coherence length of the light source, with the difference between them being less than coherence length. Under this condition, two interferometers give out an interference intensity distribution which shows the so-called "fringes of superposition" [67]. The scheme used in this modulation is sometime called "path-matched differential-interferometry" or "white-light interferometry" and has recently been exploited in interferometric fibre optical sensors.

The most commonly used low coherence light sources for such arrangements are the LED, the super-luminescent diode or multimode laser diode, in addition to broad-band sources and significant work has been done recently to develop optical fibre sensors operating by means of the coherence length modulation. As an example, an OFS for pressure measurement [22], remote displacement [60, 68], accelerometer [69], and flow speed [70] have been reported recently.

2.6. Summary

In this chapter a new kind of classification for optical fibre sensors has been introduced and discussed. The details of each "division" of the classifications were reviewed and corresponding examples given. Several points worthy of note emerge, and examples of the different schemes which have been discussed in the literature are seen in the reference matrix, Table 2.3.

Most work done in past years, in for example interferometric-based sensors, has concentrated on two major areas. The first is the "monomode light source, monomode fibre, and phase modulation" category which is represented using all types of interferometer. The second is the "broad-band, continuous spectrum light source, multimode fibre, with intensity modulation" type which covers many of the incoherent types of OFS employed.

Few-mode optical fibres and specialized fibres show significant possibilities for the development of novel types of OFS. However, their full applications have not yet been seen due to the lack of their availability at low cost, and this is likely to remain a problem.

Light modulation techniques have been investigated in different fields. The tendency for the development of sensing techniques is towards a combination of different modulation schemes together with the mixing of,

FIB \ SOU \ MOD		INT	LEN	W/F	POL	REF	TIM	COH
MON	MON	86	71	92	79	96	103	88
	TWO			105	81			
	MUL		89	102				58
	NAR		85			95		
	BRO				82			
POL	MON	87	101	84		83		
	TWO							
	MUL		90					
	NAR							
	BRO							
TWO	MON		78		100			106
	TWO							
	MUL							
	NAR							
	BRO							107
MUL	MON	91	97					
	TWO	40						
	MUL	76						
	NAR	72	99				77	
	BRO	98		94		93		
SPE	MON	104						
	TWO							74
	MUL	75						
	NAR	73						
	BRO							

Table 2.3 *Examples of different "cubic units" of the OFS space (numbers refer to references quoted).*

Key for table 2.3

1.	SON:	Source
	MON:	Monomode Light Source
	TWO:	Twomode Light Source
	MUL:	Multimode Light Source
	NAR:	Narrow Band Light Source
	BRO:	Broad Band Light Source
2.	FIB:	Fibre
	MON:	Monomode Fibre
	POL:	Polarization Maintaining Fibre
	TWO:	Twomode Fibre
	MUL:	Multimode Fibre
	SPE:	Special Fibre
3.	MOD:	Modulation
	INT:	Intensity Modulation
	LEN:	Length Modulation
	W/F:	Wavelength/Frequency Modulation
	POL:	Polarization Modulation
	REF:	Refractive Index Modulation
	TIM:	Time Modulation
	COH:	Coherence Modulation

for example, optical modulation with electronic modulation, where appropriate.

It is clear that a considerable body of work has been undertaken to develop OFS techniques, however, there are still many "blank cubes" which may be filled inside the OFS "techniques space", and in other words, this OFS techniques space has not yet been fully exploited. It is not expected that this space will be filled immediately, if ever, but this may gradually change as new kinds of light source, optical fibre or sensor approach emerge. However, it is likely that due to the basic physical mechanism and for sound commercial reasons many cubes will "remain blank" and perhaps in only a few areas will there be real commercial success with OFS techniques, where their unique advantages are seen. However, the field is very much alive and an increasing number of commercial products are appearing. This categorisation draws attention to those areas where devices do not exist and may be a stimulus to new developments with the emergence of new technology.

A number of examples have been shown to reveal the other applications, including the use of low coherence light sources such as the LED or the multimode laser diode. Such work emphasises the recent tendency towards the exploitation of these new light sources, which are both convenient and inexpensive, and operate at low voltages.

Since the use of the "CD-tpye" multimode laser diode in the field of OFS techniques has emerged only in the last few years, it is necessary fully to study the coherent characteristics of this low coherence light source in order to make better use of it in optical fibre sensor applications. The main work presented in this thesis is the results of such an investigation. From both theoretical and experimental aspects, the characteristics of a multimode laser diode in an interferometer were studied. The results show that the characteristics of a light source showing a "comb-shaped" spectrum in an interferometer are different from those of the other types of low coherence light sources, such as the narrow-band continuous spectrum sources and the broad-band continuous spectrum sources. Therefore, combining the research results on all these three types of low coherence light sources, a full overview of the coherence characteristics of the low coherence light sources can be seen (chapter 3).

In practical sensing applications, a low coherent light source is often used to illuminate a coupled dual interferometer. The scheme used is known as "white-light interferometer" or "coherence length modulation" scheme which is used in this thesis. Based upon the initial results of studies of a multimode laser diode in an interferometer, a further investigation of the characteristics of such a light source in several types of the coupled dual interferometer configurations were carried out. As a result, it can be seen that the "CD-type" multimode laser diodes are not only capable of being used as an alternative to the other type of low coherence light sources for optical fibre sensing applications, but also of giving attractive advantages of having a small numerical aperture, emitting high optical power and being of low cost. It is those advantages that make multimode laser diodes especially suitable for their use in optical fibre sensor techniques.

References:

1. D.A. Jackson, J.D.C. Jones "Extrinsic Fibre Optical Sensors for Remote Measurement: Part One", Optics and Laser Technology, 18, 243, 1986.
2. B.E. Jones "Optical Fibre Sensors and Systems for Industry", J. Phys. E: Sci. Instrum., 18, 770, 1985.
3. K.T.V. Grattan, "Fibre Optical Sensors" - the way forward", Measurement - J. Int. Meas. Confed., 5 122, 1987.
4. W.H. Glenn "Fibre Optic Temperature Sensors", OFS NATO ASI Series, Series E: Applied Sciences No. 132, 185-200, 1987.
5. A.L. Harmer "Guided Wave Chemical Sensors", OFS NATO ASI Series, Series E: Applied Sciences No. 132, pp.210-16, 1987.
6. A. Katzir "Biomedical Fibre optic Sensors", Proceedings Int. Conf. on Optical Fibre Sensors, New Orleans, 4-5, 1988.
7. R.S. Medlock "Fibre Optic Intensity Modulation Sensors", OFS NATO ASI Series, series E: Applied Sciences No. 132, 133-24, 1987.
8. K.T.V. Grattan "new Developments in Sensor Technology - Fibre & Electro - Optic", Measurement and Control, 22, 165-75, 1989.
7. R.S. Medlock "Fibre Optic Intensity Modulation Sensors", OFS NATO ASI Series, series E: Applied Sciences No. 132, 133-24, 1987.
8. K.T.V. Grattan "new Developments in Sensor Technology - Fibre & Electro - Optic", Measurement and Control, 22, 165-75, 1989.
9. S.Middlehoek and D.C. Van Duyn "Classification on Solid-State Transducers", Australasian Instrument. and Measur. Conf. 1989, Adelaide, 14th-17th November, 1-4, 1989.
10. L.Finkelstein "The formation of Engineers and Scientists in Measurement and Instrumentation", Australasian Instrum. and Measur. Conf. 1989. Adelaide 14th-17th November, 56-8, 1989.
11. H. Ishio, J. Minowa and J. Nosu "Review and Status of Wavelength-Division Multiplexing Technology", J. Lightwave Tech., LT-2, 448-463, 1984.
12. A.R. Mickilson, O. Klevhus, M. Eriksrud "Backscatter readout from Serial Microbending Sensors", J. Lightwave Tech., LT-2, 700-9, 1984.
13. Proc. of: Workshop on Single Fibre Sensor Technology, University of Kent, Canterbury, P.42, (unpublished).
14. J. Dakin, B. Culshaw "Optical Fibre Sensors: Principles and Components", 151, 198, Pub: Artec House, 1989.

15. K. Ho Tate and D. Kamatani "Reflectometry with high spatial resolution and no moving parts by means of source-coherence modulation", Proc: OFS 89 Paris, 64, 1989.
16. B.T. Meggitt, A.W. Palmer, K.T.V. Grattan "Fibre Optic Sensor using Coherence Properties - Single Processing Aspects", Int. J. Optoelectronics, 3, 451, 1989.
17. D.J. Webb, J.D.C. Jones, D,A. Jackson "Extended-range Interferometry using a Coherence-tuned Synthesised Dual-wavelength Technique with Multimode Fibre Link", Electron. Letts. 24, 1173-4, 1988.
18. C.H.F. Velzfl, R.P. Brouwer "Output Power and Coherence Length of Stripegeometry Double-heterostructure Semiconductor Laser in Incoherent Feedback", IEEE J. Quantum. Electron., QE-15, 782-6, 1979.
19. Y.N. Ning, K.T.V. Grattan, B.T. Meggitt, A.W. Palmer "Characteristics of Laser Diodes for Interferometric Use", Applied Optics, 28, 3657-61, 1989.
20. K.T.V. Grattan, A.W. Palmer, Y.N. Ning, B.T. Meggitt "Interferometric Sensors-Extension of Range Using Low Coherence Light from Laser Diode", Proc: EFOC/LAN, 1989, Amsterdam, The Netherlands, 375, June, 1989.
21. R. Kist "Source and Detectors for Fibre Optic Sensors", OFS NATO ASI Series, Series E: Applied Sciences No. 132, 267, 1987.
22. Micro-Gluhlampen-gesellschaft, Hamburg, Lanster, 1, D-2057, Manufacturer's Data.
24. D.A. Jackson "Monomode Fibre Optic Interferometers and Their Application in Sensing System", OFS NATO ASI Series, Series E: Applied Sciences No. 1-33, 1987.
25. T. Okoshi "Polarization Phenomena in Optical Fibres", OFS NATO ASI Series, Series E: Applied Sciences, 227-242, 1987.
26. B.Y. Kim "Few Mode Fibre Devices", Proc. Int. Conf. on Opt. Fibre Sensors, New Orleans, 1988. Technical Digest Series, 2, Part 1, 146-9, 1988.
27. S.Y. Huang, J.N. Blake, B.Y. Kim "Mode Characteristics of Highly Elliptical Core Two-mode Fibre Perturbations", Proc. Int. Conf. on Opt. on Opt. Fibre Sensors, New Orleans, 1988. Technical Digest Series, 2, Part 1, 14-17, 1988.
28. J.N. Blake, B.Y. Kim, H.E. Engan, H.J. Shaw "Analysis of Inter-Modal Coupling in a Two-Mode Fibre with Periodic Microbends", Opt. Lett., 12, No.4, 281, 1987.

29. G. Meltz, J.R. Dunphy, W.W. Morey, E. Snitzer "Cross-talk Fibre-Optic Temperature Sensor", Appl. Opt., 22,464, 1983.
30. W.V. Sorin, B.Y. Kin, H.J. Shaw "Phase-Velocity Measurements using Prism Output Coupling for Single- and Few-Mode Optical Fibres", Opt. Lett., 11, 106, 1986.
31. B.Y. Kim, J.M. Blake, S.Y. Huang, H.J. Shaw, "Use of Highly Elliptical Core Fibres for Two-Mode Fibre Devices", Opt. Lett., 12, 729, 1987.
32. T. Bosselmenn "Multimode-Fibre Coupled White-light Interferometric Position Sensor", OFS NATO ASI Series, Series E: Applied Sciences No. 132, pp.429, 1988.
33. C.A. Millar, B.J. Ainslie, M.C. Brierley and S.P. Craig "Fabrication and Characterisation of D-Fibres with an Accurately Controlled Core/Flat Distance", Electron. Letts., 22, 322-4, 1986.
34. R.B. Dyott, J. Beiio, V.A. Henderek "Indium-Coated D-Shaped Fibre Polarizer", Opt. Lett., 12, 287-9, 1987.
35. R.B. Dyott, P.F. Schrank "Self-Locating Elliptically Cored Fibre with an Accessible Guiding Region", Electron. Lett., 18, 980, 1982.
36. L. Li, G. Wylandgowski, D.N. Payne and R.D. Birch "Broadband Metal/Glass Single-Mode Fibre Polarisers", Electron. Lett., 22, 1020-1022, 1986.
37. J. Dakin and B. Culshaw "Optical Fibre Sensors: Principles and Components", Pub: Artec House, 249, 1989.
38. M.C. Farries, M.E. Fermann, R.I. Laming, S.B. Poole, D.N. Payne and A.P. Leach "Distributed Temperature Sensor using Nd3+ Doped Fibre", Electron. Lett., 22, 418-419, 1986.
39. A.H. Hartog "A Distributed Temperature Sensor Based on Liquid Core Fibres", IEEE J. Lightwave Tech., LT-1, 498-501, 1983.
40. G. Martens, J.Kordts and G. Weidinger "Photo-Elastic Pressure Sensor with Loss-Compensated Fibre Link", Proc: OFS 89, Springer Proc. in Physics, Springer-Verlag, 44, pp.458, 1989.
41. L. Jonssom and B. Hok "Multimode Fibre-Optic Accelerometers", Proc. 2nd Int. Conf. on Optical Fibre Sensors, Stuttgart, 5-7 Sept., (SPIE Vol.514), pp.191-4, 1984.
42. J.D. Place "Optical Control and Alarm Switch for the Process Industries", Proc. Conf. Promecon. London, pp.157-63, 19-22 June, 1984.
43. R.C. Spooner et al "Fibre Optics in Physics and Chemical Sensors" Institute of Measurement and Control Conf., Harrogate, Nov. 1985, Pub: Inst. M.C., London, 1985.

44. B. Culshaw "Optical System and Sensors for Measurement and Control", J. Phys. E: Sci. Instrum., 16, 978-986, 1983.
45. D.A. Jackson "Monomode Optical Fibre Interferometers for Precision Measurements", J. Phys. E: Sci. Instrum., 18, 981, 1985.
46. H. Ishio, J. Minowa and J. Nosu "Review and Status of Wavelength-Division Multiplexing Technology", J. Lightwave Tech., LT-2, 448-463, 1984. (See 11)
47. G. Winzer "Wavelength Multiplexing Components - A Review of Single-Mode Devices and Their Applications", J. Lightwave Tech., LT-2, 369-378, 1984.
48. M.C. Hutley "Wavelength Encoded Optical Fibre Sensors", Proc. 2nd Int. Conf. on OFS, Stuttgart, Proc. SPIE, 514, 111-6, 1984.
49. M.E. Jones and S.J. Collier "Optical Fibre Sensors using Wavelength Modulation and Simplified Spectral Analysis", J. Phys. E: Sci. Instrum., 17, 1240-1, 1984.
50. H. Ghafoori-Shiraz and T. Okoshi "Fault Location in Optical Fibres using Optical Frequency Domain Reflectry", IEEE J. Lightwave Tech., LT-4, 316, 1986.
51. S.A. Al-Chalabi, B. Culshaw, D.B.N. Davies, I.P. Giles, D. Uttam "Multiplexed Optical Fibre Interferometers: An Analysis Based on Radar System", Proc. IEE, 132A, 150-6, 1985.
52. D. Uttam and B. Culshaw "Precision Time Domain Reflectometry in Optical Fibre Systems using a Frequency Modulated Continuous Wave Ranging Technique", IEEE J. Lightwave Tech., LT-3, 971, 1985.
53. R.B. Dyott "Fibre-Optic Doppler Anemometer", IEEE J. Microwaves Opt. Acoust., 20, 13-18, 1978.
54. T.T. Nguyen, L.N. Birch "A Fibre-Optic Laser-Doppler Anemometer", Appl. Phys. Lett., 45, 1163, 1984.
55. D.A. Jackson, J.D.C. Jones, R.K.Y. Chan "A High-Power Fibre Optic Laser Doppler Velocimeter", J. Phys. E: Sci. Intrum., 17, 977-80, 1984.
56. Takashi Nakayama " Fibre LDA system " NATO ASI Series E: Appl. Sci. No. 132 OFS pp.217 (1987)
57. K.Kyuma et al, " Laser Doppler velocimeter with a novel optical fibre probe", Appl. Opt. 20, 2424-27, 1981
58. Y.N. Ning, K.T.V. Grattan, A.W. Palmer, B.T. Meggitt, and K. Weir, "A novel optical heterodyne vibration sensor scheme preserving directional information and using a short coherence length source" Optics Communications, 85, 10-16, 1991.

59. M.D. Stern "Laser Doppler Velocitmetry in Blood and Multiply Scattering Fluids: Theory", Appl. Opt., 24, 1968,.1985.

60. G. Ulbers "A Sensor for Dimensional Metrology with an Interferometer in Integrated Optics Technology" Spring proc. in phys. 44, OFS, 240, 1989.

61. K.T.V. Grattan, A.W. Palmer, B.T. Meggitt and Yanong Ning "Use of Laser Diode Source in Low Coherence Operation in Fibre Optic Sensors" Australian Instrument. and Measur. Conf., 305-8, 1989.

62. D. Trouchet, B. Laloux, and P. Graindorge "Protype Industrial Multi-Parameter F.O.S. using White Light Interferometry" Springer proc. in phys., 44, OFS, 227-233, 1989.

63. A.M. Scheggi, M. Brenci, G. Conforti, R. Faliai, G.P. Preti "Optical Fibre Thermometer for Medical Use" 1st Int. Conf. on Optical Fibre Sensors, IEE Conf. Publication, 221, 13-16, 1983, (IEE, London).

64. S.M. Scheggi, G.R. Jones "Optical Sensors for Displacement Measurement", Proc. Control, London, Jan 1984, (IEE, Colloq. Digest 1984/7).

65. B. Hok and L. Jonsson "Pressure Sensor with Fluorescence Decay as Information Carrier", Proc. 2nd Int. Conf. OFS, Stuttgart 5-7 Sept., Proc. SPIE, 514, 381-4, 1984.

66. K.T.V. Grattan, R.K. Selli and A.W. Palmer, "Ruby Decay time Fluorescence Thermometer in a Fibre-Optic Configuration" Rev. Sci. Instrum., 59, 1328-35, 1988.

67. M. Born and E. wolf "Principles of Optics" Oxford University Press, pp.360-7, 1980.

68. G. Behiem "Remote Displacement Measurement using a Passive Sensor with a Fibre-Optic Link", Appl. Opt. 24, 2335-40, 1985.

69. C.J. Zarobila, J.B. Freal, R.L. Lampman and C.M. Davis "Two Fibre - Optic Accelerometers", Proc. OFS Conf. New Orleans, USA, Pub: IEEE/OSA, 1988, Technical Digest, 2, part 1, 296, 1988.

70. B.T. Meggitt, Yanong Ning, K.T.V. Grattan, A.D. Palmer, W. Boylb the "Eighth Int. Conf. Fibre Optics and Opto-Electronics", London, April 1990, Proc. SPIE, 1314, 321-9, 1990.

71. F. Farahi et al "Optical-Fibre Flammable Gas Sensor", J. Phys. E: Sci. Instrum., 20, 435-6, 1987.

72. F.P. Milanovich et al "Remote Detection of Organochlorides with a Fibre Optic Based Sensor", Anal. Instrum. (USA), 15, 542-58, 1986.

73. I. Aeby, "Non-Destructive Measurement in Advanced Composite Materials and Structures using a Fibre Optic Sensing System", Proc. SPIE, 986, 140-7, 1989.

74. A. Safaai-Jazi, R.O. Clau, "Synthesis of Interference Patterns in Few-Mode Optic Fibre", Proc. SPIE, 986, 180-5, 1989.

75. P.B. Macedo et.al "Development of Porous Glass Fibre Optic Sensors", Proc. SPIE, 986, 200-5 1989.

76. J.K. Zientkiewcz "Self-Reference Fibre Optic Methane Detection System", Proc. SPIE, 992, 192-7, 1989.

77. G.W. Fehrenbach "Fibre Optic Temperature Measurement System Based on Luminescence Decay Time", Tech. Mess. Tm (West Germany), 56, 85-8, 1989.

78. F. Gonthier et al "Circular Symmetry Modal Interferometers in Optical Fibres", Ann. Telcommun. (France), 44, 159-66, 1989.

79. T.G. Giallorenzi "Optical Fibre Sensor Technology", IEEE, J. Quantum Electron., QE-18, 626, 1982.

80. M. Corke et al "All Fibre Michelson Thermometer", Electron. Lett., 19, 471, 1983.

81. P. Akhavanleilabady "A Dual Interferometer Implemented in Parallel on a Single Birefringent Monomode Optic Fibre", J.Phys. E: Sci. Instrum., 19, 143, 1986.

82. S.A. Al-Chalabi, B. Culshaw and D.E.N. Davies "Partially Coherence Sources in Interferometric Sensor", Proc. 1st Int. Conf. on Optic Fibre Sensors, London, Pub: IEE, 132-5, 1988.

83. H.L.W. Chan et al. "Polarimetric Optical Fibre Sensor for Ultrasonic Power Measurement", IEEE 1988 Ultrasonic Symposium Proceedings, 1, 599-602, 1988.

84. H. Tsuchida "Polarimetric Optical Fibre Sensor Using a Frequency Stabilised Semiconductor Laser", IEEE J. Lightwave Tech., LT-7, 799-803, 1989.

85. A.V.Belov "The Measurement of Chromatic Dispersion in Single-Mode Fibre by Interferometric Loop", IEEE J. Lightwave Tech., 7, 863-8, 1989.

86. E. Wittendrop-Rechenmann, Radiat. Prot. Dosim. (UK) 23, 199-202, 1988.

87. H. Takaahra, F. Togashi, T. Argaki "Ultrasonic Sensor Using Polarisation-Maintaining Optical Fibre", Can J. Phys. 66, 844-6, 1988.

88. F. Farahi, N. Takahashi, J.D.C. Jones, D.A. Jackson "Multiplexed Fibre Optic Sensors Using Ring Interferometers", J. Mod. Opt. 36, 337-48, 1988.

89. A.S. Georges "High Sensitivity Fibre-Optic Accelerometer", Opt. Lett. 14, 251-3, 1989.

90. H. Takahashi, et. al. "Laser Diode Interferometer for Small Displacement and Sound Pressure Measurements", Conf. on Precision Electromagnetic Measurements Tsukuba, Japan, 135-6, June 1988.

91. E. Theocharous "Differential Absorption Distributed Thermometer", 1st Int. Conf. on Opt. Fib. Sens. Pub IEE London, pp10-12, April 1983.

92. M.L. Henning et. al. "Optical Fibre Hygrophones with Down Lead Insensitivity", 1st Int. Conf. on Opt. Fib. Sens. IEE London, April 1983. pp 25-7.

93. K. Spenner et. al. "Experimental Investigations on Fibre Optic Liquid Lever Sensors and Refractometer", 1st Int. Conf., on Opt. Fib. Sens. IEE London, April 1983, pp 75-8.

94. E.R. Cox and B.E. Jones "Fibre Optic Colour Sensors Based on Fabry-Perot Interferometry", 1st Int. Conf. on Opt. Fib. Sens. IEE London, April 1983, pp 122-6.

95. K. Shibata "A Fibre Optic Electric Field Sensor Using the Electro-Optic Effect of Bismnth Germinate", 1st Int. Conf. on Opt. Fib. Sens. IEE London, April 1983, pp164-6.

96. S.C. Rashleigh "Polarimetric Sensors: exploiting the Axial Stress in High Birefringement Fibre", 1st Int. conf. on Opt. Fib. Sens. IEE London, April 1983, pp210-3.

97. A.J.A. Brumsma and J.A. Vogel "Ultrasonic Noncontact Inspection System with Optical Fibre Methods", Appl. Opt. 27, 4690-5, 1988.

98. K. Iwamoto and I. Kamato "Pressure Sensors Using Optical Fibres", Appl. Opt. 29, 375-7, 1989.

99. T. Okamoto and I.Y. Yamaguchi "Multimode Fibre Optic Mach-Zehnder Interferometer and its Use in Temperature Measurement", Appl. Opt. 27, 3085-7, 1988.

100. S.y. Huang et. al. "Mode Characteristics of Highly Elliptical Core Two-Mode Fibres Under Perturbation", Proc. Int. Conf. On Opt. Fib. Sens. (OFS-88) Tech. Digest (Pub IEEE/OSA), pp.14-9, 1988.

101. E. Sakaoa et. al. "Polarisation Maintaining Fibres for Fibre-Optic Gyroscopes", Proc. Int. Conf. On Opt. Fib. Sens. (OFS-88) Tech. Digest (Pub IEEE/OSA) pp.18, 1988

102. D.T. Dong and K. Hotate "Frequency Division Multiplication of Optical Fibre Sensors Using an Optical Delay Line with a frequency Shifter", Proc. Int. Conf. On Opt. Fib. Sens. (OFS-88) Tech. Digest (Pub IEEE/OSA), pp.76, 1988.
103. A.D. Kersey and A Dandridge "Tapped Serial Interferometric Fibre Sensor Array with Time Division Multiplexing", Proc. Int. Conf. On Opt. Fib. Sens. (OFS-88) Tech. Digest (Pub IEEE/OSA), pp.80, 1988.
104. H. Hosokawa et. al. "Integrated Optical Microdisplacement Sensor Using a Y Junction and a Polarisation Maintaining Fibre", Proc. Int. Conf. On Opt. Fib. Sens. (OFS-88) Tech. Digest (Pub IEEE/OSA), pp.137, 1988.
105. H. Koseki et. al. "Optical Heterodyne Gyroscope Using Two Reversed Fibre Coils", Proc. Int. Conf. On Opt. Fib. Sens. (OFS-88) Tech. Digest (Pub IEEE/OSA), pp.168, 1988.
106. G. Kotrotsios and D. Pariaux "White Light Interferometry for Distributed Sensing on Dual Mode Fibres", Springer Proc. in Phys. 44, OFS, 1989.
107. S.Y. Huang, H.G. Park and B.Y. Kim "Passive Quadrature Phase Detector for Coherence Fibre Optic System", Springer Proc. in Phys., 44, OFS, p38, 1989.

Chapter 3

Fibre-optic interferometric systems using low coherence light sources

Abstract:

With the increasing interest in the use of optical fibre interferometer measurement systems, the importance of the incorporation of low coherence light sources is becoming of particular significance. In this work, the optical characteristics of different types of such sources in interferometers are reviewed and examples are given. Their advantages in term of increased unambiguous range, immunity to perturbation and high resolution and dynamic range are discussed.

3.1 Introduction:

The most frequently used light sources in interferometric systems are various types of single mode (or narrow-band spectrum), high coherence laser devices, especially the single mode HeNe lasers. Two fundamental problems associated with these single mode light source interferometers are their short unambiguous operating range which is due to the periodic nature of the output, and the lack of identification of the interference order when the interferometer is switched on. By contrast, the use of low coherence light sources in these interferometers can help to overcome some of the above problems [1, 2, 3], and thus to extend the range and applicability of these sensors. A considerable amount of research effort has been expended in the investigation and the development of fibre-optic interferometric systems using low coherence light sources in recent years [2, 3, 4, 5].

In this chapter, the optical characteristics of different types of low coherence light sources are outlined, the basic configuration of the low coherence interferometer and theoretical consideration related to it are described. Examples of several types of the fibre-optic interferometric systems with different types of low coherence light sources are reviewed.

3.2. Optical characteristics of low coherence light sources

3.2.1. Basic configuration of a white light interferometer and the classification of light sources

An interferometric system using a low coherence light source is also known as "the white-light interferometer". Although there are different types of configuration proposed or developed, the basic arrangement is the same, and one commonly used is constructed using two interferometers. The first of them, with a large "static" optical path difference, L_1 (which is much greater than the coherence length of source, L_C, i.e., L_1>>Lc), acts as a sensing interferometer, which converts the measurands into the change of optical path difference (OPD). The second works as the reference interferometer, in which the large "static" OPD induced by the first is compensated with the OPD of the second. Thus, the OPD of the second interferometer acts as an optical delay line in which the two incoherent optical signals in the two arms of the first interferometer are brought together and become coherent. In this case, although the two values of OPD, L_1 and L_2, are much greater than the coherence length of the light source used, the difference between them is less than L_c, i.e., $L_1 >> L_c$, $L_2 >> L_c$ and $|L_1 - L_2| < L_c$. Thus interference fringes can be observed from the combined output of these interferometers. The fringes produced are known as "fringes of superposition" [6]. It is these superposed fringes that play a main role in the use of low coherence interferometric systems.

Dependent on the spectral distribution of the light source itself, these low coherence sources may be divided into three groups: the broad-band continuous spectrum, the narrow-band continuous spectrum and the comb -shaped spectrum group. Due to the fact that the spectral distributions of these light sources are different, their optical characteristics, especially their coherence characteristics, are also different. This determines the different application areas for these light sources.

3.2.2. Broad - band continuous spectrum light sources

Frequently used examples of this group of light sources are the tungsten lamp, the mercury lamp, and the continuous output xenon lamp. The spectral distribution in general, black body radiation characteristics, can be described by Planck's law [7]:

$$L = \frac{2hc}{\lambda^5}\left[\exp\left(\frac{hc}{\lambda kT}\right) - 1\right]^{-1} \qquad (3.1)$$

where

L = spectral radiance
λ = wavelength
T = temperature
c = speed of light
h = Planck's constant
k = Boltzmann's constant.

Taking a typical tungsten lamp (supplied by RAC) for example, Figure 3.1 shows the typical normalised spectral distribution of this light source operated at 2850 K. It can be seen that the optical output is in the spectral range 400 - 2800 nm. Because of this broad-band spectral distribution, the coherence characteristics of this group of light sources are usually very poor, with the coherence length being of a distance equal to a few wavelengths for a typical white light source [8]. Therefore, the sources in this group are frequently termed as incoherent. However, in a balanced interferometer, the interference fringes generated by this type of light sources have an unique characteristic, i.e., a fixed internal "zero" position which corresponds to the "balanced position" where the optical path length in the signal arm is equal to that in the reference arm. This characteristic may be employed to provide a "position mark" in the interferometric system, so that the absolute displacement can be measured [9].

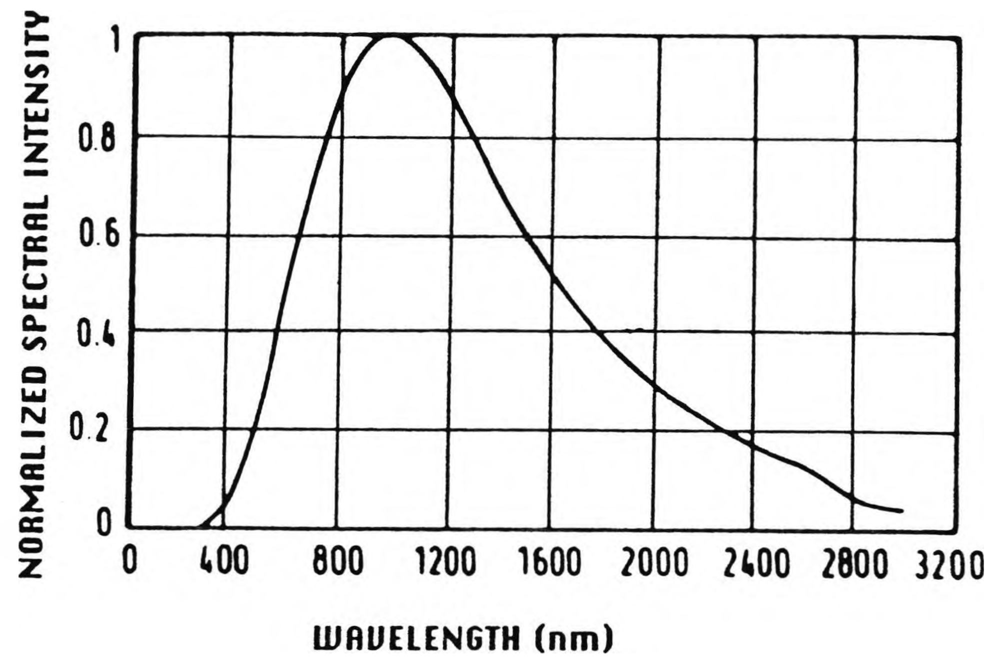

Figure 3.1. *Normalised spectral distribution of a tungsten lamp at T=2850 K (Ref. 7).*

3.2.3. Narrow-band continuous spectrum light sources

The light emitting diode, or LED, and the superluminescent LED belong to this group of light source, which is widely used in various fibre-optic interferometric systems. The radiation from an LED is produced by spontaneous emission via an electro-luminescent process in the semiconductor materials. There are at least two types of LED frequently used: the surface emitting LED and the edge emitting LED. The optical power of the edge emitting LED, with a beam of typical half-power width of 25^{o} to 30^{o}, is generally a few times lower than that of the surface emitting LED. However, the radiation coupling efficiency from the edge emitting LED into the optical fibres is relatively higher than that from the surface emitting LED. The spectral distribution of an LED may be described by a Gaussian spectral distribution [2], which is symmetric about the central wave number σ_0 and having a half-width $\Delta\sigma$, i.e.,

$$i(\sigma) = \frac{1}{\sqrt{\sigma\pi}} \exp\left[- \left(\frac{\sigma - \sigma_0}{\Delta\sigma} \right)^2 \right] \tag{3.2}$$

where $i(\sigma)$ is the spectral density, and σ is wave number. Figure 3.2 shows the normalised emission spectrum for various forward current values for an GaAlAs LED [10]. The bandwidth of its output spectrum is much narrower than that of the ordinary white light source, being typically 20-80 nm [11], and as a consequence its coherence length is of the range from a several micrometers to tens of micrometers [2, 11]. When an LED device is used in a balanced interferometer, the output interference fringes still have a fixed internal "zero" position which produces the same result as is obtained in an interferometer with a white light source. However, due to the longer coherence length, the output from an interferometer with an LED source will give a few more interference fringes. The amplitude of these sinusoidal fringes has its maximum value at the fixed internal "zero" position where the two values of the OPDs, L_1 and L_2, are the same, and decreases as the difference of L_1 and L_2 increases. When $|L_1 - L_2| > L_c$, the fringe visibility will become zero, where L_c is the coherence length of the LED.

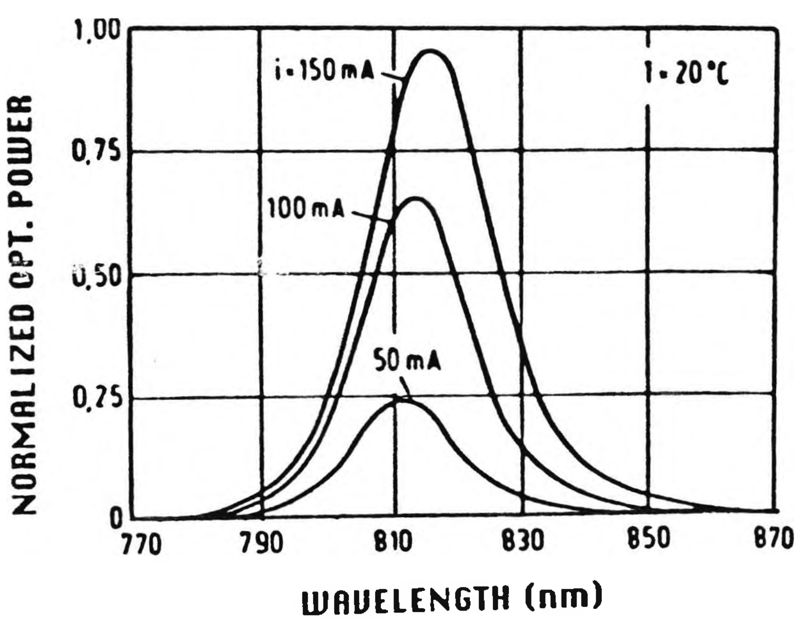

Figure 3.2. *Normalised AlGaAs - LED emission spectral distribution for various forward current values (Ref. 7).*

Superradiant diodes, (SRD) [7] or superluminescent diodes (SLD) [12] are another widely used narrow-band spectrum light source. In SRD operation, the lasing action is suppressed or avoided by use of an antireflection (AR) coating on the emitting facet of the semiconductor and by incorporating a rear absorbing section. Therefore, the SRD device is able to emit a high optical power, for example, 22.5 mW in the SRD mode at a very low injection current, such as 100 mA. The spectral distribution as shown in Figure 3.3 is about half as broad as for a LED, typically 20 nm. The coherence length of a SRD device is thus about 50 mm.

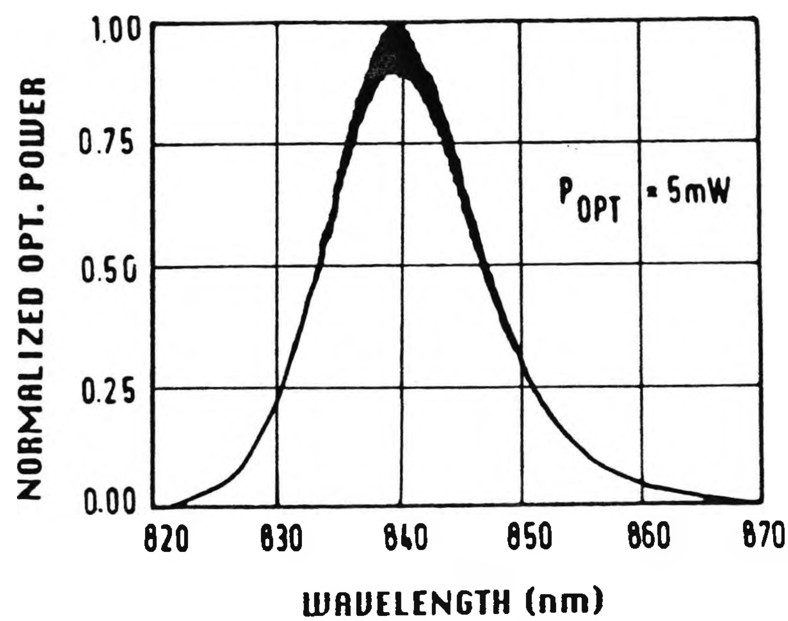

Figure 3.3 *Normalised spectral distribution of a SRD (Ref. 7)*

3.2.4. "Comb-shaped" spectrum light sources

This group of light sources includes all types of multimode laser devices and the multimode laser diode. The spectral distribution of this group of light sources consists of a series of equally separated single lasing modes, with each of them having a Lorentzian spectral shape [13, 14], and the spectral envelope of all the lasing modes may be considered as a Gaussian distribution [5]. The details of the output characteristics of an interferometer using such a light source are shown in chapter 5.

3.3 Basic configurations and their theoretical background

3.3.1 Interferometers using a continuous spectral distribution light source

For light sources with a continuous spectral distribution, one of the earliest theories used to analyse the intensity distribution of the optical output from a coupled dual interferometer (two Fabry-Perot cavities) was given by Fabry and Buisson [15]. Following that analysis, Born and Wolf discussed the details of the theoretical consideration [6]. According to their theory, if the light source has unity intensity with a spectral density $i_{(i)}(k_o)$, then, under the conditions of $L_1 >> L_c$, $L_2 >> L_c$ and $|L_1 - L_2| < L_c$, where L_1, L_2 are the OPDs of two cavities respectively, and L_c is the coherence length of the light source, the transmitted output intensity, I(t), of the interferometer is given by:

$$I_{(t)} = \frac{T_1^2 T_2^2[1-(R_1 R_2)^2]}{(1-R_1^2)(1-R_2^2)[1-(R_1 R_2)]^2} \int \left(\frac{i_{(i)}(k_o)}{1+B \sin^2(k_o \varepsilon/2)} \right) dk_o \qquad (3.5)$$

where

$B = (4R_1R_2)/(1-R_1R_2)^2$

$\varepsilon = | L_1 - L_2 |$ is the difference of the two OPDs.

$k_o = 2\pi\Delta\lambda/\bar{\lambda}_o{}^2$ is the wave number,

$\Delta\lambda$ is the wavelength range about a mean wavelength $\bar{\lambda}_o$,

R_1, R_2 are the reflectivities of the two cavities respectively.

T_1, T_2 are the transmissivities of the two cavities respectively.

Therefore, the intensity maxima of these distributions occur when $k_o\varepsilon$ is an integral multiple of 2π, when

$$\varepsilon = m\lambda_o \qquad | m | = 0, 1, 2, ... \qquad (3.6)$$

For a white light source, there is a central white fringe in the position where $L_1 = L_2$, with coloured maxima and minima on either side, and further away there is what appears to the detector to be uniform illumination.

3.3.2. Interferometers using a comb-shaped spectral distribution light source

For light sources with a comb-shaped spectral distribution, a recent theoretical analysis and experimental investigation were reported [16,17,18]. In the theoretical considerations reported, three assumptions were made, which are:

(i) each single lasing mode of the multimode laser diode can only interfere with itself, hence

(ii) different lasing modes, which do not interfere between them, can be summed from single intensity superposition consideration,

(iii) the total output intensity from the two interferometers is proportional to the sum of the output of all the 2m+1 modes of the multimode laser diode.

Based on this, the output intensities of several types of dual interferometer configurations were studied. The details of those work are shown in chapters 6 to 7.

3.4. Examples of the fibre-optic interferometric systems with different types of low coherence light sources

3.4.1. Systems with broad-band spectrum light sources

Fibre-optic interferometric systems with broad-band spectrum light sources have been investigated and developed by several research groups [3, 19,20,21]. The basic working principle of these systems is the use of the "internal zero position" to determine the variation of the OPD in the sensing interferometer.

One of the examples of this type of fibre-optic interferometric system was reported by Bosselmann [3]. In his system, two Michelson interferometers are connected with a multimode optical fibre, as shown in Figure 3.4. The internal zero position of the sensing interferometer can be obtained by adjusting the OPD of the reference interferometer to match that of the sensing one, i.e., $L_1=L_2$. When the OPD of the sensing interferometer is changed by ΔL_1, which is caused by the measurand to be measured, and ΔL_1 is greater than the coherence length of the light source (i.e.: $\Delta L_1=|L_1-L_2|>L_c$

), the output interference fringes or the fringes of the superposition will disappear. However, by adjusting the OPD of the reference interferometer to match ΔL_1, i.e., ΔL_1 is matched by ΔL_2 (the change of L_2), which can be measured with an additional single mode light sourced interferometer, the balanced position will be recovered, and ΔL_1 is given by ΔL_2 directly. Using this system, a measuring range of 22 mm with the resolution of 0.00001 mm was reported [3].

Based upon almost the same principle, a trench depth measurement system was developed by Takada et al [21]. In their system, instead of employing a "sensing interferometer" to induce the OPD change, the surface of the cell island and the surface of the trench bottom were used to reflect the irradiated light, as shown in Figure 3.5. Thus, two kinds of the reflected waves, with an OPD of twice of the trench depth, d, are produced. When the coherence length is less than 2d, these two waves are no longer correlated. Under this condition, as the OPD of the "reference interferometer" is scanned, the trench depth of the cell is transformed into the OPD between the centre of the central interference region and the centre of one of two sideband interference regions or shifted interference regions. By using this system, the measurement error was within ±0.2 μm for trench depth of 2 - 5 μm. Because the multimode fibre was used in the system facilitates wafer arrangement, the system can be introduced into a in-process measurement system.

3.4.2. Systems with narrow-band spectrum light sources

The dual interferometric system with a LED light source has been researched and developed for more than one decade. The theoretical analysis of the system has been described in detail elsewhere [22]. One of the first proposed systems, which used a tunable reference interferometer to compensate a passive sensing interferometer, was reported by Cielo [23]. In this system, as shown in Figure 3.6, two single-mode optic fibre Fabry-Perot cavities are connected, with one of them being a hydrophone element, other acting as a reference cavity. When the two OPDs are adjusted to the same length, the optical output of the system exhibits the superposed interference fringes. In this system, the detected signal is unaffected by any phase perturbation in the fibre between the two cavities. This is due to the detected intensity depending only upon the matching of the spectral responses of the two cavities.

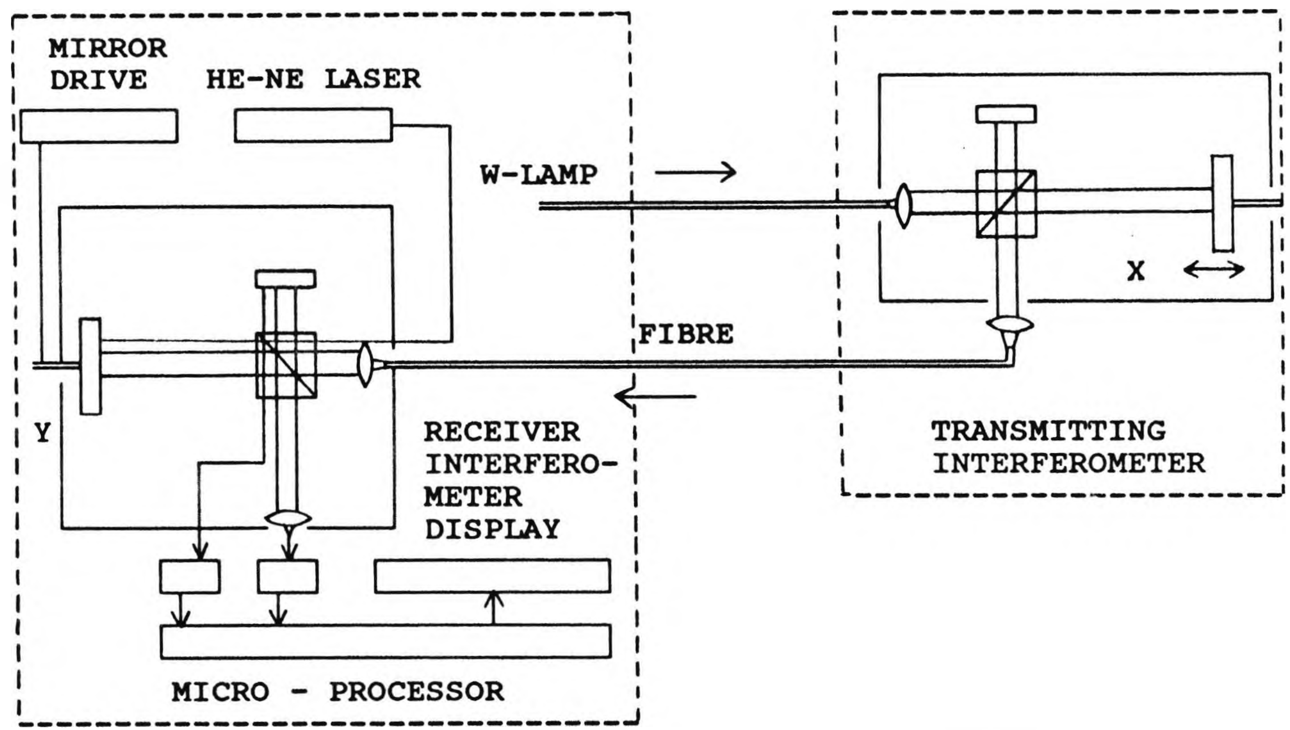

Figure 3.4. *Schematic optical arrangement of the "white - light interferometer" (Ref.3).*

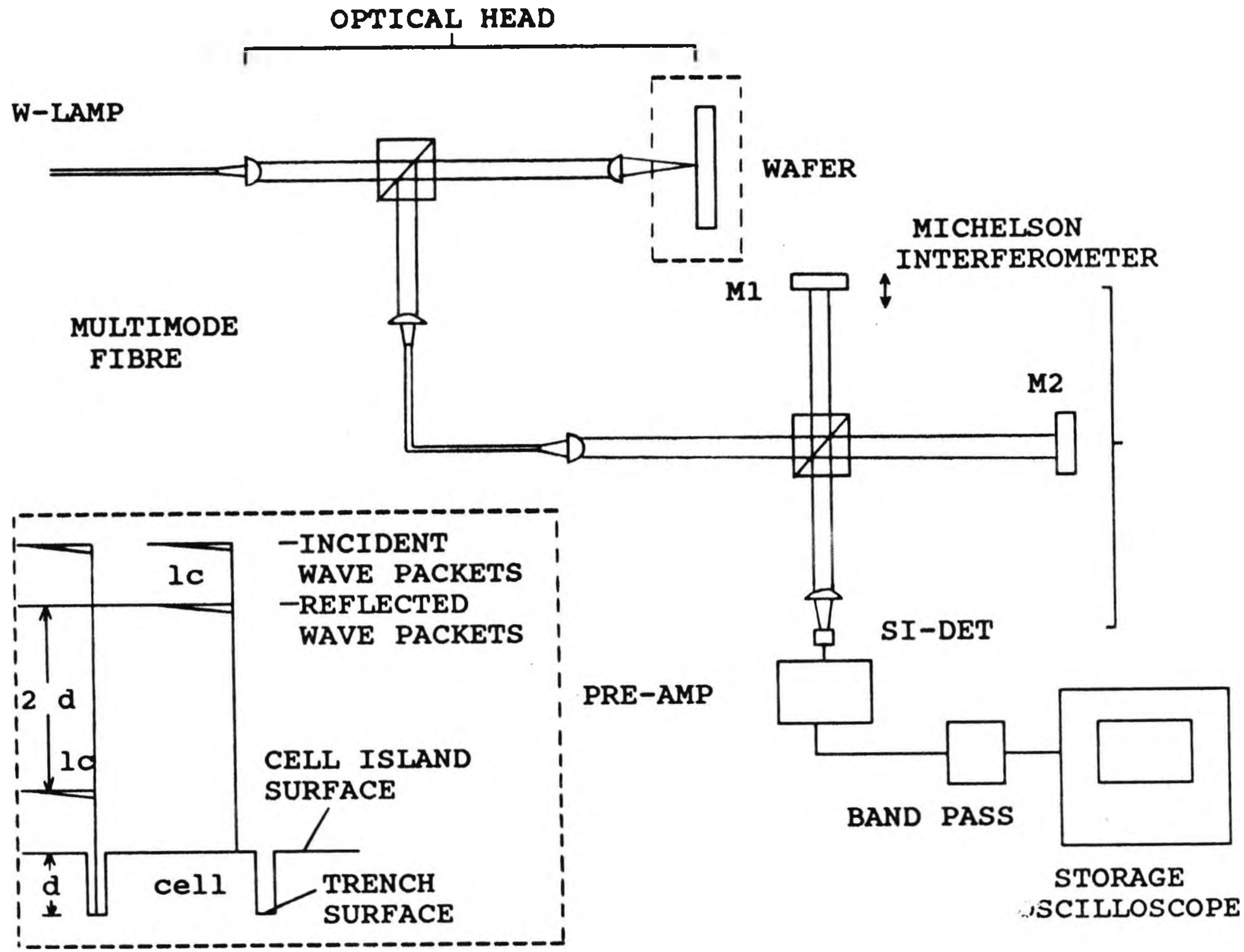

Figure 3.5. *Experimental arrangement of the system used to measure the trench depth of DRAM's capacitor cell (Ref. 25).*

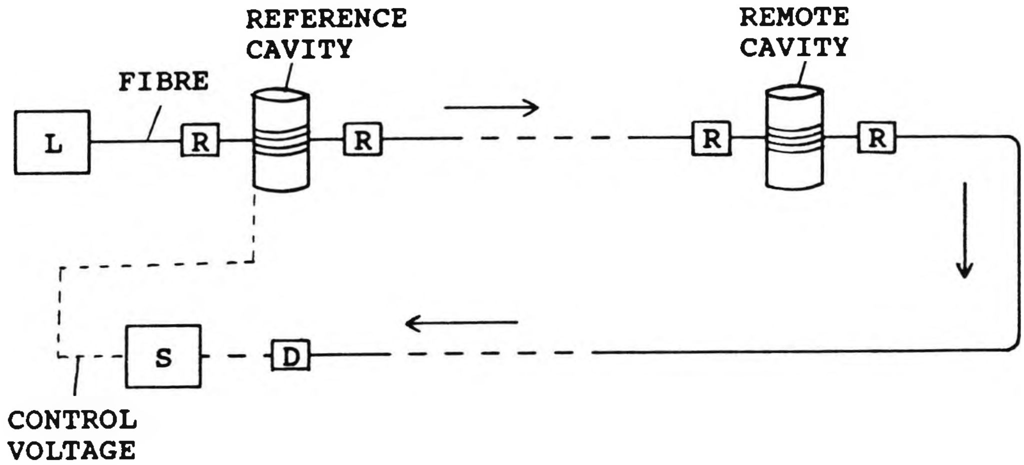

Figure 3.6. *Double - cavity configuration: L, light source coupled to the fibre; R reflectors; D, photodiode; S servocontrol electronics (Ref. 23).*

Another type of coupled dual Fabry-Perot interferometer, which was used to measure pressure, was reported by Beheim et al [2]. In their system, shown in Figure 3.7, a diaphragm is used to modulate the mirror separation of the Fabry-Perot sensing cavity, and the change of this separation is matched by the OPD of the reference Fabry-Perot cavity, which is controlled by an electronic servo control unit. The two cavities are linked with a multimode fibre. The mirror separation of the reference cavity is determined by measuring the capacitance of its metal-coated mirrors. Using this system, the pressure range from 0 to 3.8 MPa was obtained. A least-squares fit for the measured data yields a standard deviation of 3.4 KPa or 0.1 % of full scale in the measurement.

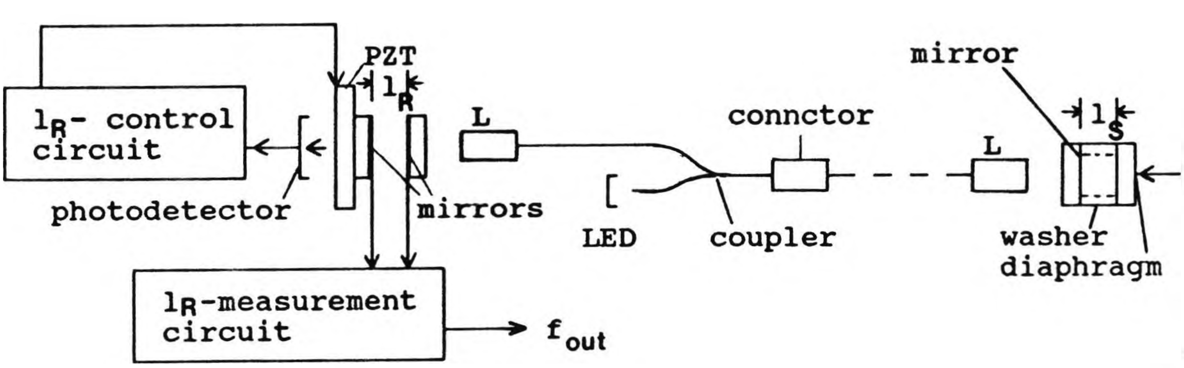

Figure 3.7. *Schematic diagram of a pressure sensing instrument (Ref. 2)*

In order to minimise the requirement of the source stability, a low coherence light source interferometric system using a dual-wavelength technique was developed and reported by Webb et al [24]. In their system, as shown in Figure 3.8, an interference filter with a 10 nm passband entered on 803 nm is placed at the front of one of the detectors. Therefore, by combining the output with the optical output from the original source, which has a peak wavelength of 815 nm and a bandwidth of 50 nm, two outputs were available, corresponding to sources at 815 and 803 nm. By using the pseudo-heterodyne technique, two electronic carrier frequencies can be generated at the outputs. By use of this experiment arrangement, a resolution which corresponds to a mirror displacement of 8.5 nm, with a dynamic range increased from 47.5 to 900, i.e., a factor of roughly 21, was achieved.

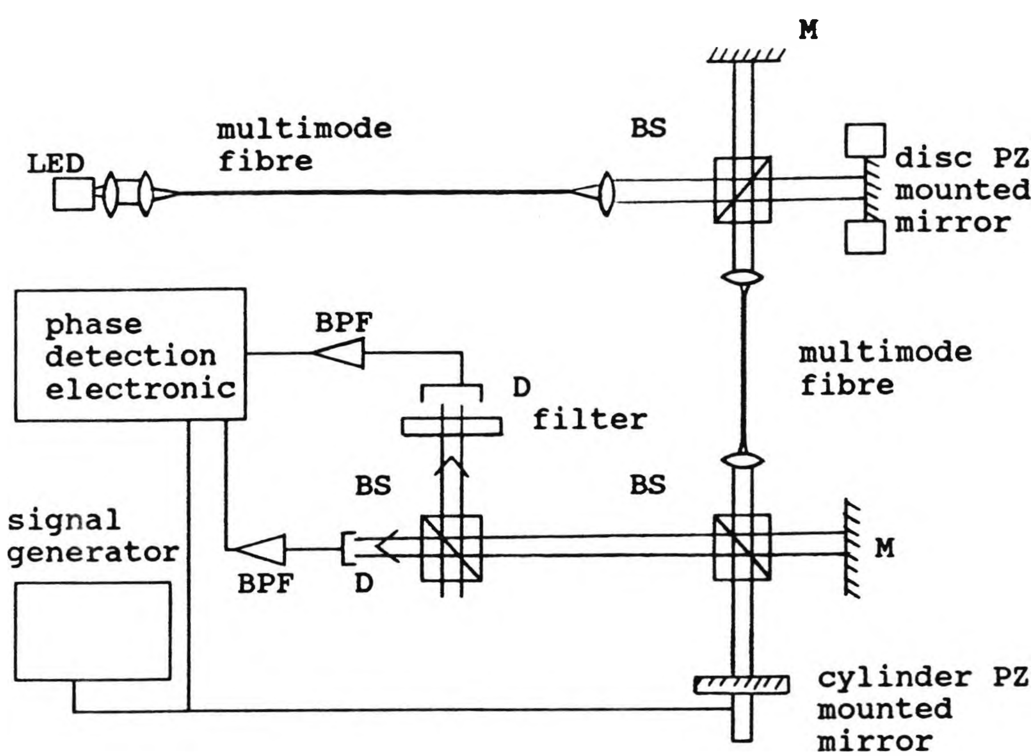

Figure 3.8. *Experimental arrangement using a coherence-tuned, Synthesised dual - wavelength technique (Ref. 24)*

Again, a number of variations of fibre-optic interferometric systems have been developed or proposed, such as a Mach-Zehnder and a Michelson coupled interferometer for temperature measurement [20], a Michelson and a Fabry-Perot coupled interferometer for remote displacement measurement [25], and the coupled dual Mach-Zehnder interferometer for Doppler-shift measurement [26].

Another important characteristic of interferometric systems using LED light sources is that they can be used with several remote interferometric sensors in communication system. This is the so called "coherence multiplexing" scheme. The first reported work on sensor multiplexing aspects of this scheme was by Al-Chalabi et al [26]. The basic principle of this scheme can be described as follows, when a low coherence light source is used to illuminate the sensing interferometers, which have different large "static" OPDs which are significantly greater than the coherence length, a reference interferometer may be used selectively to reconstruct the interference associated with a particular sensor element by appropriately tuning its OPD to match the "static" OPD of that particular sensor element. Based upon this simple principle, a number of schemes have been investigated and proposed. A detailed discussion of these schemes is given in other published work [27,28,29].

3.4.3. Systems with a comb-shaped spectrum light source

With the increase of the availability of the multimode laser diode, which was developed recently in commercial quantities for use with the compact disc (CD) player, the possibility of wide use of this high-output, multimode, low-coherence source with small emitting area in optical fibre interferometric systems becomes very significant. A number of research groups have reported both theoretical and the experimental results on work in this area [5, 14, 16, 30, 31]. From these reports, the detail characteristics of a multimode laser diode in a single interferometer [5] and a dual coupled interferometer [16] can be seen in both theoretical simulation and experimental analysis. For application aspects, several optical fibre interferometric systems were proposed, and the feasibilities of these proposals have been demonstrated in chapters 8 and 9.

By using a multifunction integrated optical circuit, a miniature laser vibrometer system was demonstrated by Suchoski et al [30]. In this system, as shown in Figure 3.9, a pigtailed 830 nm multimode laser diode is used as the light source. The sensing interferometer consisted of the fibre end and the surface of the vibrating body is a Fabry - Perot interferometer with a common - path fibre to deliver and receive the light. The reference interferometer, formed with a proton exchanged multifunction integrated optical circuit and a fibre delay line, is a Mach-Zehnder type, in which one of two arms is serrodyne modulated by a ramp current at the frequency of 5.35 MHz. Thus, a carrier frequency of 10.5 MHz, which is the second harmonic of the ramp frequency, can be achieved. Because the phase modulator is formed inside the reference interferometer, the light coupling problems that would otherwise be experienced are considerably minimized.

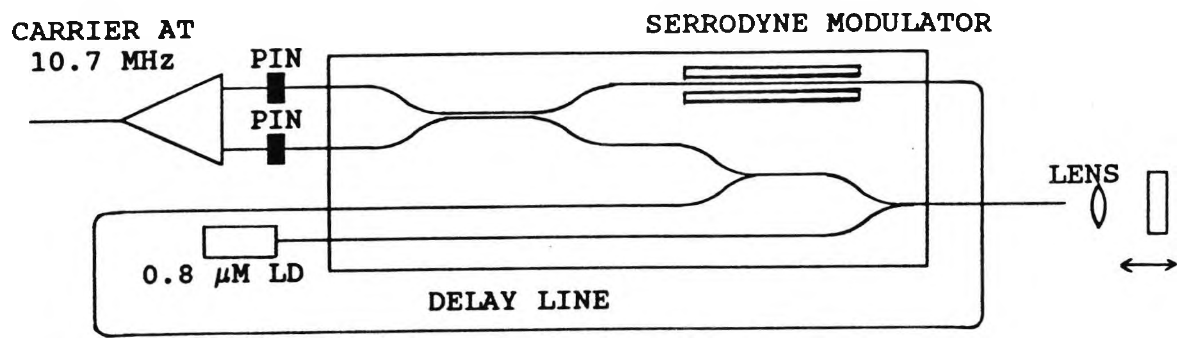

Figure 3.9. *The fibre-optic laser vibration sensor using a multifunction integrated optic circuit for signal processing and common-path interferometry to provide a phase insensitive fibre-optic probe (Ref. 30).*

3.5. Conclusions

Research and development of fibre-optic interferometric systems with different types of low coherence light sources have become a very active during recent years. As a branch of optical fibre interferometry, the interferometric systems using low coherence light sources are already seen to exhibit a number of advantages over conventional ones. First, it is possible to increase the unambiguous range of the interferometric system. Secondly, the systems are immunity to the perturbation of the transmission medium (either in free space or in an optic fibre link), i.e. the outputs of such systems are high insensitivity to loss variations in the fibre transmission link. Third, high resolution (1 nm) and dynamic range (10^5 to 10^6) can be achieved [16]. Finally, since the inexpensive low coherence light sources and multimode fibres used in the system are inexpensive, it is possible to employ such systems for a variety of measurands at relatively low cost.

References:

[1] D.A. Jackson " Monomode optical fibre interferometers for precision measurement ", J. Phys. E. 18, 981, 1985

[2] G, Beheim, K. Fritsch and N. Poorman "Fibre-linked interferometric pressure sensor", Rev. Sci. Instrum. 58(9), 1655-9, 1987

[3] T. Bosselmann "Multimode fibre coupled white-light interferometric position sensor", Optical Fibre Sensors, NATO ASI Series. Series E: Applied Sciences No. 132, 429-32, 1987

[4] C. Mariller and M. Lequime, "Fibre-linked white-light birefringent temperature sensor", Proc. Soc. Photo-Opt. Instrum. Eng. 798, 121-130, 1987

[5] Y.N. Ning, K.T.V. Grattan, B.T. Meggitt, and A.W. Palmer "characteristics of laser diodes for interferometric use", Appl. Opt. 28, 3657-61, 1989

[6] M. Born & E. Wolf, "Principle of Optics", Oxford University Press, pp360-7, 1980

[7] R. Kist "Source and detectors for fibre optic sensors" Optical Fibre Sensors NATO ASI series E: Applied Sciences No. 132, 267, 1987

[8] Proc. of: Workshop on single fibre sensor technology, University of Kent, Canterbury, p42, (unpublished).

[9] T. Bosselmann, and R. Ulrich,"High accuracy position-sensing with fibre coupled white light interferometers", Proc. 2nd Int. Conf. on Optical Fibre Sensors, Stuttgart (Berlin: VDE), pp. 361-4, 1984

[10] Kersten, R.Th.,"Einf hrung in die optische Nachrichten technik", Springer-Verlag Berlin, Heidelberg, New York, 1983

[11] A.S. Gerges, F. Farahi, T.P. Newson, J.D.C. Jones and D.A.Jackson "Fibre-optic interferometric sensors using a low coherence source: dynamic range enhancement", Int. J. of Opto electronics, 3, 311-22, 1988

[12] S.K.K. Norman, Y.L. Kam, and B.C. Nadav, " High power GaAlAs superluminescent diode for fibre sensor applications ", OFS'88, 1988 Technical digest series 2, PP.451, 1988

[13] S. Saito, Y. Yamamoto, "Direct observation of Lorentzian line shape of semiconductor laser and linewidth reduction with external grating feedback", Electron. Lett. 17, 325-327, 1981

[14] T. Okoshi, Kikuchi, A. Nakayama. " Novel Method for high resolution measurement of laser output spectrum", Electron. Lett. 16, 630-632, 1980

[15] C. Fabry and H. Buisson, Journ. de Phys. (5), 9 (1919), 1.

[16] Y.N. Ning, K.T.V. Grattan, B.T. Meggitt, and A.W. Palmer, " Characteristics of a multimode laser diode in a dual interferometer configuration ", IEEE / OSA J. Lightwave Technology, LT-12, 1773-8, 1990

[17] Y.N. Ning, K.T.V. Grattan, A.W. Palmer and B.T. Meggitt, "Coherence Length modulation of a multimode laser diode in a dual Michelson interferometer configuration", Applied Optics, 31, 1332-7, 1991

[18] Y.N. Ning, K.T.V. Grattan, A.W. Palmer and B.T. Meggitt "Characteristics of a multimode laser diode source in several types of dual-interferometer configurations", OE/Fibres, San Jose, AC, USA. Proc. SPIE 1367, 1991.

[19] C.Delisle and P. ielo, Can. J. Phys. 53, 1047, 1975

[20] C.Mariller, M. Lequime "Fibre-optic white-light Birefringent temperature sensor" SPIE 798, Fibre Optic Sensors II, pp.121, 1987

[21] K.Takada, K. Chida, J. Noda and S. Nakajima,"Trench depth measurement system for VLSI DRAM's capacitor cell using optical fibre and Michelson interferometer" IEEE J. Lightwave Technology, LT-5, pp. 881, 1987

[22] B.T. Meggitt, W.J.O. Boyle, K.T.V. Grattan, A.W. Palmer and Y.N. Ning, "Fibre optic Anemometry using an optical delay cavity

technique " Int. Conf. Fibre optics and opto-electronics, London, SPIE 1314, 321-9, 1990

[23] P.G. Cielo " Fibre optic hydrophone: improved strain configuration and environmental noise protection ", Appl. Opt. 18, pp. 2933, 1979

[24] D.J. Webb, J.D.C. Jones and D.A. Jackson, "Extended-range interferometry using a coherence-tuned, synthesised dual wavelength technique with multimode fibre link", Electron. Lett. 24, pp1173-5, 1988

[25] G. Behein, "Remote displacement measurement using a passive interferometer with a fibre-optic link", Appl. Opt. 24, pp.2335, 1985

[26] S.A. Al-Chalabi, B. Culshaw, D.E.N. Davies, "Partially coherence sources in interferometric sensors" Proc. First Int. Conf. Optical Fibre Sensors, pp. 132-135, 1983 7

[27] J.L. Brooks, R.H. Wentworth, R.C. Youngquist, M. Tur, B.Y. Kim, and H.J. Shaw "Coherence multiplexing of fibre-optic interferometric sensors", J. Lightwave Technology. LT-3, pp. 1062, 1985

[28] A.D. Kersey and A.D.Dandridge, "Phase noise reduction in coherence multiplexed interferometric fibre sensors", Electron. Lett., 22, pp. 616-618, 1986

[29] A.M. Yurek, A.B. Tveten, A.D. Dandridge and A.D. Kersey, "1.3 µm operation of a coherence multiplexed interferometric sensor", Springer Proc. in Phys., 44, Optical Fibre Sensors pp 179, 1989

[30] P. G. Suchoski, J.P. Waters and M. R. Fernald,"Miniature laser vibrometer system with multifunction integrated optic circuit", IEEE Photonics technology letters, 2, 81-2, 1990

[31] R Jones, M. Hazell and R. Welford " A generic sensing system based on short coherence interferometry" Int. Conf. Fibre optics and opto-electronics, London, April, 1990

Chapter 4

An all fibre vibration monitoring scheme based on the pseudo-quadrature recombination heterodyne scheme

Abstract:

An all fibre common-mode interferometer which allows the measurement of the movement (speed and distance) of a vibrating body is presented. An electronic signal processing scheme is used, and this is contrasted with the measurement of velocity through an optical processing technique, which is however, more complex and expensive to implement. The overall simplicity of the electronic technique, the low cost of components and the use of an all-fibre arrangement make this system easy implement where the limited information is required, and suitable for the monitoring purposes.

4.1. Introduction:

In this chapter, a new technique for measuring frequency and displacement of a vibrating object is presented. This scheme may be described as an "electronic pseudo-quadrature recombination" one and is an electronic analogue to an optical signal processing scheme. Both schemes are discussed in detail in this chapter. Although this novel electronic signal processing scheme gives less information than that of the optical signal processing scheme, extreme simplicity and obvious cheapness of this new scheme indicates that development for a different market is potentially desirable.

Section 4.2 of the chapter gives an analysis of the detected signal in an interferometer used to measure a vibration, and the following section (section 4.3) gives a summary of the various modulation schemes available for processing this type of signal. The electronic and optical quadrature recombination schemes are described in detail in the section 4.4.

The demodulation scheme used for the experimental work is detailed in the section 4.5, and the experimental arrangements and results for both electronic and optical quadrature recombination schemes are given in the section 4.6. This chapter is finished with a conclusion, section 4.7.

4.2.The analysis of the detected signal:

The schematic experimental arrangement for vibration measurement is shown on figure 4.1. The vibration characteristic of the moving object, for example,

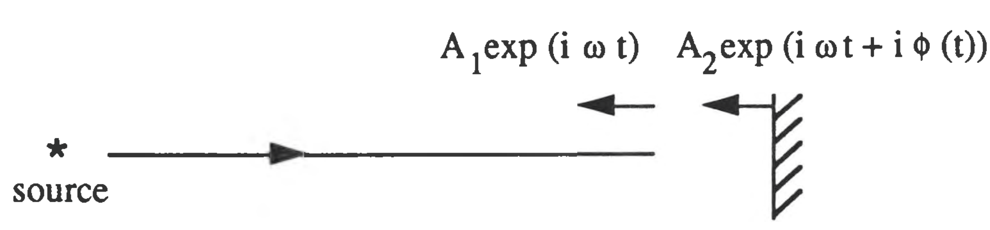

Figure 4.1 *Schematic reflections from the fibre end and vibrating body.*

the mirror in figure 4.1., is determined by analysis of the optical signal returned from the device illuminated. In order to simulate the output of the interferometer, it is assumed that there are no multireflections between the end of fibre and the moving mirror. This assumption is made based on the fact that the reflectivity of the end of the fibre is only 0.04. Light reflected from the fibre end interferes with that reflected from the moving mirror. The radiation electric field from the fibre end is given by

$$E_1 = A_1 \exp(i\omega t) \tag{4.1}$$

and from the vibrating object is given by

$$E_2 = A_2 \exp[i\omega t + i\phi(t)] \tag{4.2}$$

where A_1 and A_2 are amplitudes of electric fields. $\phi(t)$ is a phase difference, given by

$$\phi(t) = 2\pi n [L_o + L_s \sin(\omega_s t)]/\lambda \tag{4.3}$$

or

$$\phi(t) = \phi_o + \phi_s \sin(\omega_s t) \tag{4.4}$$

where L_o is twice the cavity length at zero displacement, L_s is twice the maximum magnitude of the displacement measured from either side of L_o, λ is the wavelength of the light source, and ω_s is the frequency of vibration. $\phi_o = 2\pi n L_o/\lambda$ is the static phase difference, and $\phi_s = 2\pi n L_s/\lambda$ is the amplitude of the phase change induced in the interferometer. These radiation fields enter the detector forming the output intensity I, given by

$$I = (E_1 + E_2)(E_1^* + E_2^*) \tag{4.5}$$

where E_1^* and E_2^* are the conjugate values of E_1 and E_2 respectively. For simplicity, if it is assumed that $A_1 = A_2$, the intensity can then be written as

$$I = k [1 + \cos(\phi(t))] \tag{4.6}$$

where k is a constant. Substituting equation 4.4 into 4.6, the output current of the photodiode may be written as the following equation:

$$I_d = \varepsilon \{1 + k \cos[\phi_o + \phi_s \sin(\omega_s t)]\} \tag{4.7}$$

where ε is a constant and

$$\cos[\phi_o + \phi_s \sin(\omega_s t)]$$
$$= \{ \cos\phi_o [J_o(\phi_s) + 2\Sigma J_{2n}(\phi_s) \cos(2n\omega_s t)]$$
$$- \sin\phi_o [2\Sigma J_{2n+1}(\phi_s) \sin((2n+1)\omega_s t)] \} \quad (4.8)$$

where J_n is the Bessel function of order n. The spectrum of I_d can be considered as one of a phase modulated signal with a zero carrier frequency. When the interferometer is operating at normal conditions, ϕ_o will fluctuate randomly in time due to the environmental effects such pressure and temperature changes, therefore, the amplitude of the Bessel components will fluctuate in the same way. This signal fluctuation problem is the so called "fading problem" and can be solved by different signal processing schemes such as the passive homodyne and quadrature recombination heterodyne schemes. In this work, only the first harmonic, $\sin(\omega_s t)$, is able to be measured, the rest of the high frequencies will be filtered out in the signal processing.

4.3. Summary of modulation schemes for the detection of a vibration

There are a number of techniques which can be used to recover the frequency and amplitude information from the detected signal which is described by equation 4.7. These techniques are usually classified into two groups: homodyne and heterodyne signal recovery schemes. A common feature of the homodyne signal recovery schemes (active homodyne and passive homodyne) is that the recovery signal is always centred about a zero carrier frequency, therefore, the directional information contained in the original signal is lost. In contrast, in the heterodyne signal recovery schemes, a high frequency carrier is introduced into the light beam, hence, the output signal from the photodiode is centred about this high frequency carrier. The directional information can be obtained by comparing the frequency of the detected signal with that of the carrier frequency, i.e., when the frequency of the detected signal is less than the carrier frequency, the object is moving away from the sensor, while the former is greater than the latter, the object is moving towards the sensor. A fundamental requirement of the heterodyne signal processing schemes is a high frequency carrier for the demodulation. The heterodyne schemes can be classified into three types: synthetic heterodyne, pseudo-heterodyne and quadrature recombination heterodyne. The classification depends upon the technique used to introduce the high frequency carrier. In this section, the principles of both homodyne and heterodyne signal recovery schemes are outlined briefly.

4.3.1. Active homodyne

In the scheme of the active homodyne, the interference is always maintained at its maximum sensitivity point (quadrature point), where the optical phase difference is $2\pi\,(2n+1)/2$. This maintenance may be achieved by two different methods. In the first method [1], a phase modulator is employed in the reference arm of the interferometer as part of the servo-feedback loop, by which the quadrature condition between the phases of the light in each arms of a interferometer is monitored and maintained. While in the second one [2], the quadrature condition is maintained by changing the laser driving current, and hence, the wavelength of the solid state laser. This wavelength variation allows the optical phase difference $\phi(t)$ to be used to maintain the quadrature condition. The modulating signal can be directly recovered from the feedback signal [3].

4.3.2. Passive homodyne

For the passive homodyne signal processing scheme [4], in addition to the normal detector output, $I_c = \varepsilon\,\{1 + k\cos[\phi_o + \phi_s\sin(\omega_s t)\,]\,\}$, a second quadrature output $I_s = \varepsilon\,\{1 + k\sin[\phi_o + \phi_s\sin(\omega_s t)\,]\,\}$ is required. The high frequencies of these two quadrature output signals can be then removed by filtering. The new signals are given by

$$I_{cf} = \varepsilon\, k\, \sin(\phi_o)\, J_1\,(\phi_s)\, \sin(\omega_s t) \qquad (4.9)$$

and

$$I_{sf} = \varepsilon\, k\, \cos(\phi_o)\, J_1\,(\phi_s)\, \sin(\omega_s t) \qquad (4.10)$$

these signals can be combined to produce an output signal I, which does not suffer from the fading problem, i.e.:

$$I = \sqrt{[\,(I_{cf})^2 + (I_{sf})^2\,]} = \varepsilon\, k\, J_1\,(\phi_s)\, \sin(\omega_s t) \qquad (4.11)$$

4.3.3. Synthetic heterodyne

In the synthetic heterodyne signal processing scheme [5], a phase modulator is employed in one arm of the interferometer to shift the frequency of light in this arm with respect to the frequency of light in another arm. The output signal, in which the carrier frequency and signal frequency are added together is capable of being demodulated by an ordinary phase demodulation technique such as a phase locked loop, or carrier phase tracing. The conventional Bragg cell may be used as a frequency or phase modulator device, but unfortunately, due to practical difficulties, it becomes inefficient to couple light from the fibre to and from the Bragg cell. Again, the size of the Bragg cell is too large to be compatible with the dimensions of the fibre. A considerable effort however has been made to develop new methods for producing a phase modulated carrier in an optical fibre [6, 7].

4.3.4. Pseudo - heterodyne

The pseudo-heterodyne scheme can be used in an unbalanced interferometer [8]. Instead of using a phase modulator, the phase carrier is induced by ramping the absolute frequency of the injected laser light, the optical output is then a moving fringe pattern which is created by a linear frequency increase of the laser light frequency. Although the optical output has a complex spectrum, composed of components at the fundamental and harmonics of the ramping frequency, it is possible to concentrate most of the power in the Nth harmonic of the ramp frequency by adjusting the ramp rate in such a way that the optical output fringe pattern is driven over N full fringes during each ramp period [9]. By employing a bandpass filter around the Nth harmonic of the ramp frequency, a strong frequency carrier is generated. This carrier, after being filtered, is free from the distortion caused by the high harmonics associated with the ramp fly-back. When the interferometer output is limited over one complete fringe per cycle, most optical light power will be concentred in the first harmonic, which gives out a frequency carrier at the ramp frequency.

4.3.5. Quadrature recombination heterodyne

Another signal processing scheme is that of quadrature recombination [10], which requires two optical quadrature outputs from two optical quadrature channels in an interferometer. These optical outputs are received by two photodiodes respectively and then multiplied by the quadrature components of a high frequency electronic carrier. Then two products are linearly combined to produce a phase modulated signal with the high frequency carrier [11, 12].

In this work, another approach was carried out to process the output signal from a common-mode optical fibre Fabry-Perot interferometer. This may be described as a pseudo-quadrature recombination scheme, which may be considered as an electronic equivalent to the optical quadrature recombination scheme. The details of this scheme is described in the next section.

4.4. Theoretical considerations of the two quadrature recombination schemes

In the pseudo-quadrature recombination scheme, instead of using two photodiodes to obtain the signals from two optical quadrature channels, the "quadrature signals" are generated with a wide-band 90^o phase shifter [13] from only one optical channel, i. e., when an optical output signal form an interferometer is received and converted into an electronic signal by a photodiode, the electronic signal is then shifted by 90^o in phase through using a wide-band 90^o phase shifter, forming another quadrature signal. Those two signals are then multiplied by the quadrature components of a high frequency electronic carrier. Then two products are linearly combined to produce a phase modulated signal with the high frequency carrier. Unfortunately, the direction information, which is in the form of the phase relationship between true quadrature signals, cannot be obtained by this method. This can be seen in the following theoretical explanations:

According to equation 4.4, if ϕ_o is fixed, the sign of $\phi(t)$ may be positive or negative as the time, t, increases, thus

(i) For the true quadrature signals generated by using the quadrature recombination scheme:

when $\phi(t) > 0$,

$$\sin[\,\phi(t)\,] = \sin|\,\phi(t)\,| \text{ and } \cos[\,\phi(t)\,] = \cos|\,\phi(t)\,| \qquad (4.12)$$

$\phi(t)<0$,

$$\sin[\ \phi(t)\ ] = -\sin|\ \phi(t)\ |$$

$$\text{and} \quad \cos[\ \phi(t)\ ] = \cos|\ \phi(t)\ | \tag{4.13}$$

Therefore, for true quadrature signals, according to equations 4.12. and 4.13., the sign of cos[$\phi(t)$] is always positive, and the sign of sin[$\phi(t)$] changes in the same way as $\phi(t)$ does. Thus after being processed using a quadrature recombination scheme mentioned in the section 4.3.5, these two quadrature output signals, give out a true phase modulated signal with a carrier frequency of ω_c, and this can be written as

$$\sin[\ \pm|\phi(t)|\ ]\cos(\omega_c t) + \cos[\ \pm|\phi(t)|\ ]\sin(\omega_c t)$$

$$= \sin[\ \omega_c t \pm |\phi(t)|\ ] \tag{4.14}$$

(ii) for the pseudo quadrature signals:

A pair of "quadrature" signals is generated electronically by shifting the phase of the original signal by 90^o. When $\phi(t)>0$,

$$\sin[\ \phi(t)\ ] = \sin|\phi(t)|$$

$$\text{and} \quad \cos[\ \phi(t)\ ] = \cos|\phi(t)| \tag{4.15}$$

but when $\phi(t)<0$,

$$\sin[\ \phi(t)\ ] = -\sin|\phi(t)| \tag{4.16}$$

The phase shifter cannot tell the difference between $|\phi(t)|$ and $-|\phi(t)|$, (therefore, $\sin|\phi(t)|$ and $-\sin|\phi(t)|$) and only shifts them by 90^o in phase. The electronic output signal, $-|\phi(t)|$, after being phase shifted by 90^o will become:

$$-\sin|\phi(t) + 90^o| = -\cos|\phi(t)| \tag{4.17}$$

Note the difference between signs of the cosine terms in equations 4.13 and 4.17. It is this difference that causes the different results between the true and pseudo- quadrature recombination schemes.

By using the quadrature recombination processing scheme, i.e., after inducing a carrier the frequency ω_c, and the two products being linearly combined, the output signal in the pseudo- quadrature recombination scheme is then given by

$$\pm\sin|\phi(t)|\cos(\omega_c t) \pm \cos|\phi(t)|\sin(\omega_c t)$$
$$= \pm\sin[\,\omega_c t + |\phi(t)|\,] \qquad (4.18)$$

By comparing equation 4.14. and 4.18., it can be seen that the former gives out a true frequency modulation signal, while latter gives out only a signal modulated by the absolute value of the detected signal. This means that the direction of the movement cannot be determined by the pseudo-quadrature recombination scheme. Therefore, when a phase-locked loop is used to demodulate these signals, the former can give the velocity of the vibrating mirror, while the latter only gives the speed of the vibration. However, from the results given in Equation 4.18., it can be seen that the information on frequency and amplitude can be obtained through this scheme. Another difference between the ture- and pseudo- quadrature recombination schemes is that, in the former, the fading problem is solved, whilst in the later, the fading problem still remain due to the presence of the static phase difference.

4.5. Demodulation scheme

Employing a phase-locked loop (PLL) to demodulate a phase modulated signal is one of the most common methods used in signal processing. The basic construction of a phase-locked loop is shown in figure 4.2. There are three main parts in a phase-locked loop, i.e., a voltage controlled oscillator (V.C.O.), a phase detector and a low pass filter with an amplifier.

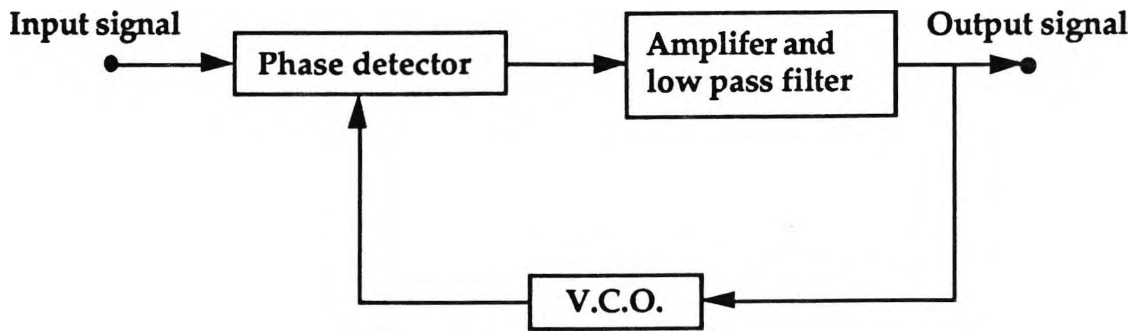

Figure 4.2. *Basic construction of a phase-locked loop.*

The function of the V.C.O. is to generate a reference frequency which is set at the phase carrier frequency by an external resistor-capacitor network and is controlled by a control voltage from a low pass filter. The V.C.O. output frequency is fed to the phase detector where it is compared to the phase of the incoming signal. After comparing the phase angle of these signals, the phase detector gives out an error voltage which is an average voltage proportional to the difference in phase angle between the input frequency and the V.C.O. frequency. The error voltage is then filtered and amplified by the low pass filter. Finally, the output of the low pass filter is fed back to the V.C.O., thus completing the loop.

When the phase-locked loop is working in the capture range, the V.C.O. will change its frequency to reduce the phase difference between the two signals. If the phase difference is reduced to zero, i.e. the two frequencies are the same, the loop is said to be "phase-locked". In this condition, the output signal from the PLL is linearly related to the frequency of the input signal. Therefore, when the frequency of the input signal changes, the error voltage from the phase detector will change which will cause the V.C.O. frequency to follow, or track the input frequency. Then the output from the low pass filter which is connected with the V.C.O. will be a demodulated signal.

4.6. Experimental arrangement and results

4.6.1. The pseudo quadrature recombination

A schematic configuration of the experimental arrangement is shown in figure 4.3., The arrangement can be divided into two physical parts: the optical part and the electronic processing part. The former is used to deliver light from the light source to the vibrating mirror and receive the reflected light from the mirror. The later is used to process the electronic signal generated from the detector by means of the pseudo quadrature recombination scheme with a phase locked loop demodulation.

As shown in figure 4.3., a light beam from a HeNe laser (single mode, 4 mW) is launched into one of a four-port optical fibre coupler through a objective lens (X 40). The light beam inside the fibre is split into two beams with one of them being damped by the index matching oil and another becoming the sensing beam. The light reflected from the fibre end interferes with the one reflected from the moving mirror at the detector. The detector (BPX65) converts the optical intensity into an electronic signal. Figure 4.4

shows a typical electronic signal generated by a vibrating mirror, which responds to equation 4.7. The detected signals is then amplified in the detector electronic circuit, which is shown in figure 4.5. The two stage amplifier has a gain of 100 times.

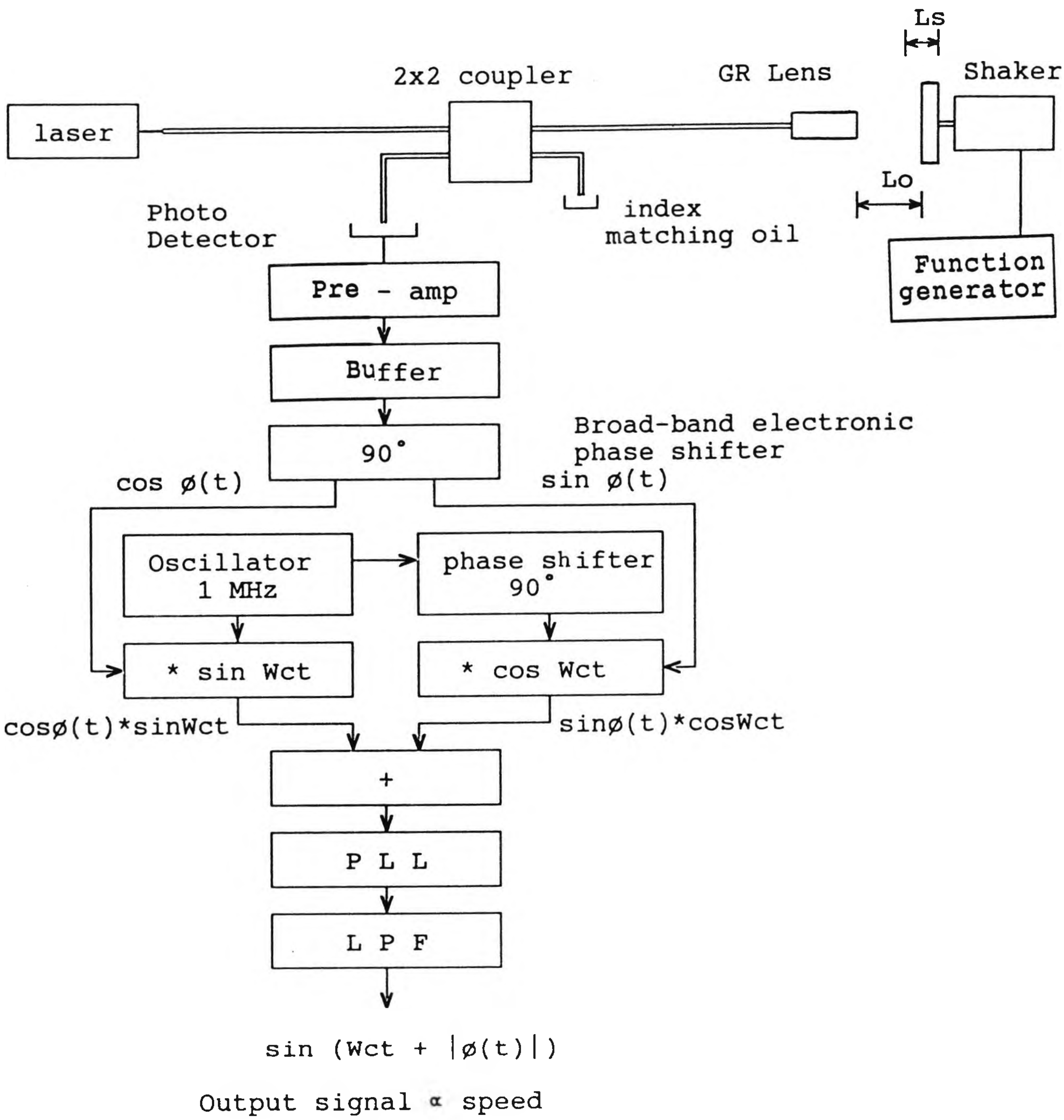

Figure 4.3 *Schematic pseudo-quadrature recombination scheme.*

+	*Adder*
PLL	*Phase Locked Loop*
LPF	*Low Pass Filter.*

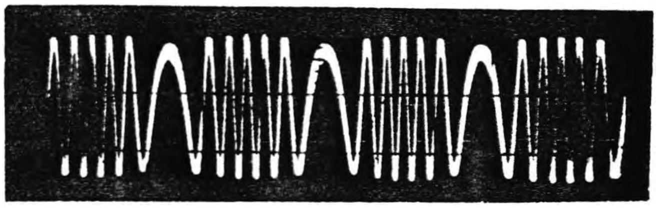

Figure 4.4. *A typical electronic output signal generated by a vibration body.*

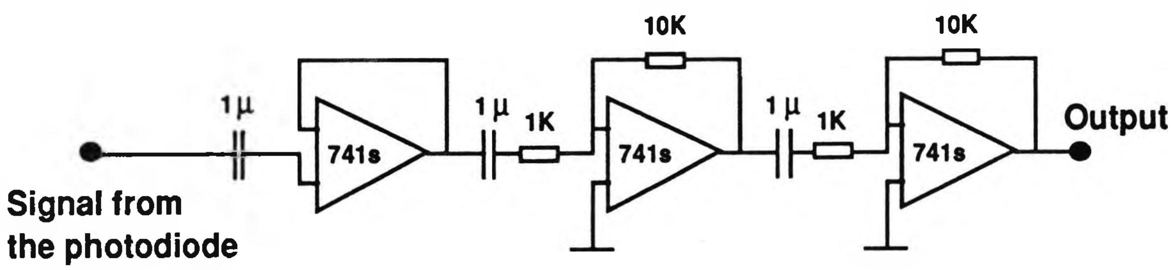

Figure 4.5. *The Pre-amplify circuit for the detected signal.*

This detected signal is then fed into the wide-band 90^0 phase shifter to form a pair of pseudo quadrature signals, which are represented mathematically by equations from 4.15. to 4.17., and are shown in figure 4.6.

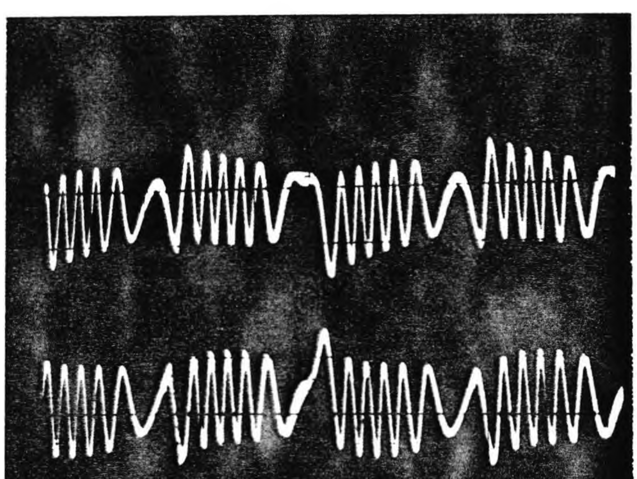

Figure 4.6. *A pair of pseudo quadrature signals*

Figure 4.7. shows the Lissajous figure obtained by applying these pseudo quadrature signals to the X and the Y plates of the oscilloscope. The thickness of the circle indicates that the process of the phase shifting will induce a amplitude modulation in these quadrature signals. The bandwidth of the phase shifter is in the range from 10Hz to 23 kHz with a error less than 2^0 (as shown in figure 4.8.). The electronic circuit of the 90^0 phase shifter is shown in figure 4.9. The op-amp used in the shifter is type TL062 with a unity-gain bandwidth of 1 MHz.

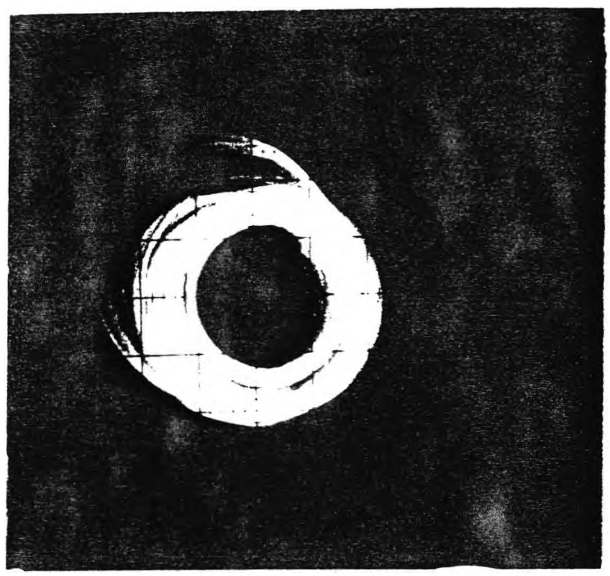

Figure 4.7. *The Lissajous figure obtained by applying the pseudo quadrature signal to the X and Y plates of a oscilloscope.*

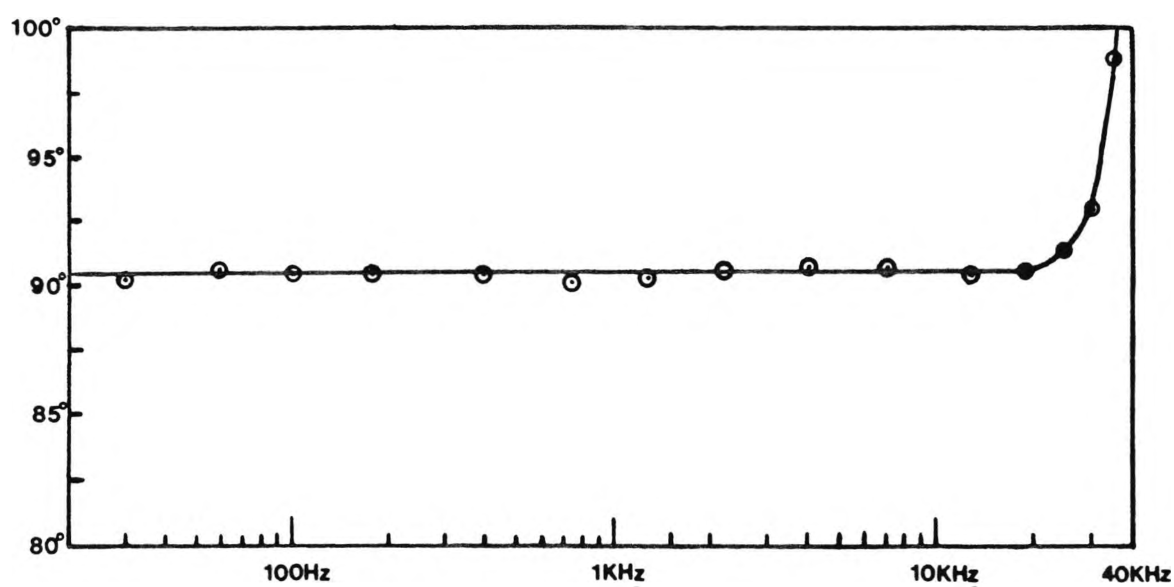

Figure 4.8. *The Band-width of the phase shifter varied from 10 Hz to 23 kHz with a error being less than 2^0*

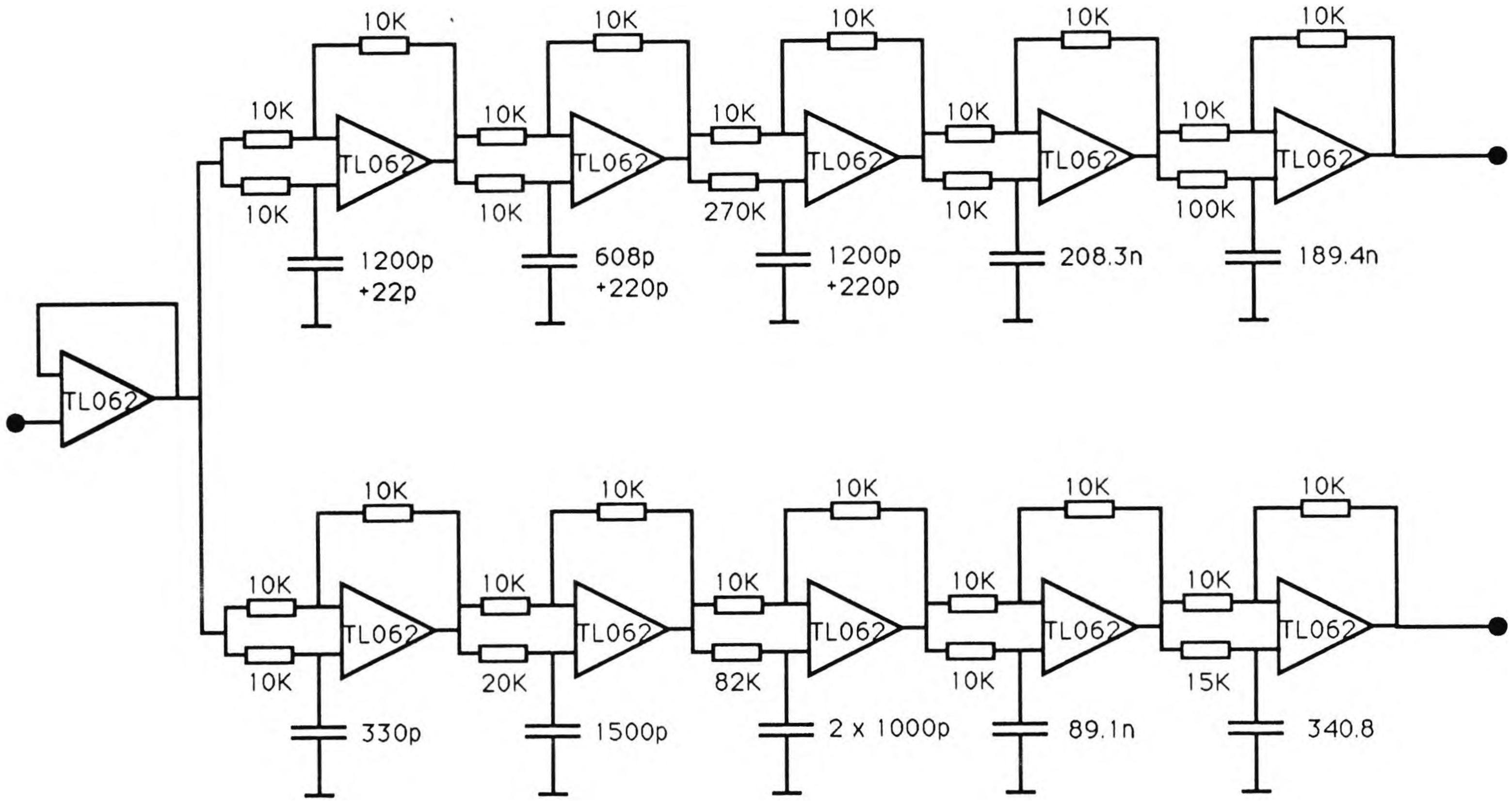

Figure 4.9. *The electronic circuit of the 90° phase shifter.*

The pseudo quadrature signals are then multiplied with $\sin(\omega_c t)$ and $\cos(\omega_c t)$ respectively, (shown in figure 4.10.), the later being generated by a 1 MHz oscillator and a 90^0 phase shifter at the frequency of 1 MHz respectively. The electronic circuit of the oscillator and the 90^0 phase shifter is shown in figure 4.11. The products (shown in figure 4.12.) are added together forming a signal modulated by the absolute value of the signal $\phi(t)$, which corresponds to equation 4.18. The electronic circuit of the amplifiers and the adder are shown in figures 4.13 and 4.14 respectively. The multipliers used in the arrangement are type MC1495l with a 3.0 dB bandwidth of 3 MHz. The op-amps used to build the oscillator and the phase shifter are type 741S.

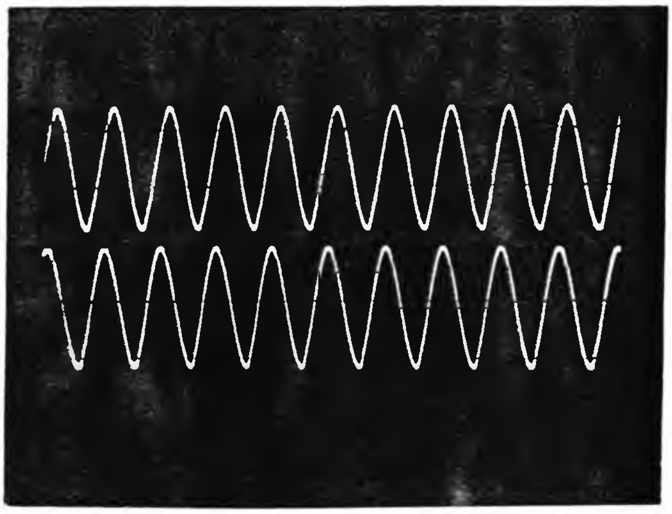

Figure 4.10. *The quadrature high frequency carrier signals.*

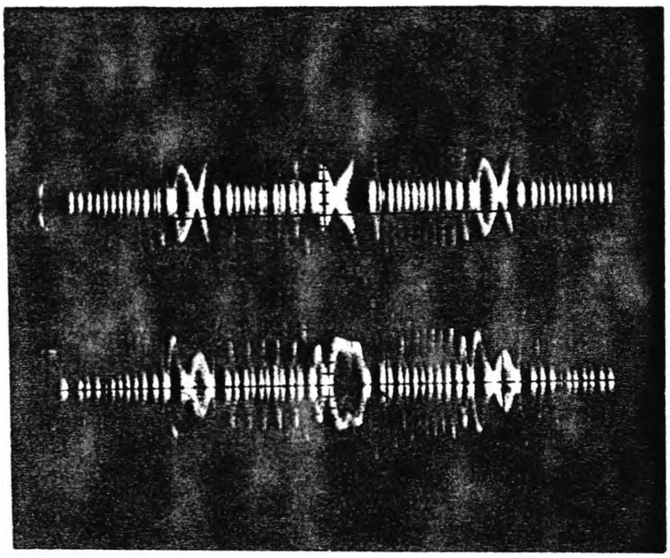

Figure 4.12 *The products of the high frequency carrier signals with the pseudo quadrature signals.*

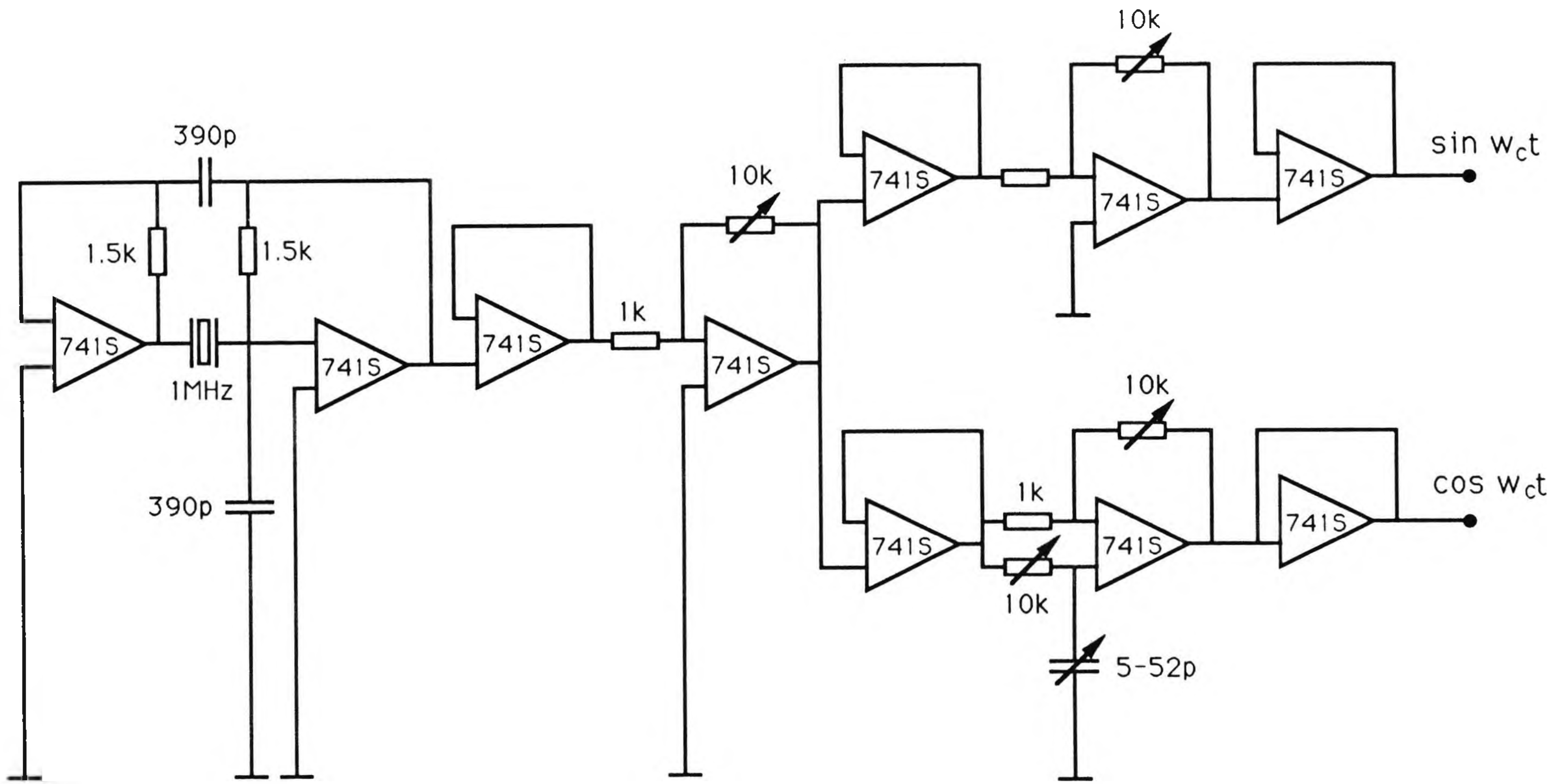

Figure 4.11. *The electronic circuit of a 1 MHz oscillator and a 90^o phase shifter at the frequency of 1MHz.*

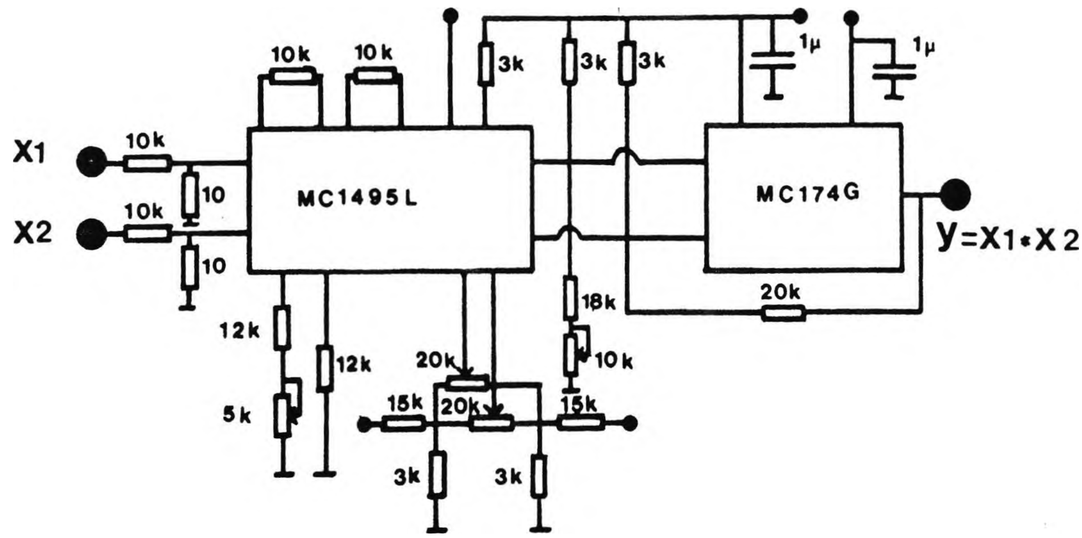

Figure 4.13. *The electronic circuit of the multiplier.*

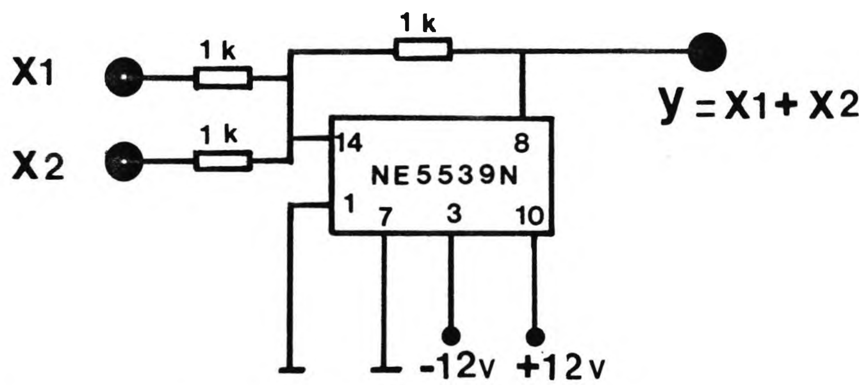

Figure 4.14. *The electronic circuit of the adder*

Finally, the phase-locked loop is used to demodulated this pseudo quadrature recombination signal. Because the directions of motion are not detected, the movement of the vibrating mirror at two opposite directions are treated equally in this arrangement. Therefore, the output frequency from the phase locked loop is twice of the vibration frequency. Since the amplitude of the output from the phase locked loop is proportional to the frequency difference between the input detected signal and one generated in the V.C.O., the vibration speed is proportional to the amplitude of the output signal of the phase locked loop. By integrating this output signal the amplitude of the vibration may be obtained. This means that apart from the direction of the motion, the fundamental frequency and the amplitude of vibration may be determined by the pseudo quadrature recombination scheme. The comparison between the input signal (the signal used to drive the mirror vibrating) and the output signal from the phase locked loop is shown in figure 4.15.a,b. It can be seen that the frequency of the output signal is twice of the input vibration frequency, and the value of the output signal is proportional to the vibration speed. The electronic circuit of the phase locked loop is shown in Figure 4.16. The phase locked loop chip used is NE564, with a locked range and a capture range being about 70% of f_0 and 30% of f_0 respectively, where f_0 is the central frequency of V.C.O. In this experiment, the central frequency of V.C.O. was set at 1150.928 kHz, the capture range was 632.045 kHz (from 851.079 to 1483.124 kHz). Figure 4.17. shows the experimental results of the variation of the demodulated output voltage as a function of the output frequency of the V.C.O..

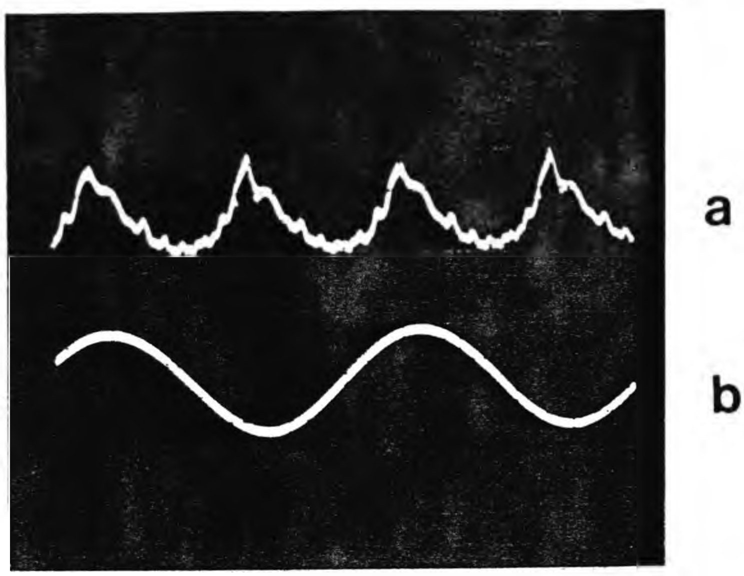

Figure 4.15. *a: Output signal from the phase locked loop in the pseudo quadrature recombination scheme.*
b: Input signal used to drive the mirror vibrating.

4.6.2. The true quadrature recombination scheme

In order to compare the results between the pseudo and the true quadrature recombination schemes, a optical arrangement was built to produce a pair of true quadrature signals. Figure 4.18 shows the schematic configuration of the experimental arrangement. The polarisations of the light beams at different positions are shown in figure 4.18. The 90^o phase difference between the two beams with two polarisations is introduced by a quarter wavelength plate. The polariser 1 and polariser 2, shown in figure 4.18., are used to select the light beam with different polarisations. The quadrature signals are then converted into electronic signals by two detectors respectively. These detected signals are shown in figure 4.19. Figure 4.20. shows the Lissajous figure obtained by applying these quadrature signals to the X and the Y plates of the oscilloscope. In contrast

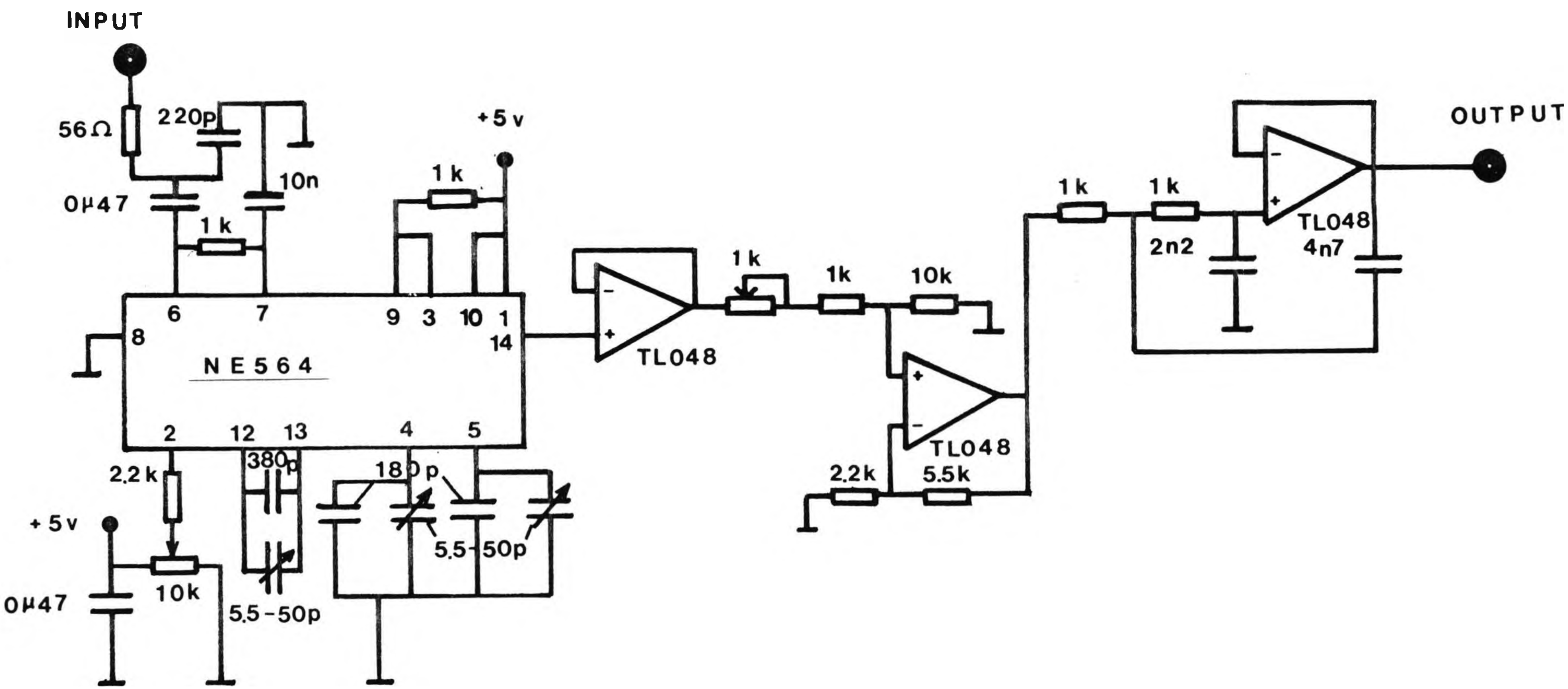

Figure 4.16. *The electronic circuit of the phase locked loop.*

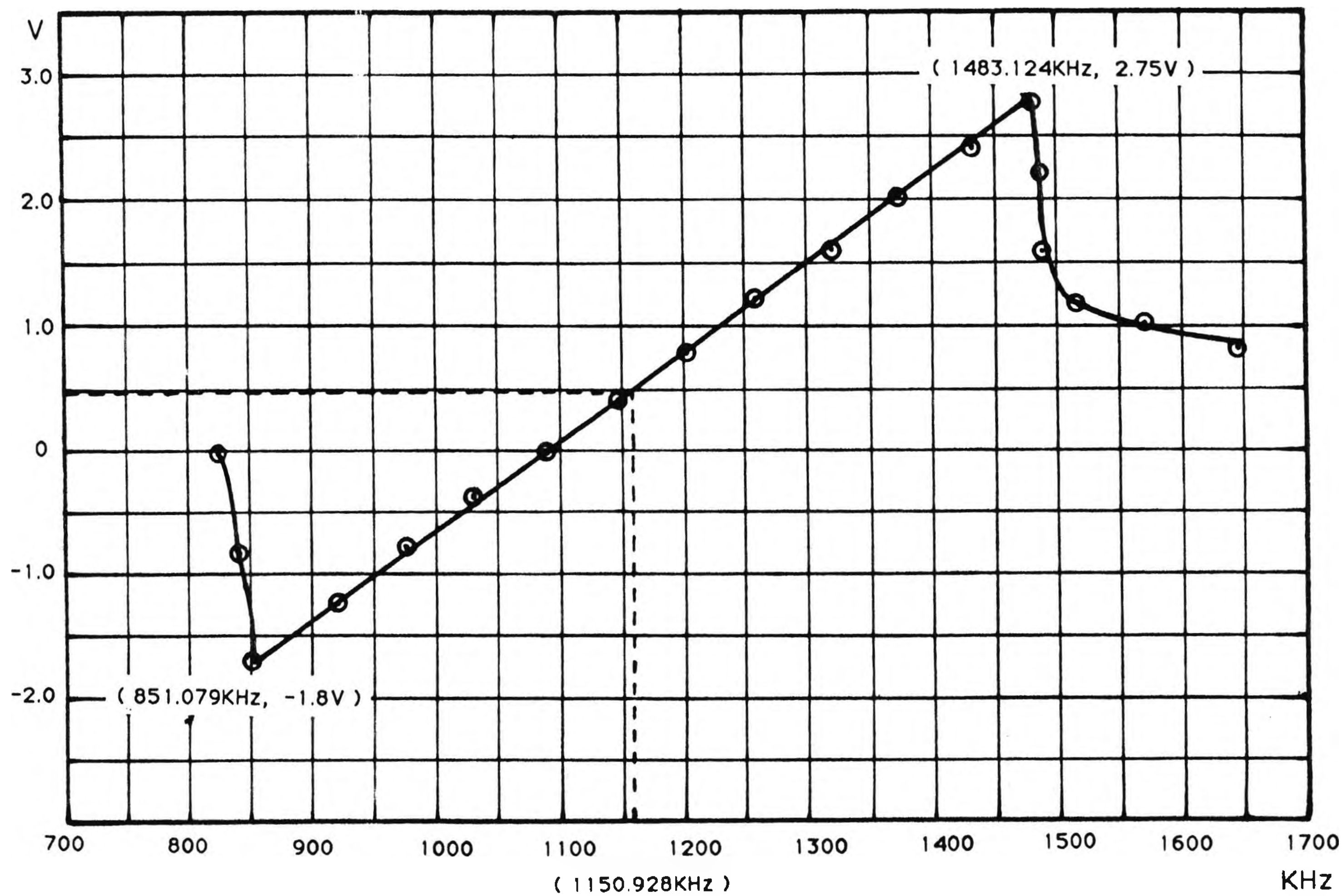

Figure 4.17. *Experimental results of the demodulated output voltage v the VCO output frequency.*

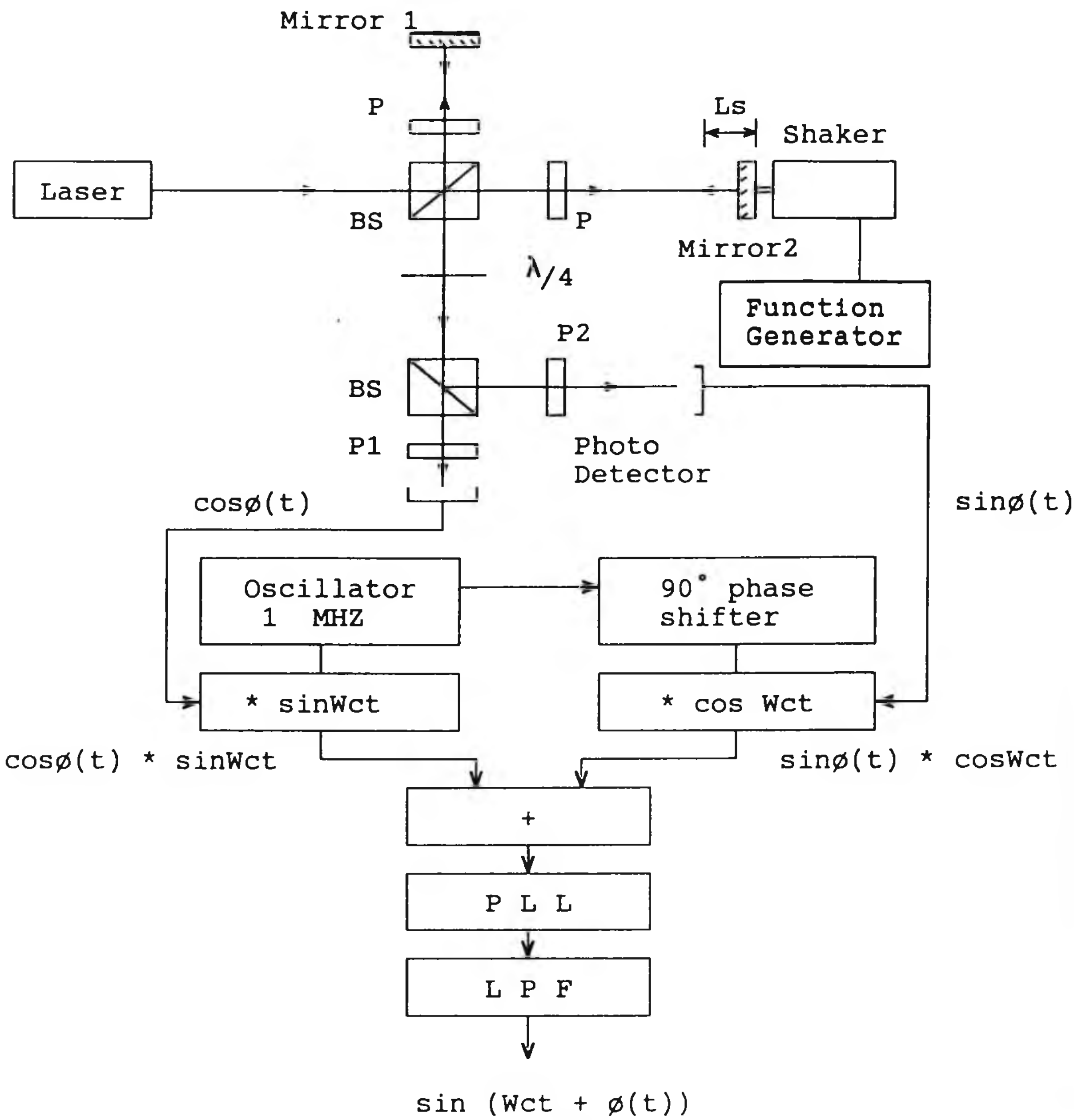

Figure 4.18. *Schematic configuration of the true quadrature recombination scheme.*

P:	*Polariser*
BS:	*Beam Splitter*
λ/4:	*Quarter wave plate*
+:	*Adder*
PLL:	*Phase Locked Loop*
LPF:	*Low Pass Filter.*

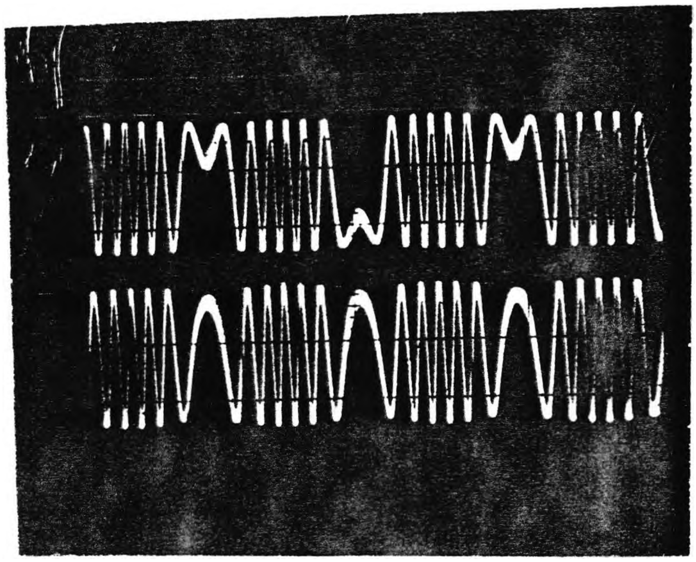

Figure 4.19. *A pair of true quadrature signals.*

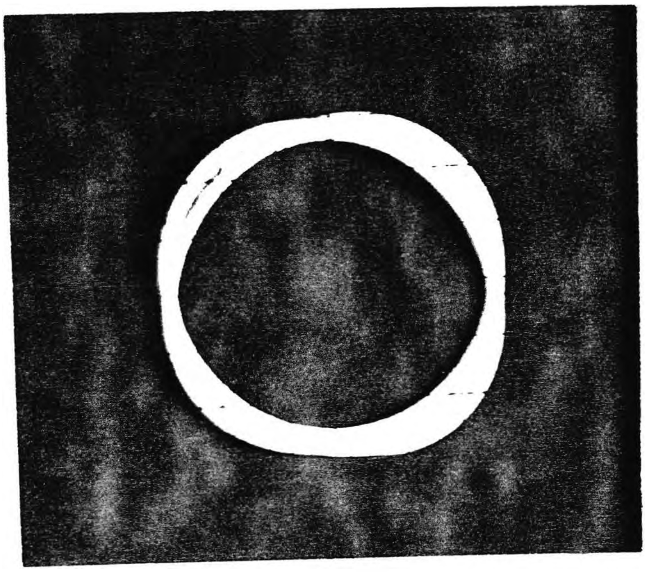

Figure 4.20. *The Lissajous figure obtained by applying the true quadrature signal to the X and Y plates of a oscilloscope.*

to the previous electronic scheme, the figure shown on the oscilloscope are truly circular instead of a tracing of oscillation shown in figure 4.7. As shown in figure 4.18., a oscillator and a 90^0 phase shifter are used to induce the quadrature carrier signals with a frequency at 1 MHz (figure 4.10.). The products of the detected quadrature signals with the quadrature carrier signals are shown in figure 4.21. The combination of these products is given by equation 4.14.. The output signal from the phase locked loop (figure 4.22a.) shows that the frequency, amplitude and direction of a vibration are recovered through the true quadrature recombination scheme. This result may be compared to the result of the pseudo quadrature recombination scheme where direction has been lost, as shown in figure 4.15.

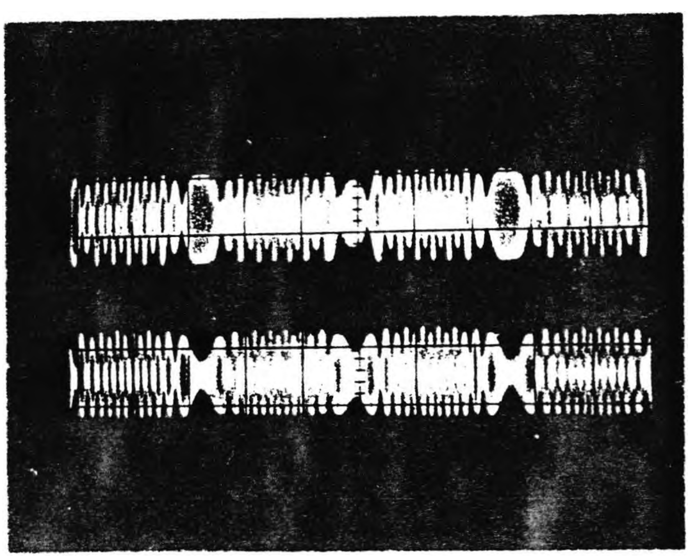

Figure 4.21. *Products of a pair of true quadrature signals with a pair of quadrature high frequency carrier signals.*

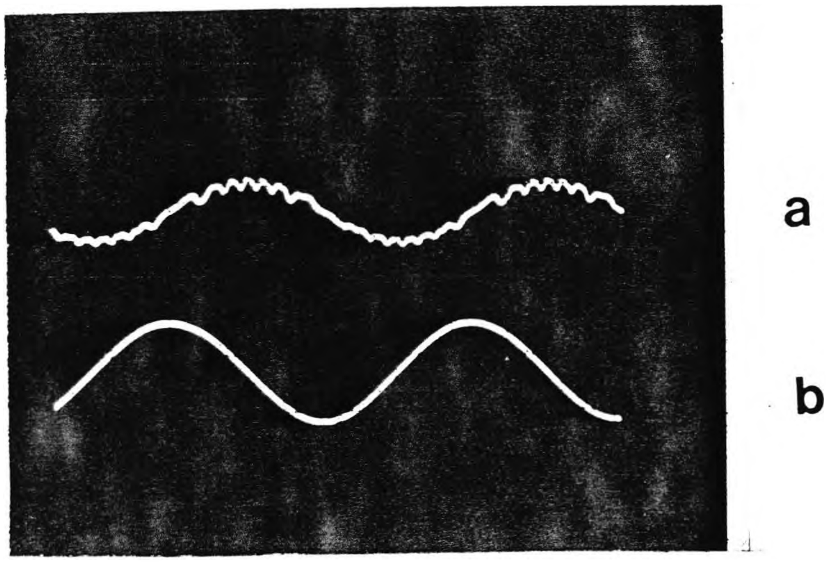

Figure 4.22. *a: Output signal from the phase locked loop in the true quadrature recombination scheme.*
b: Input signal used to drive the mirror vibrating.

4.7. Conclusion

By comparing the configurations and the results of the pseudo and true quadrature recombination schemes, the following conclusions can be drawn:

(1). As the pseudo quadrature signals do not have the phase information which can be used to determine the direction of the moving body, the pseudo quadrature recombination scheme can only be used to measure the speed of a vibrating body instead of the velocity. The latter can be measured by the true quadrature recombination scheme.

(2). The pseudo quadrature recombination scheme shows extreme simplicity in the configuration by virtue of the all fibre interferometer and direct electronic processing, comparing to the true quadrature recombination scheme.

(3). The work reported here only demonstrates the results of two type quadrature recombination schemes in principle, rather than a detailed study of the range of velocity/speed which can be measured.

References:

[1] D.A. Jackson, R. Priest, A. Dandrige and A.B. Tveter, "Elimination of drift in a single-mode optical fibre interferometer using a piezoelectrically stretched coiled fibre" Appl. Opt., pp2926-9, 1980

[2] A. Dandrige and A.B. Tveter, "Phase compensation in interferometric fibre optic sensors " Opt. Lett. 7, pp279, 1982.

[3] D.A. Jackson "Monomode fibre optic interferometers for precision measurement" J. Phys. E. .18, pp981, 1985.

[4] S.K. Sheem, T.G. Giallorenzi and K.P., Koo "Optical techniques to solve the fading problem in fibre interferometers" Appl. Opt., 21, pp689, 1982.

[5] J.H. Cole, B.A. Danver and J.A. Bucaro, "Synthetic heterodyne interferometric demodulation" IEEE J. Quantum Electron QE-18, pp694-7, 1982.

[6] B. Culshaw, P.R. Ball, A.A. Sadler, J.C. Pond, "Data collection using optical fibres " Electronics and Power 27, pp148, 1981.

[7] C.D. Butter, G.P. Hocker, "Fibre optical strain gauge" Appl. Opt., 17, pp2867 1978.

[8] A.D. Jackson, A.D. Kersey, M. Corke and J.D.C. Jones "Pseudo-heterodyne detection scheme for optical interferometers" Electron. Lett. 18, pp1081-3, 1982.

[9] A.D. Kersey, M. Corke, J.D.C. Jones, A.D. Jackson "Signal recovery techniques for unbalanced fibre interferometric sensors illuminated by laser diodes" The first international Conf. on Optical fibre sensors, pp43, 1983.

[10] A.D. Kersey, M. Corke and D.A. Jackson "Linearised polarimetric optical sensor using a heterodyne-type signal recovery scheme" Electron. Lett. 20, pp209-11, 1984.

[11] Y.N. Ning, B.T. Meggitt, K.T.V. Grattan, A.W. Palmer, "An all fibre low cost 'rangefinder' for small vibration measurements" OE/LASE 89, Society of photo-optical Instrumentation Engineers proceedings, SPIE. 1043, pp284-290, 1989.

[12] Y.N. Ning, K.T.V. Grattan, A.W. Palmer and B.T. Meggitt, "A novel detection scheme for vibration monitoring using optical techniques" Optics and Laser in Engineering, 15, 115-126, 1991.

[13] C.J. Gibbins, Suningdale and Berkshire, Wireless World, august 48, 1980.

Chapter 5

An investigation of the characteristics of laser diodes for interferometric sensor use

Abstract:

Multimode laser diodes may be used as one of the low coherence light sources in such applications that the measurement range of interferometric fibre optic sensors needs to be extended. In order to determine the operational characteristics of these devices, the characteristics of two commercial multimode laser diodes were investigated. Reasonable trends in the comparison between the theoretical and experimental results were seen. Both results show that the spectral envelope of a multimode laser diode determines the profile of the each interference region, and the fine spectral structures within this envelope modifies the spatial periodic distribution of the interference regions and their peak values. This is the consequence of one being the Fourier transform of the other. As a result, the measurement volume of this type of interferometric system will be limited to inside the interference region of the interferometer and may be defined by determining the order of the interference region.

5.1. Introduction:

One of the most commonly used light source in an interferometer is the single mode , high coherence laser device, for example the He-Ne laser. The two fundamental problems associated with a single mode laser light sourced interferometer is the short unambiguous operating range which is limited by the periodic nature of the optical transfer function [1, 2], and the lack of identification of the order of interference when the interferometer is switched on. By contrast, the use of low coherence length light source such as the LED [3] or even a white lamp [4] in the interferometer can help to overcome some of these problems.

One of the drawbacks, for practical applications of an LED, is its large emitting area, and thus light is not easily coupled into an optical fibre. However, the availability of the multimode laser diode, developed recently in commercial quantities for use with the compact disc player, open up the possibility of the wider use of this high output, multimode, low coherence source with a small emitting area, in this application. High light output levels may be achieved as the diode is operating in its normal lasing mode, typically 3 to 5 mW.

In this chapter, the coherence properties of two multimode laser diode light sources are presented. Both are GaAlAs index guided laser diodes. Because they are inexpensive and in volume production, the potential of employing these devices in the optical fibre sensing system is very high.

5.2. Experimental arrangement:

The optical configuration employed to investigate the characteristics of these laser diodes in an interferometer is shown in figure 5.1. This represents a basic Michelson interferometer with the imbalance in one arm provided by an oscillator-driven vibrator attached to mirror M_2, operating at a known frequency of 200 Hz. The micrometer shown in figure 5.1 was adjusted to allow the mirror M_1 to scan along the optic axis of the system in this dynamic case study. The pattern of the familiar Doppler-shifted interference fringes produced in such an interferometer when the optical path difference $2\Delta L'$ (twice the mirror scan distance) between the two interferometric arms in the Michelson interferometer arrangement is within the coherence ranges of the light source, is shown by figure 5.2. The peak-to-peak value of this detected signal against the change of the micrometer was recorded. The photodiode and the detector amplifier circuit used in this arrangement are the same as those used in the experiment mentioned in the chapter 4.

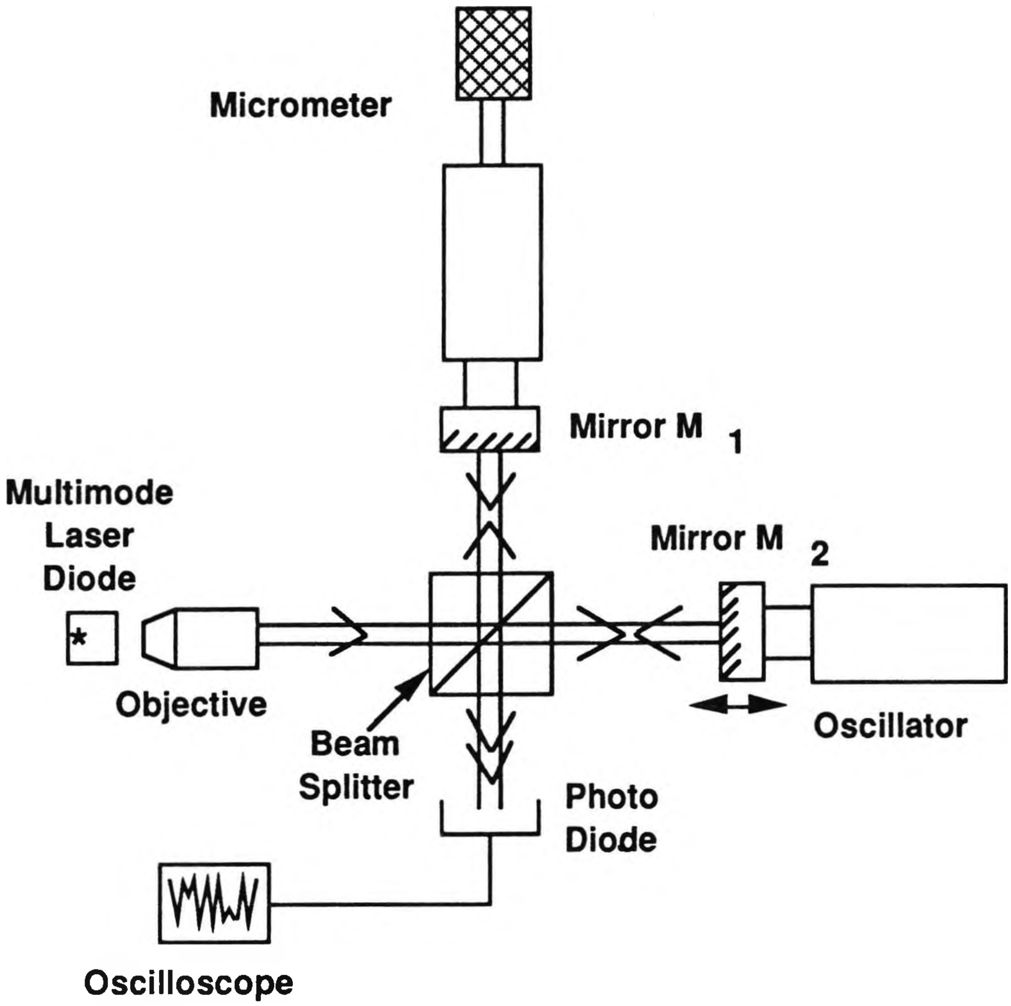

Figure 5.1. *Schematic arrangement of a Michelson interferometer.*

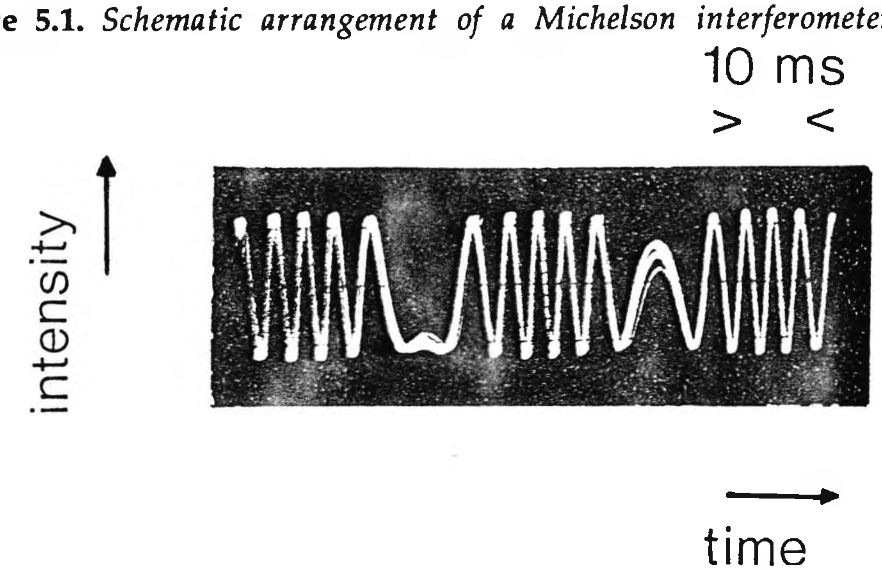

Figure 5.2. *Interference signal recorded on the photodiode in the interferometer.*

5.3. The theoretical analysis:

5.3.1. The theoretical model of a multimode laser diode:

In order to analyse the characteristics of a multimode laser diode, a theoretical model is established based on following assumption: the spectral envelope of the multimode laser diode is a Gaussian distribution and the spectral shape of a single lasing mode may be considered to be a Lorentzian one [7, 8] where the normalised signal intensity is $S_j(\sigma)$ and, with the wave number $\sigma_j = 1/\lambda_j$, this may be written as [9]

$$S_j(\sigma) = \frac{2\delta'\sigma/c}{(\delta'\sigma)^2 + 4(\sigma-\sigma_j)^2} \tag{5.1}$$

The total radiation electric field E for all the modes is then described as

$$E = \sum_{j=-m}^{+m} \int_{-\infty}^{+\infty} \sqrt{S_j(\sigma)}\, \exp\left[-\pi\left(j\frac{\Delta\sigma}{\delta\sigma}\right)^2 + i\omega t\right] d\sigma \tag{5.2}$$

where m is the order of the lasing modes,
$\Delta\sigma$ is the difference between adjacent model wave numbers,
$\delta\sigma$ is the envelope full width of all modes,
σ is the wave number,
σ_j is the wave number of the jth lasing mode,
$\delta'\sigma$ is the spectral width of the lasing mode,
ω is the frequency of light, and
c is the velocity of light.

This is illustrated by figure 5.3.

5.3.2. The theoretical simulation of the optical output of the interferometer

In order to simulate the optical output of the Michelson interferometer configuration, which is shown in figure 5.1, a mathematical model was developed, based on the assumptions mentioned in 3.3.2.

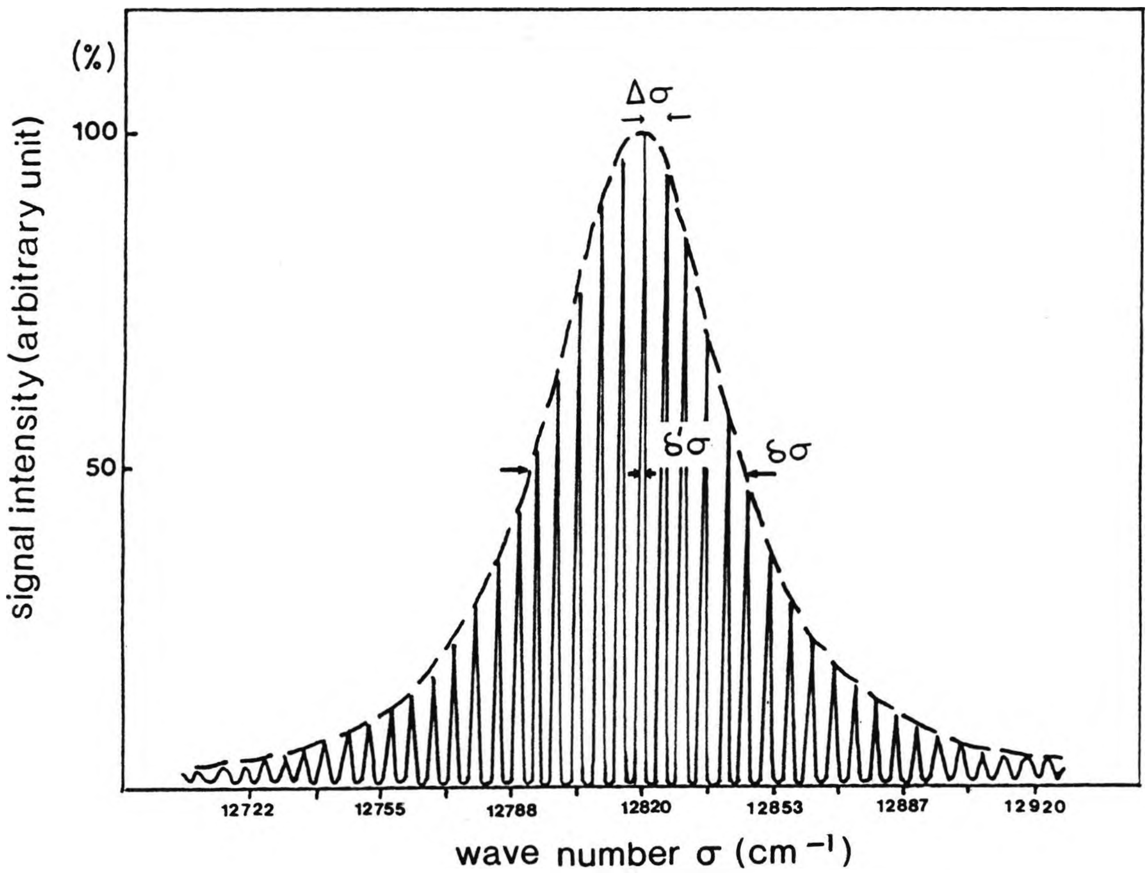

Figure 5.3. *Schematic output spectral characteristics of the "CD-type" laser diode used in this work.*

For rays normal to the mirrors of the Michelson interferometer, the phase difference, ϕ_1, between the beams reflected from mirror M_1 and mirror M_2 is given by:

$$\phi_1 = 2\pi\,(2\Delta L'/\lambda) = 2\pi\sigma L \tag{5.3}$$

where $\sigma = 1/\lambda$ (the wave number) and $2\Delta L'$, is the optical path difference introduced by the Michelson interferometer, given by L.

The radiation electrical fields, which are generated by the jth lasing mode, and are reflected from the two mirrors may be written as

$$E_{j1} = \sqrt{S_j(\sigma)}\ \exp\left[-\pi\left(j\frac{\Delta\sigma}{\delta\sigma}\right)^2 + i\omega t\right] \tag{5.4}$$

$$E_{j2} = \sqrt{S_j(\sigma)}\ \exp\left[-\pi\left(j\frac{\Delta\sigma}{\delta\sigma}\right)^2 + i\omega t + i2\pi\sigma L\right] \tag{5.5}$$

where the additional factor in the expression for E_{j2} is due to the phase difference ϕ.

The resulting intensity , dI_j, of an element of the jth mode is given by

$$dI_j = (E_{j1} + E_{j2})\,(E_{j1} + E_{j2})^*$$

$$= S_j(\sigma)\exp\left[-2\pi\left(j\frac{\Delta\sigma}{\delta\sigma}\right)^2\right][\,2+2\cos(2\pi\sigma_j L)\,]\,d\sigma \tag{5.6}$$

Thus for one full mode, this can be integrated to given I_j

$$I_j = \int_{-\infty}^{+\infty} S_j(\sigma)\exp\left[-2\pi\left(j\frac{\Delta\sigma}{\delta\sigma}\right)^2\right][2+2\cos(2\pi\sigma_j L)\,]\,d\sigma \tag{5.7}$$

The solution of this integral gives both a term not changing with the optical path difference L, and one with a dependence on that quantity, denoted by I_j', where

$$I_j' = 2\exp\left[-2\pi\left(j\frac{\Delta\sigma}{\delta\sigma}\right)^2\right]\int_{-\infty}^{+\infty} S_j(\sigma)\cos(2\pi\sigma_j L)\,d\sigma$$

$$= \frac{1}{c}\sqrt{\frac{2}{\pi}}\exp\left[-2\pi\left(j\frac{\Delta\sigma}{\delta\sigma}\right)^2\right]\exp(-\delta'\sigma L/2)\cos(2\pi\sigma_j L) \tag{5.8}$$

as

$$\int_{-\infty}^{+\infty}\left[\frac{2\delta'\sigma/\pi}{c(\delta'\sigma)^2 + 4c(\sigma-\sigma_j)^2}\right]\cos(2\pi\sigma L)\,d\sigma$$

$$= \sqrt{\frac{1}{2c^2}}\cos(2\pi\sigma_j L)\exp\left(-\frac{\delta'\sigma|L|}{2}\right) \tag{5.9}$$

Now considering all the intensity in all modes, I has a value given as:

$$I = \sum_{j=-m}^{+m} I_j = \sum_{j=-m}^{+m} \exp\left[-2\pi\left(j\frac{\Delta\sigma}{\delta\sigma}\right)^2 - \frac{\delta'\sigma|L|}{2}\right]\cos(2\pi\sigma_j L)$$

$$= \exp\left(-\frac{\delta'\sigma|L|}{2}\right)\sum_{j=-m}^{+m} \exp\left[-2\pi\left(j\frac{\Delta\sigma}{\delta\sigma}\right)^2\right]\cos(2\pi\sigma_j L) \qquad (5.10)$$

It can be seen from this intensity function that as the total output from the multimode laser diode is proportional to the sum of all the outputs of the 2m+1 modes of the laser diode, therefore, the interfered optical output is a kind of superposition fringes [10]. These superposed fringes appear periodically as the optical path difference L is varied, forming a constructive interference pattern.

Constructive interference for a particular value of L occurs when the path difference between adjacent sets of laser modes is a multiple of 2π, i.e., $2\pi\sigma_j L = 2N\pi$, or $2\pi(2\Delta L')/(\lambda_o + j\Delta\lambda) = 2N\pi$, where $\Delta L'$ is mirror scanned distance, N is an integer, and the integer j denotes the order of the mode. For example, the difference between the phase angle of the fundamental laser line and its first shifted line is $2\pi(2\Delta L')[\,1/\lambda_o - 1/(\lambda_o+\Delta\lambda)\,] = 2\pi$, thus

$$L = 2\Delta L' = \frac{\lambda_o^2}{\Delta\lambda} \qquad (5.11)$$

5.4. Experimental results and comparison

5.4.1. Experimental results

Results are presented on the characteristics of the interferometer with the displacement of the mirror M_2 provided by the vibrator, representing a displacement which would be induced in a practical fibre optic interferometer sensor by the action of the measurand. Conversion of effects such as a small vibration or pressure changes, etc., to a measurable displacement are relatively easy to achieve by adjustment of the mechanical configuration of the sensors to give the movement of the mirror.

As the mirror M_1 is scanned along the optic axis , the peak amplitudes of the Doppler-shifted interference fringes produced for both multimode laser diodes are obtained, and results are illustrated by figure 5.4(a) for the Sony diode (SONY, SLD104AU) and figure 5.4(b) for the Sharp diode (SHARP, LTO23). These figures show that, as the mirror scans along the optic axis, there are periodic regions in which constructive interference occurs. Maximum output from the detector occurs when the two optical paths in the interferometer have exactly equal lengths. This so-called zero-order region is labelled on figures 5.4(a) and 5.4(b), and results are given for both diodes as the optical path difference in the interferometer is adjusted. Only one direction of the adjustment is shown in figure 5.4, but there is a certain symmetry of output as the path difference changes in either positive or negative direction, lying to either side of the zero-order region. In figure 5.4(a), there a systematic error after the third order interference region. This may be explained that after the third region was recorded, the alignment of the experimental arrangement was slightly changed by some unexpected source.

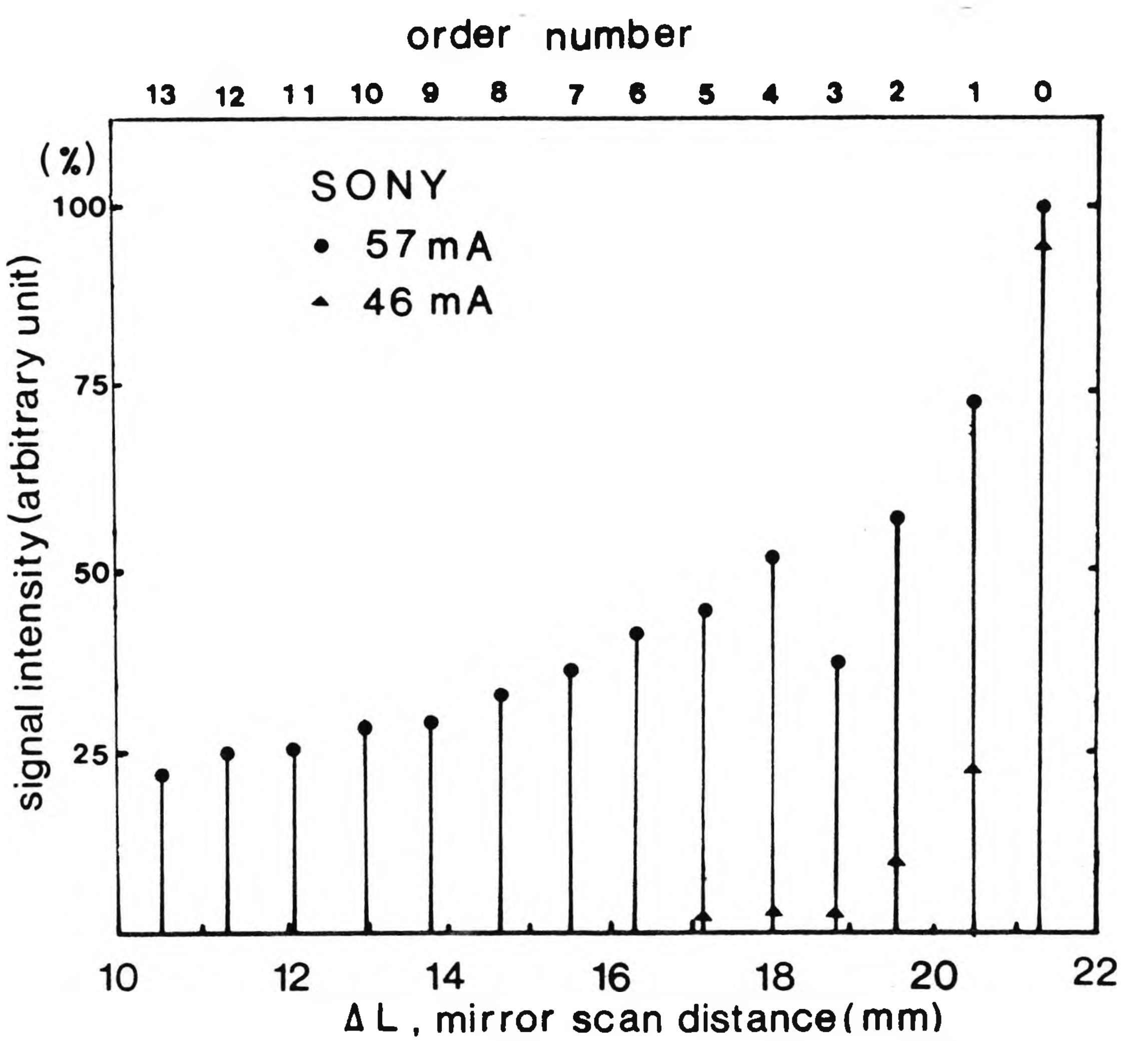

Figure 5.4(a). *Intensity of signal representing the peaks of the Doppler shifted interference fringes. SONY laser diode: driving currents: 57 and 46 mA.*

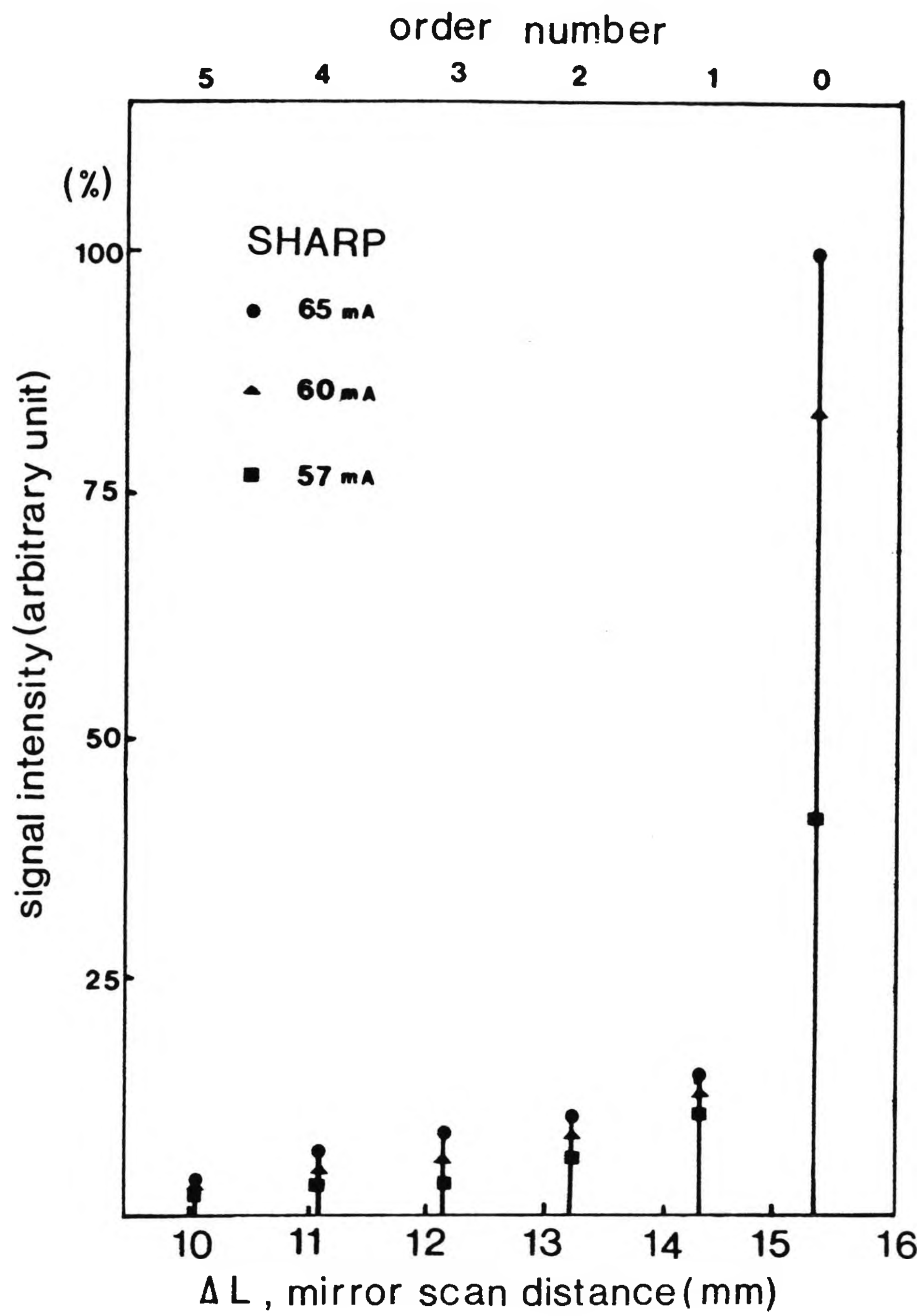

Figure 5.4(b). *Intensity of signal representing the peaks of the Doppler shifted interference fringes. SHARP laser diode: driving currents: 65, 60 and 57 mA.*

Figure 5.5 illustrates details of the maximum constructive interference region i.e., zero-order region. This figure shows the manner in which the output in this zero-order region typically reduces with the current applied to the laser diode being reduced over a drive-current region of 50 mA - 65 mA. The output is shown over the range of mirror scan distance, ΔL'. The results are shown for one of the devices, the Sharp LT023 MDO laser diode.

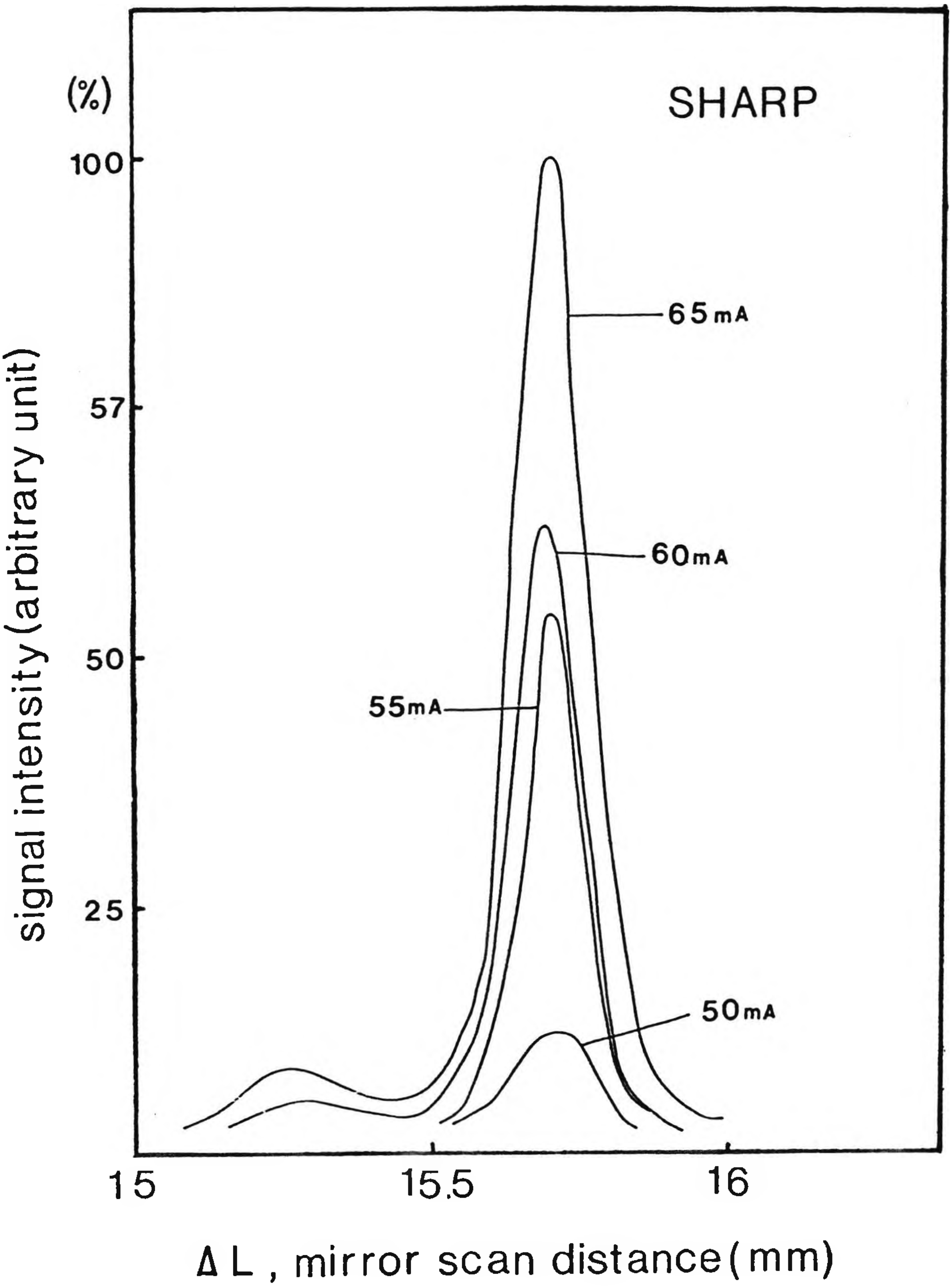

Figure 5.5. *Intensity of "zero - order" interference region for SHARP laser diode, drive current 50, 55, 60 and 65 mA.*

Figures 5.6(a) and 5.6(b) show detailed plots of light output intensity when the mirror scan distance $\Delta L'$ covers the zero- and first-order regions. Particularly noteworthy in these results is the much smaller region of $\Delta L'$ over which an output is seen for these orders of the Sony laser diode (figure 5.6a) and the Sharp diode (figure 5.6b) in the same driven-current conditions. It can be seen, from these figures, that the output is 0.84 mm for the Sony device and 1.07 mm for the Sharp. These spacings, ΔL, can be calculated from equation 5.11, i.e., $\Delta L = \lambda_o^2/\Delta\lambda$, where λ_o is the centre line of the radiating wavelength and $\Delta\lambda$ is the difference between adjacent modal wavelengths supported by the laser diode.

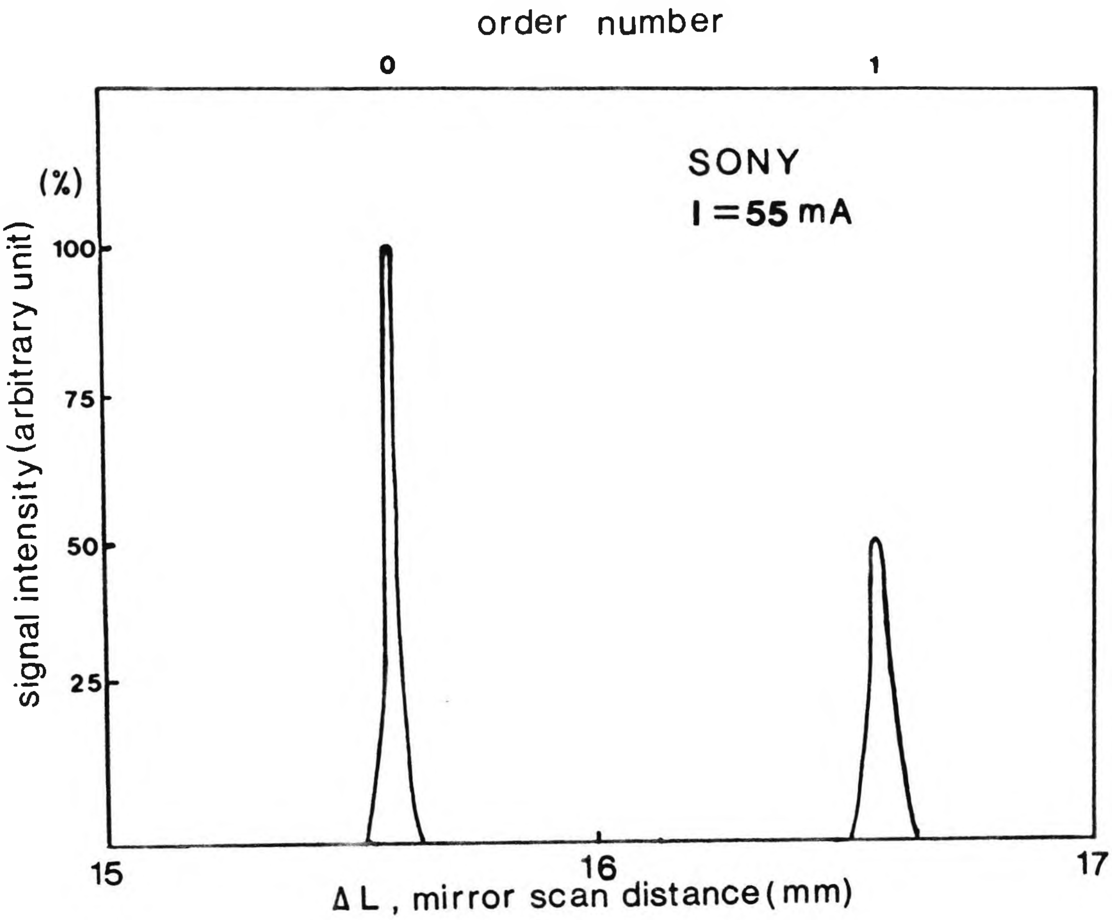

Figure 5.6.(a) *Intensity of signal representing zero and first order regions. SONY diode: drive current 55 mA.*

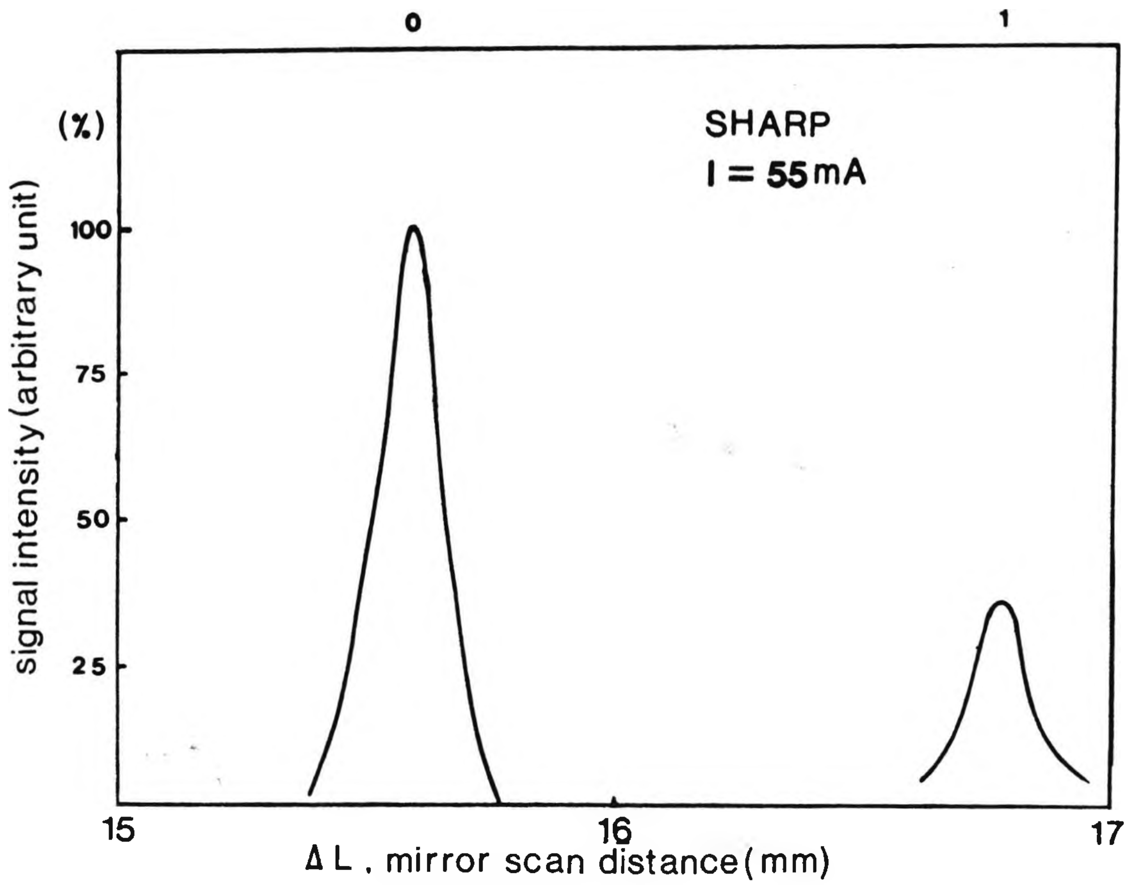

Figure 5.6 (b). *Intensity of signal representing the zero and first order regions. SHARP laser diode: driving current: 55 mA.*

5.4.2. Comparison between the experimental and the theoretical results

The theoretical intensity was calculated using a simple computer programme according to equation 5.10. Results are plotted in figure 5.7(a) for the case of m = 7, $\Delta\lambda$ = 0.3 nm, $\delta\lambda$ = 4 nm, λ_o = 780 nm and $\delta'\lambda$ = 0.15 nm, which are typical of the Sony laser diode, where $\Delta\lambda$, $\delta\lambda$, and $\delta'\lambda$ are related to the inverse of $\Delta\sigma$, $\delta\sigma$, and $\delta'\sigma$, respectively.

Figure 5.7(a) shows a plot of the peak amplitudes of each interference order as a function of the optical path difference change, $\Delta L'$. It can be seen that constructive interference occurs only over a narrow region and not over the broad range. This compares closely with figure 5.4(a) which is the experimental results obtained for the Sony diode. For example, the ratios of the first four peaks is 100:73:57:38 in figure 5.7(a) and 100:77:58:42 in figure

5.4(a) (normalised to the zero-order peak in each case), which reflects the experimental situation. However, the theoretical prediction shows that the

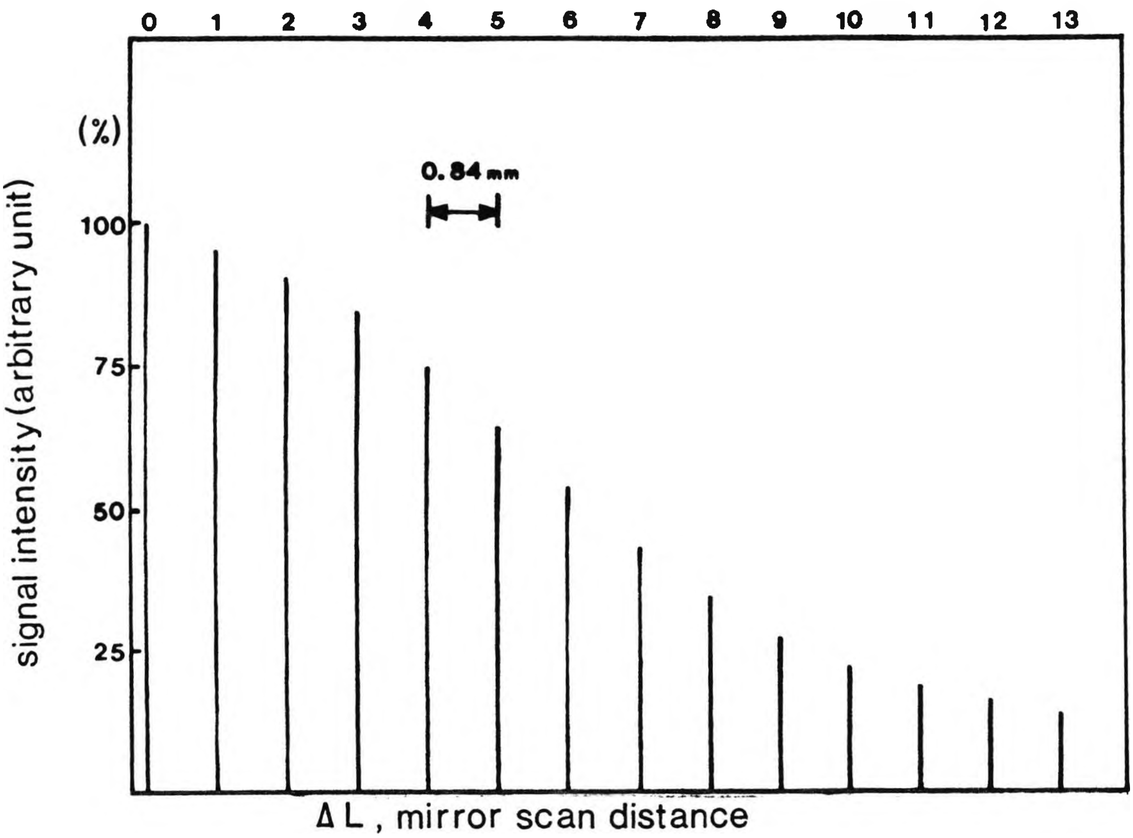

Figure 5.7.(a). *Calculated signal intensity of peaks of Doppler shifted interference fringes. SONY diode: 0.15 nm.*

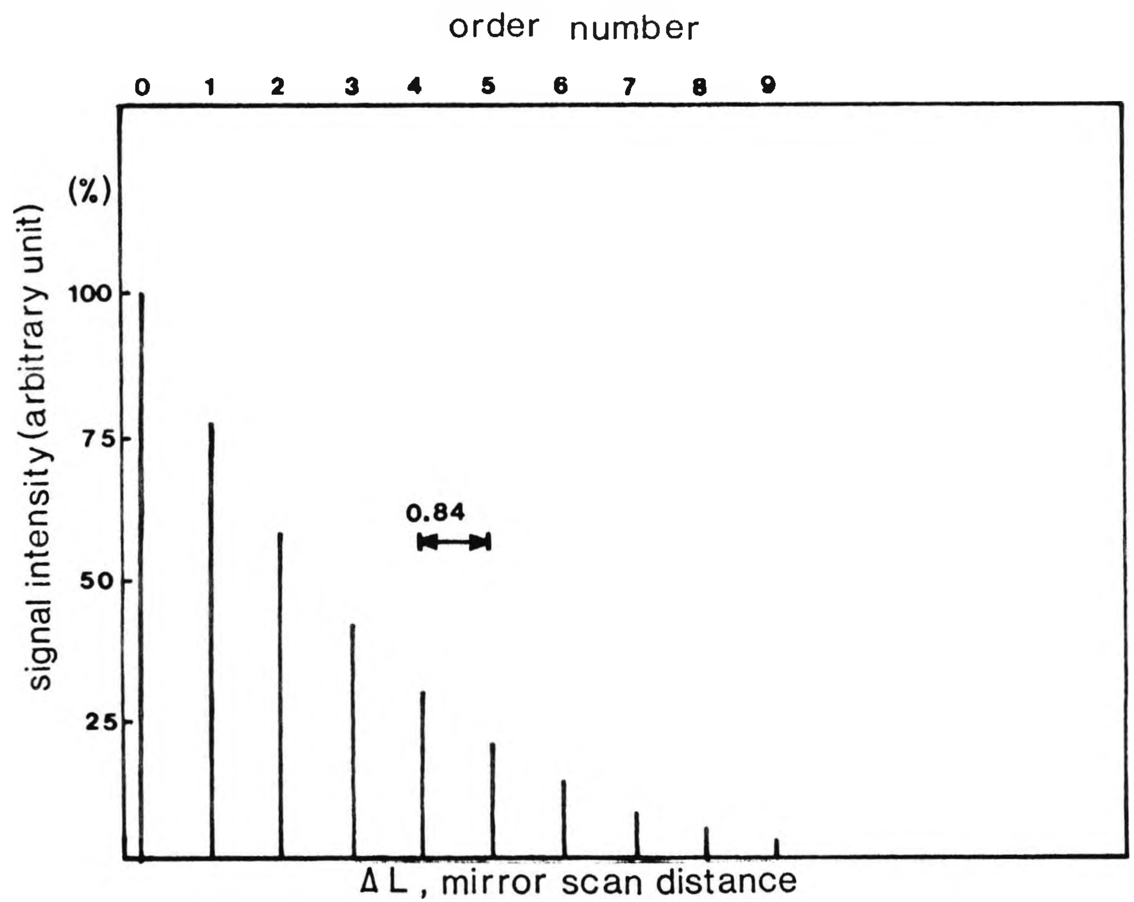

Figure 5.7.(b). *Calculated signal intensity of peaks of Doppler shifted interference fringes. SONY diode: 0.05 nm.*

intensity has reduced to <3% of the zero-order peak by the 10th position, whereas experimentally this does not occur. This may partially be explained by the assumption of $\delta'\lambda = 0.15$ nm which was obtained from an approximate measurement from manufacturer's published data [ ]. If that is decreased to a value of $\delta'\lambda = 0.05$ mm, the resulting pattern is shown in figure 5.7(b). In this figure, the pattern extends beyond the 10th order. However, the trend is clearly revealed by the theoretical data for the assumed value of $\delta'\lambda = 0.15$ nm.

It can be seen that the intensity distribute of each interfered region in the optical output from the interferometer is not the same with most of the energy being concentrated on the zero-order region. This result can be explained by the two facts: first, the envelope of all peaks of the interference regions is a exponential function of the optical path difference, with its half-width being inversely proportional to the half-spectal-width of the single lasing mode. Thus as the optical path difference increases, the peak values in the higher order regions will drop exponentially. Second, in the practical interferometer, the light beams are not perfectly collimated, and the mirrors are not perfectly normal to the light beams, those facts will bring down the interfered intensities in the high order regions as well.

Figure 5.8 shows detailed computed plots of the shape of the regions of constructive interference shown as the zero- and first-order on figure 5.7(a). This can be compared to the equivalent experimental results of figure 5.6(a) where the zero- and first-orders were obtained for the Sony diode. The experimental separation between the orders, ΔL, is in very good agreement, with a value of 0.83 mm experimentally and 0.84 mm theoretically. However, the half-width of the theoretical interference region is much greater than that of the experimental system at 0.22 mm as compared to 0.02 mm in the zero-order region and 0.04 mm in the first-order region. This is in part due to the fact that, in the theoretical model, the energy is distributed into only 15 modes for ease of calculation whereas experimentally there are many more modes present. Also, the value $\delta\lambda$ (corresponding to $\delta\sigma$ in figure 5.3) is an approximation at 4 nm and the half-width of the zero- and first-order regions are dependent on this parameter. However, these results show a good agreement in the separation of the constructive interference regions.

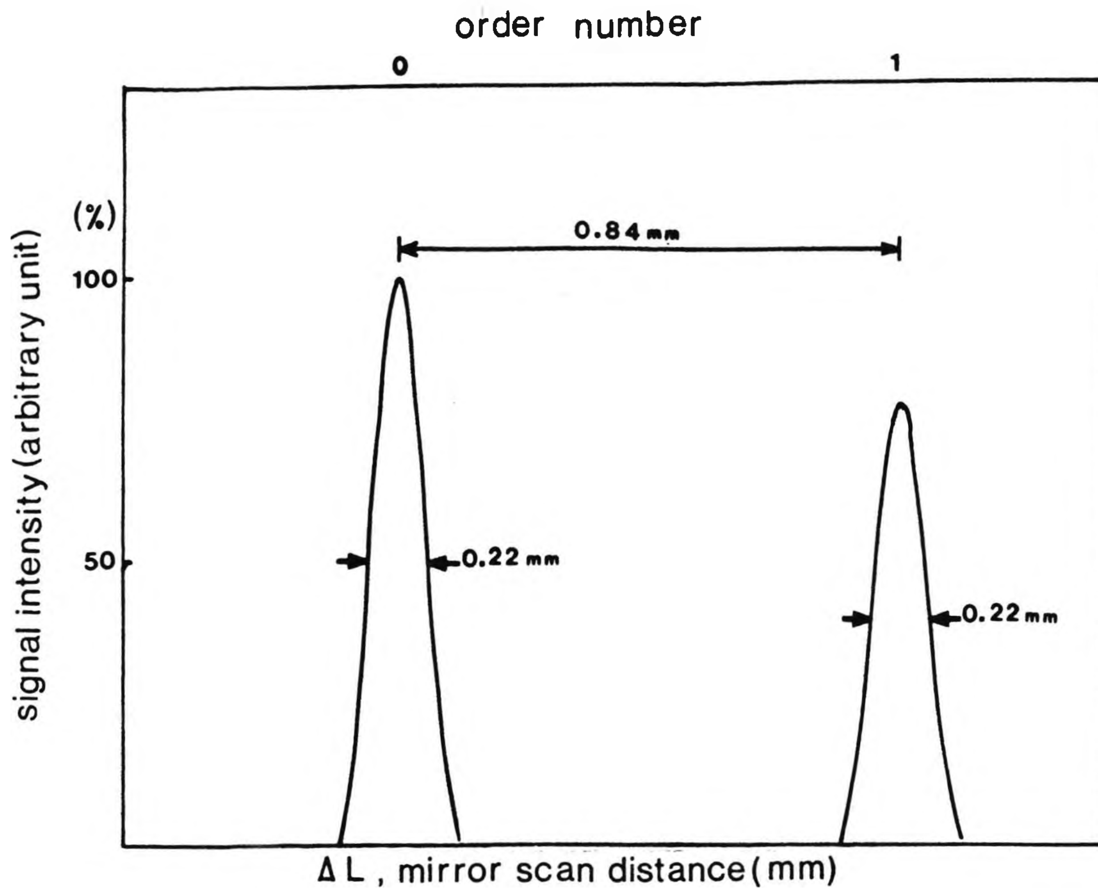

Figure 5.8. *Calculated signal intensity representing the zero and first order interference regions for SONY laser diode.*

5.5. The optical fibre version of the experimental arrangement

In order to verify the feasibility of using a multimode laser diode in a practical optical fibre interferometric sensor, an optical fibre version of the experimental arrangement was built, shown in figure 5.9. The optical output of the fibre interferometer was recorded and compared with that of the open path arrangement shown in figure 5.1.

It can be seen, from figure 5.9, that the beam splitter in figure 5.1 is replaced by an 2 X 2 optical fibre coupler, and the two arms in the open path interferometer are replaced by one optical fibre (port 3 of the coupler in figure 5.9). The multimode laser diode used in this arrangement is ML-4406, which was more easy to be obtained, manufactured by Mitsubish, with a optical output of 3 mW at the driven current of 55 mA. In this experimental arrangement, the vibrating mirror is fixed on the micrometer shown in figure 5.9, hence, the optical path difference in the interferometer can adjusted by scanning the micrometer.

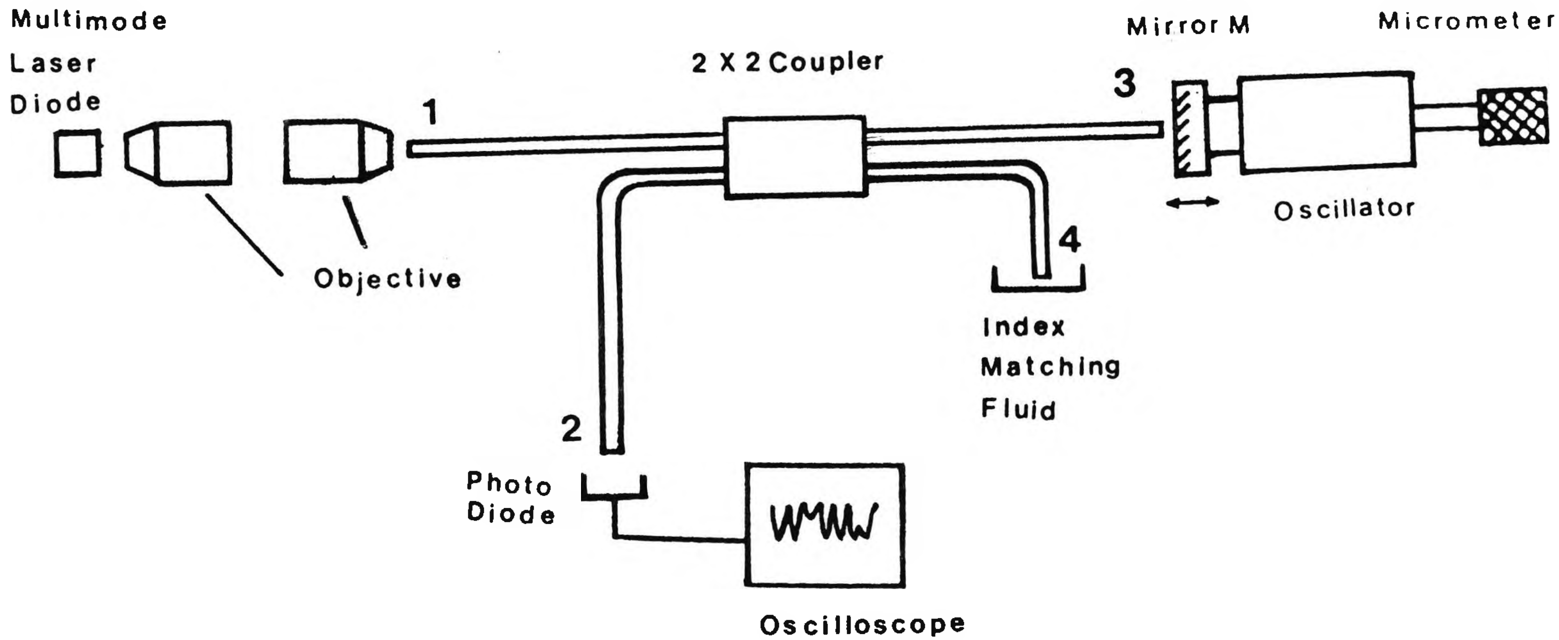

Figure 5.9. *The optical fibre version of the experimental arrangement.*

Light beam in the fibre port 3 is divided by the end face of the fibre. Therefore, the light beam reflected from the fibre end interferes with that reflected from the vibrating mirror on the photodetector. The output signal from the photodetector is similar to that obtained from the open path interferometer shown in figure 5.2.

Figure 5.10 shows the detailed plots of light output intensity when the mirror scan distance ΔL' cover the zero- and first-order regions. By comparing the plot shown in figure 5.10 with those shown in figures 5.6(a) and 5.6(b), it can be seen that the characteristics of the multimode laser diode studied in the open path interferometer do not change in the optical fibre one. Therefore, the characteristics of the multimode laser diode in the interferometer can be employed to develop new types of optical fibre sensors.

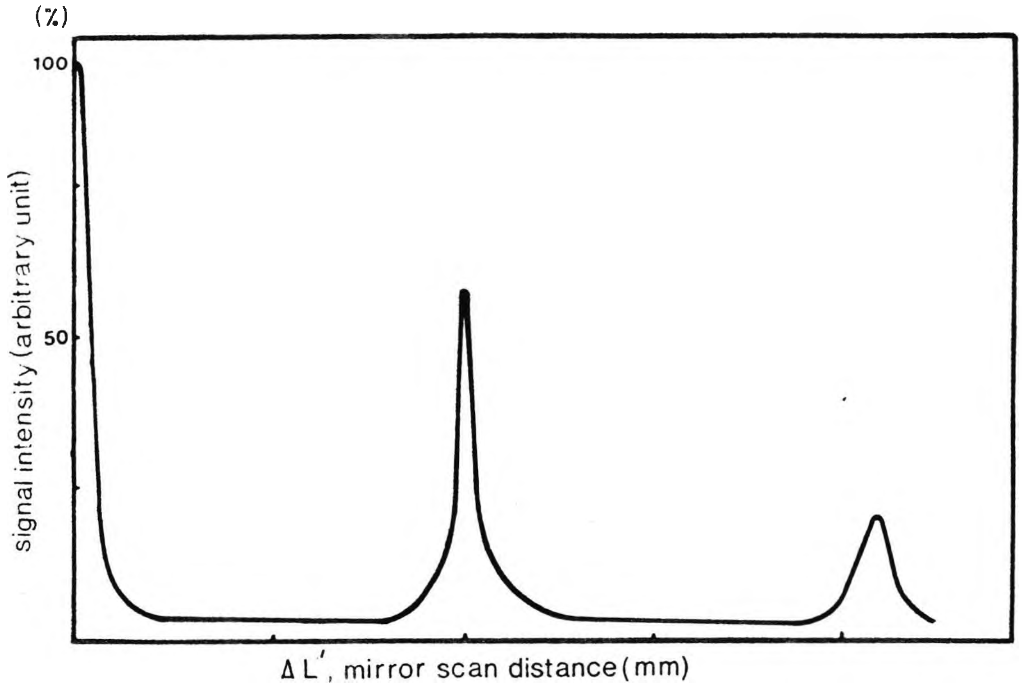

Figure 5.10. *Intensity of signal representing the half zero region, first and second order interference regions.*

5.6. Conclusion

The theoretical results shown support the experimental results when they indicate that the maximum energy output from these laser diodes will be in the zero-order interference region. The rapid decrease of energy shown in the experimental results when they move to the higher order regions indicates that the assumption of a Lorentzian distribution of energy in a single laser lasing mode is a reasonably representation of the physical laser system. However, the experimental results do show that these types of laser diodes will be very useful as optical sources in sensors requiring low coherence, especially for multiplexed systems where high light power coupled into optical fibre is needed.

Thus a reasonable agreement between theoretical and experimental results is observed and useful interference regions with a simpler configuration are seen. The experimental results obtained in this work using a multimode laser diode as the light source device are not similar to those obtained previously using a narrow-band continuous spectral light source such as a LED. Both types of sources have their spectra contained under a Gaussian-type envelope, but the LED shows a spectral continuum with a Half-spectrum-width of 20 nm to 80 nm [3], therefore, the coherence length of the LED is about 50 μm. While the spectrum of the multimode laser diode consists a set of discrete spectral lines (about 20), each having a Lorentzian line shape. The half-spectrum-width of its spectrum is about a few nanometers, thus the coherence length of the a multimode laser diode is much longer than that of the LED. Because the spectral structures of two light sources are not the same, the optical outputs from an interferometer are different. It is the spectral envelope shape that determines the profile of the interference region, while the fine spectral structures within this envelope modifies the spatial distribution of the interference pattern and the peak values. This is the consequence of one being the Fourier transform of the other.

The high-resolution range of the devices is illustrated by, for example, the characteristics of the Sharp device. With a coherence range of above 0.1 mm in the zero-order, this is equivalent to above 250 fringes when light of 0.8 μm wavelength is used in an interferometer of the Michelson type, i.e., one fringe per half wavelength (0.4 μm) over the coherence range. It is obvious, therefore, in the important field of multiplexing in optical fibre systems, these laser diodes will have considerable application.

References

[1] R.B. Dyott "The fibre optic Doppler anemometer" IEE J Microwaves Opt Accurst 2, 13, 1978.

[2] D.A. Jackson "Monomode fibre optic interferometers and their application in sensing system" Optical Fibre Sensors, NATO ASI series, series E: Applied Sciences, NO.132, pp.1-33, 1987.

[3] G. Beheim, K. Fritsch and N. Poorman "Fibre-linked interferometric pressure sensor" Rev. Sci. Instrum. 58(9), pp.1655-9 1987

[4] T. Bosselmann "Multimode fibre coupled white-light interferometric position sensor" Optical Fibre Sensors, NATO ASI series, series E: Applied Sciences, NO.132, pp.429-32, 1987.

[5] C. Mariller and M. Lequime,"Fibre-optic white-light birefringent temperature sensor" Proc. Soc. Photo-Opt. Instrum.Eng. 798, 121-130, 1987

[6] A.S.Gerges, Farahi, T.P. Newson, J.D.C. Jones, and D.A. Jackson, "Interferometric fibre-optic sensor using a short coherence length source", Electron. Lett. 22, 238-239, 1987

[7] S. Saito, Y. Yamamoto, "Direct observation of lorentzian line shape of semiconductor laser and linewidth reduction with external grating feed back", Electron. Lett. 17, 325-327 1981

[8] T. Okoshi, K. Kikuchi, A. Nakayama, "Novel method for high resolution measurement of laser output spectrum", Electron. Lett. 16, 630-632 1980

[9] K. Peterman and G. Arnold, "Noise and distortion characteristics of semiconductor lasers in optical fibre communication system", IEEE J.Quantum Electron. QE-18, 543-544, 1982

[10] M. Born and E. Wolf "Principles of optics", Oxford University Press, 360-367, 1980

Chapter 6

Coherence length modulation scheme based on a coupled Michelson : Fabry-Perot interferometer using a multimode laser diode

Abstract

In this Chapter, several experimental and theoretical investigations of the use of multimode laser diodes in a coupled Michelson : Fabry - Perot interferometer are presented. The results obtained indicate that two "side-band" or "shifted" interference regions can be generated around the original interference region through the use of this dual interferometer configuration. By changing the optical path difference (OPD) or the thickness of the Fabry-Perot cavity, the position of the "shifted" interference regions can be adjusted in a controlled and reproducible way. Therefore, the volume where a measurement may be made using this scheme which is otherwise limited inside the interference region can be defined by setting the OPD of the second interferometer. The results obtained show that the "coherence regions" of such diodes can be varied over a large range of optical path imbalance of the interferometers allowing the interference region in fibre optic sensors to be tailored to specific sensor applications.

6.1. Introduction

As mentioned in chapter 4, if a common-mode optical fibre interferometer is used to measure flow speed, it is difficult to define the geometry of the measurement volume. This is largely due to the fact that if a highly coherent light source is employed in the interferometer, light scattered back from anywhere along the optical axis will interfere with that reflected from the fibre end, and thus only from the interference fringes, it not easy to define the position where the measurement is taken. From the results shown in chapter 5, it can be seen that if a low coherence light source is used in a common-mode interferometer configuration, the interference regions are limited to a certain number of positions along the optical axis of the interferometer. However, if only one interferometer is used in this operation, the problem of defining the geometry of the measurement volume still remains unsolved.

In order to overcome this problem, the coherence length modulation technique based on a coupled Michelson-Fabry Perot interferometer configuration was studied. The results show that by employing a second interferometer, the interference region can be "shifted" along the optical axis of the first interferometer. In this chapter, the details of this work are described. The experimental results verify the theoretical prediction from the mathematical model developed in this work.

In the section 6.2, the principle of coherence length modulation and early work done are outlined. The experimental arrangement used in this work is presented in the section 6.3. A theoretical simulation of the interferometer configuration (shown in figure 6.1.) is presented in section 6.4. Then, by comparing the experimental results with the theoretical ones, it is shown in section 6.5 that there is a good agreement between these experimental and theoretical results. This chapter ends with a further discussion, section 6.6.

6.2. The principle of the coherence length modulation and the early work

"Coherence region" is a term used to describe a region where phase modulation can be achieved. The coherence region is limited by the

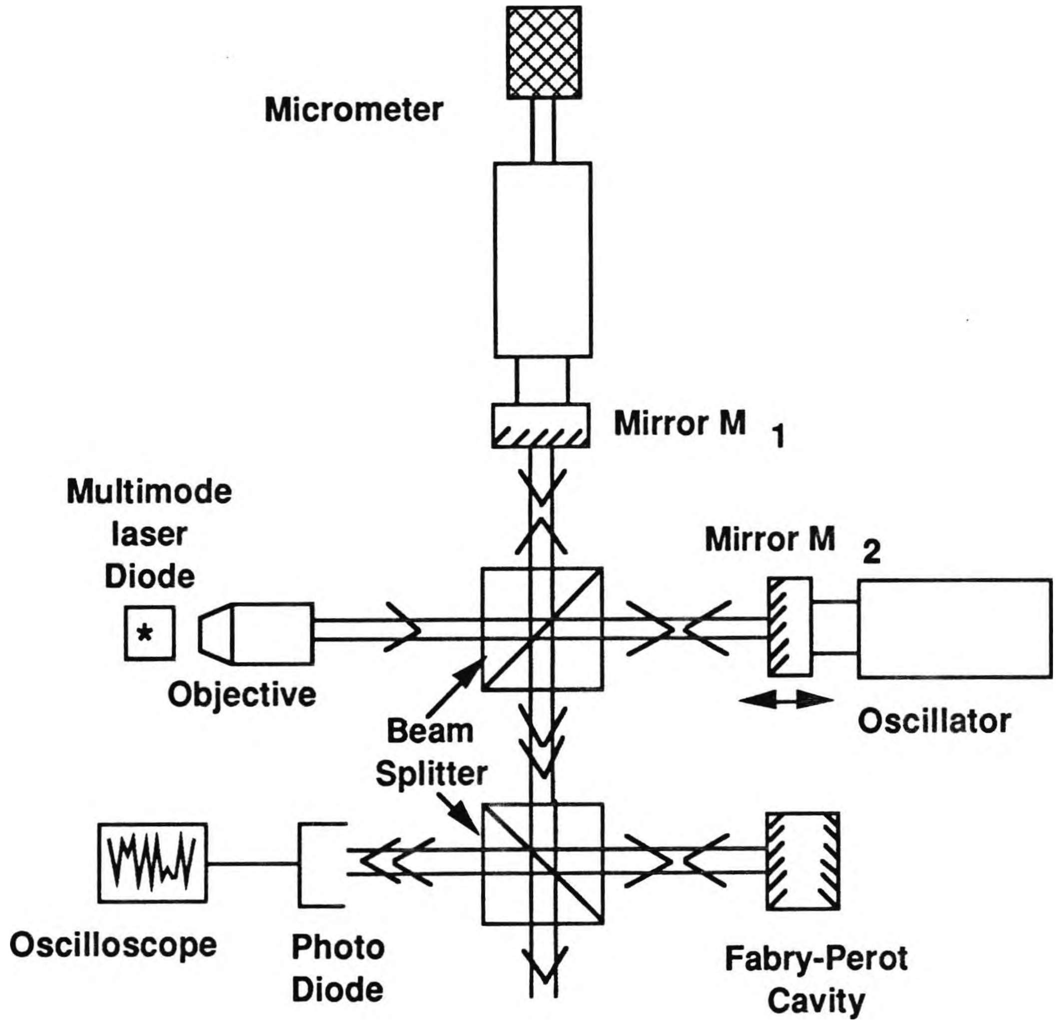

Figure 6. 1. *Schematic optical arrangement of the coupled Michelson : Fabry-perot interferometer used in this work.*

coherence length. When the optical path difference of the interferometer is greater than the coherence length of the light source, the interferometer is working inside a "non-coherence region". In order to achieve the phase modulation in this case, a coherence length modulation technique can be used to "shift" this unbalanced interferometer from the non-coherence region into the coherence one, where the interferometer is balanced or near balanced. The basic function of this modulation is to compensate the large optical path difference between beams in the sensor interferometer, where this large optical path difference cannot be reduced due to the limitation of the sensor configuration. For example, when a common-mode optical fibre interferometric sensor is employed to measure the flow speed (figure 6.2.),

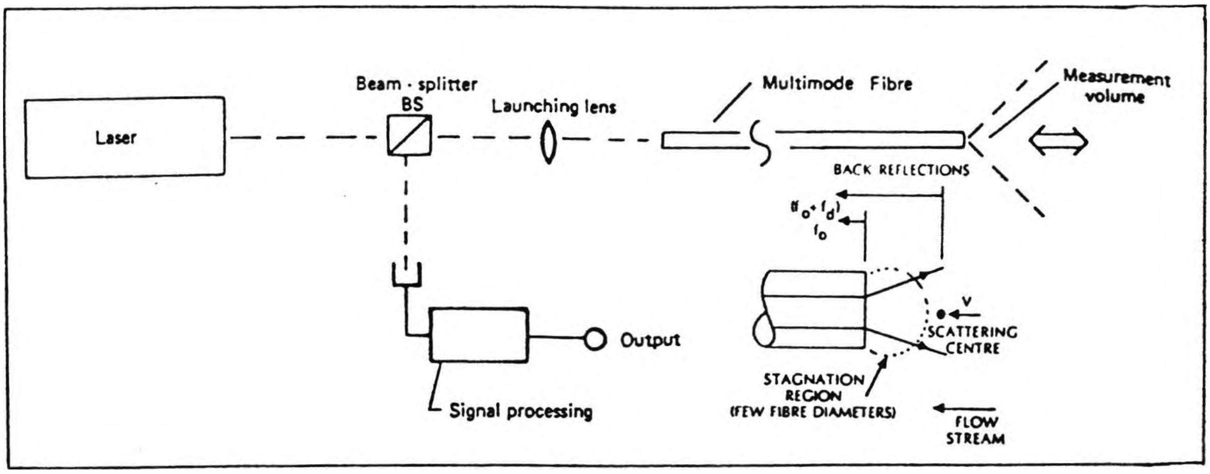

Figure 6.2. *Simple fibre -optic laser velocimeter (Ref.1).*

the ideal measurement volume should be away from the end of the fibre, in order to avoid the "stagnant region" caused by the presence of the fibre. Therefore the optical path difference between the light beam reflected from a fibre end and the beam reflected from the measurement volume will be large compared with the coherence length if a low coherence light source was used. In this case, these two light beams will not interfere with each other. However, by employing a second interferometer to compensate this large optical path difference, the working region of the first interferometer can be shifted from the original incoherent region into the "coherence region", and therefore phase modulation can be achieved.

The basic arrangement employed to achieve this modulation is a two-coupled interferometer, also known as "white-light interferometer" [2] or "coherence modulated interferometer" [3]. In order to introduce the coherence length modulation, two requirements should be met:

(a) the optical path differences of the two interferometers (L_1, L_2) are greater than the coherence length of the light source (L_c), i.e., $L_1 >> L_c$, $L_2 >> L_c$.

(b) the difference between these two optical path differences is less than the coherence length of the light source, i.e., $|L_1-L_2|<L_c$,

Under these conditions, this two-coupled interferometer gives an intensity distribution which is the so-called "fringes of superposition" [4].

The light sources often used in the coherence length modulation are low-coherence ones such as the light emitting diode devices (LED), white light sources and multimode laser diodes. The characteristics of an LED in a dual interferometer were investigated both theoretically and experimentally by Al-Chalabi et al [5]. The applications of a dual interferometer with a LED light source were considered with slowly changing measurands such as pressure [6], position [2] or strain [7]. One of the two-coupled interferometers is employed as a sensing one to induce the optical path difference variation caused by the measurand, and the second interferometer is used as a reference one. When the optical path difference of the reference interferometer is adjusted to match that of the sensing one, the superposition fringes appear in the optical output of the reference interferometer. These fringes can be used as a "position mark" to define the changed position which is induced by the sensing interferometer. The separation between the original position and the changed one was measured by an additional single mode He-Ne laser in the reference interferometer. With this laser reference, a 22 mm measuring range with 0.00001 mm resolution was reported by T.Bosselmann [2].

The multimode laser diodes investigated in the last chapter may be employed as another type of low coherence light source. The characteristics of the optical output from a coupled Michelson : Fabry - Perot interferometer using a multimode laser diode light source are described in detail in the following sections.

6.3. The experimental arrangement

Figure 6.1. illustrates the dual interferometer system which was investigated in this work. As shown in figure 6.1., the first interferometer is a Michelson one, which may be considered as a sensing interferometer, and the second reference interferometer is a Fabry-Perot cavity formed by the two planes of a piece of glass slice. By using this glass-slice cavity, it become more easy to align the system. In figure 6.1., the mirror M_1 is mounted on a

micrometer for fine adjustment along the optical axis. The mirror M_2 is attached to a vibrator which is driven at 200 Hz and induces a simulated input signal. Light from the multimode laser diode is collimated by a X10 objective lens, and the parallel beam is injected into the Michelson interferometer. The light beam coming out from the Michelson interferometer is then reflected by the second interferometer cavity, which is linked with the Michelson interferometer through a beam splitter, and detected by a high sensitivity Si photodiode/amplifier (EG&E HUV 1100BQ). The detected signal (as shown in figure 6.3) is then displayed on an oscilloscope. The peak-to-peak value against the variation of the mirror scanned distance were recorded and plotted out [8].

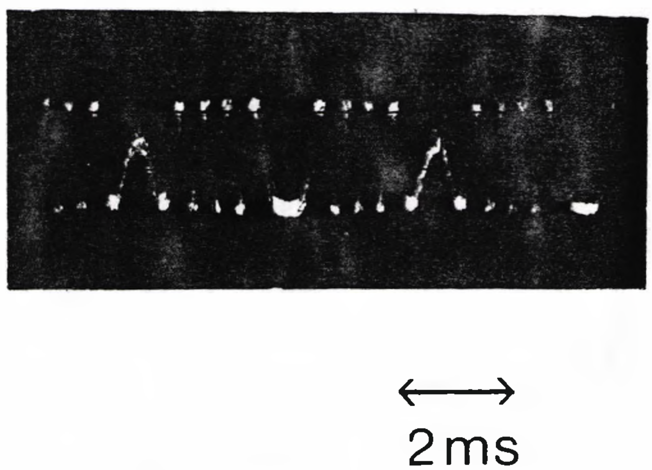

Figure 6.3. *Interference signal recorded on the photodetector in the interferometer.*

6.4. Theoretical considerations

The simulation of the optical output of the configuration shown in figure 6.1 was made based on the same assumptions used in section 5.3.2.

For the light beam normal to the mirrors of the Michelson interferometer, the phase difference, ϕ_1, between the beams reflected from mirror M_1 and mirror M_2 is given by

$$\phi_1 = 2\pi\,(2\Delta L_1)/\lambda = 2\pi\sigma L_1 \qquad (6.1)$$

where $\sigma=1/\lambda$ (the wave number) and ΔL_1 is the mirror scanned distance. The optical path difference, L_1, introduced by the Michelson interferometer, given by $2\Delta L_1$.

The corresponding radiation electric fields, E_{j1} and E_{j2}, which are generated by the jth lasing mode of the laser diode, and are reflected from the two mirrors in the Michelson interferometer, may be written as:

$$E_{j1} = \frac{A_o}{2} \exp\left[-\pi\left(j\frac{\Delta\sigma}{\delta\sigma}\right)^2\right]\exp(i\omega t) \tag{6.2}$$

$$E_{j2} = \frac{A_o}{2} \exp\left[-\pi\left(j\frac{\Delta\sigma}{\delta\sigma}\right)^2\right]\exp[\, i(\omega t + 2\pi L_1\sigma_j)\,] \tag{6.3}$$

where $\Delta\sigma$ is the difference between adjacent model wave numbers of full width $\delta'\sigma$.

$\delta\sigma$ is the envelope full width of all the modes.

σ_j is the wave number of the jth lasing mode.

These lasing modes are illustrated schematically in figure 5.3.

These radiation fields enter and are reflected within the Fabry-Perot cavity, undergoing multiple reflections, and so the electric fields of the light E_{jr1}, E_{jr2} thus reflected from the Fabry-Perot cavity, respectively can be written as

$$E_{jr1} = \frac{[\,1 - \exp(i\phi_2)\,]\sqrt{R}}{[\,1 - R\exp(i\phi_2)\,]} E_{j1} \tag{6.4}$$

$$E_{jr2} = \frac{[\,1 - \exp(i\phi_2)\,]\sqrt{R}}{[\,1 - R\exp(i\phi_2)\,]} E_{j2} \tag{6.5}$$

where R is the reflectivity of the cavity, ϕ_2 is the phase difference caused by the Fabry-Perot cavity and this may be written as

$$\phi_2 = 2\pi L_2 \sigma_j \tag{6.6}$$

where σ_j is the wave number of the radiation and L_2 is the optical path difference caused by the reflection from the cavity itself. Hence the total radiation electric field for the jth lasing mode of the diode is

$$E_{jr} = E_{jr1} + E_{jr2} \tag{6.7}$$

The intensity so represented is given by the product shown below in equation 6.8 i.e.:

$$I_{jr} = (E_{jr1} + E_{jr2})\,(E_{jr1}{}^{*} + E_{jr2}{}^{*}) \tag{6.8}$$

Substitution of equations 6.4 and 6.5 into the above yields an expression for I_{jr} as:

$$I_{jr} = \frac{1}{2}\left[\frac{B\,(1 + \cos\phi_1)\sin^2\left(\frac{\phi_2}{2}\right)}{1 + B\sin^2\left(\frac{\phi_2}{2}\right)}\right]\exp\left[-2\pi\left(j\,\frac{\Delta\sigma}{\delta\sigma}\right)^2\right] \tag{6.9}$$

where $B = 4R/(1 - R)^2$ and the intensity, I, in all the 2m+1 modes can then be calculated from the summation below, i.e.

$$I = \sum_{j=-m}^{j=+m} I_{jr} \tag{6.10}$$

In order to simulate the optical output from the coupled Michelson: Fabry-Perot interferometer shown in figure 6.1., a calculation was performed using a computer program on a PC computer.

6.5. Experimental results and comparison with calculation

The configuration of the experiment arrangement is shown in figure 6.1. The first interferometer used was a Michelson interferometer and the second one was a Fabry-Perot cavity. The light source used was a multimode laser diode device ("CD" type, Mitsubishi ML4406) emitting at a wavelength of 780nm. The situation considered initially is that when the Michelson interferometer only is used and the optical path difference , L_2, of the Fabry-Perot cavity is set to zero, so that it effectively represents a single reflecting surface. As the mirror M_1 is scanned by the micrometer away from the balance position of the Michelson interferometer, (which corresponds to $L_1 = 0$), the fringe visibility reduces and the a.c. signal received by the detector falls off. As the mirror is scanned through a distance of 0.05 mm, corresponding to $L_1 = 0.1$ mm, the a.c. signal drops to half the peak value, reflecting the width of the "zero-order" region. As L_1 is increased, a first order interference region is seen at $L_1 = 2.10$ mm, as shown in figure 6.4., and subsequent orders of interference are seen at integer multiples of this value, as shown in figure 6.5. This result is similar to that described in the chapter 5, for example, the experimental result shown in figure 5.6b.

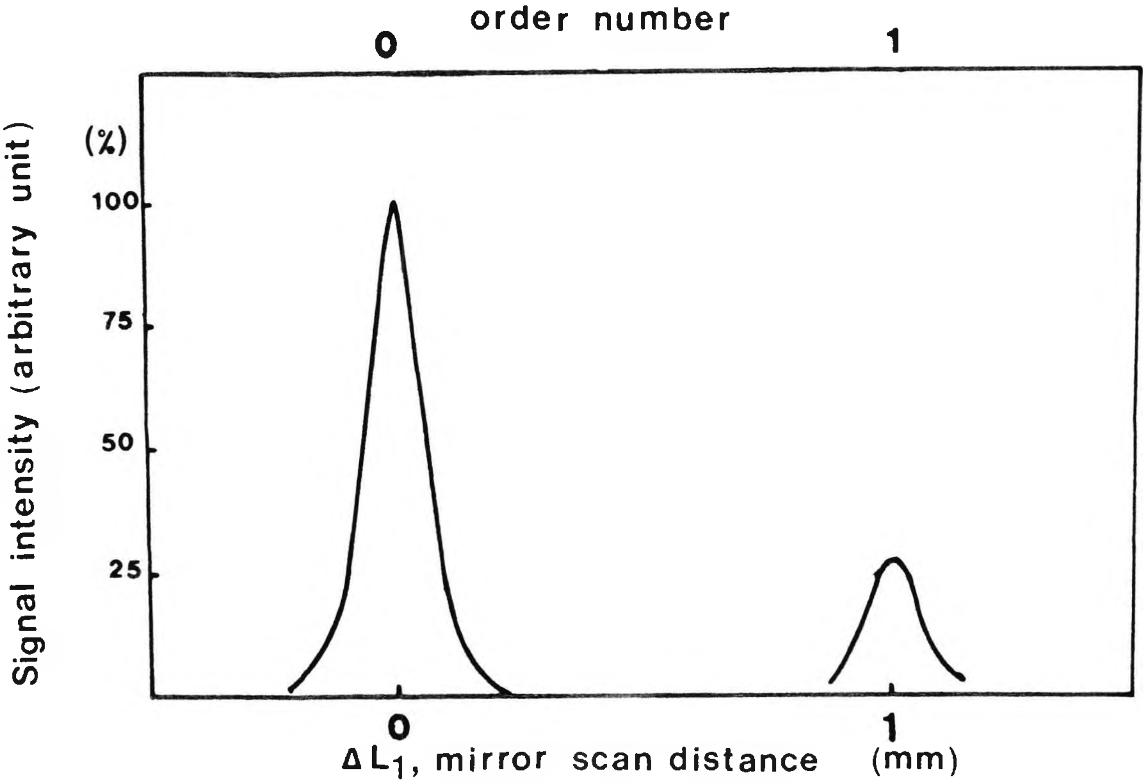

Figure 6.4 *Output signal intensity (arbitrary unit) v ΔL_1 (mm) with no Fabry - Perot interferometer, showing the first and second order of the original interference regions.*

However, a contrast is seen in the case where L_2 is non-zero and the Fabry-Perot cavity becomes operational. The operation of two interferometers must then be considered, and two "sideband" regions of interference can be seen accompanying each central interference order, as is shown in figure 6.6. As the thickness of the Fabry-Perot cavity is increased and the reflective surfaces are drawn apart, the optical path difference, L_2, increases. The effect is shown in figure 6.7, where the separation between the "sideband" region and the original region is seen to increase. For example, in figure 6.6, with L_2 = 0.435 mm (the cavity thickness between the two planes of the glass slice is 0.145 mm and the refractive index is 1.5), the average separation of the sideband from the central band was 0.22 mm, which would imply an optical path difference of 0.44 mm i.e. twice the separation. This represents good agreement with the value of L_2 used. Similarly, in figure 6.7, a second situation is illustrated for a cavity thickness of 0.139 mm. This implies a value of L_2 of 0.417 mm, and the average band separation is given by 0.213 mm, which implies a value of L_2 of 0.426 mm. In this second case also, excellent agreement is seen.

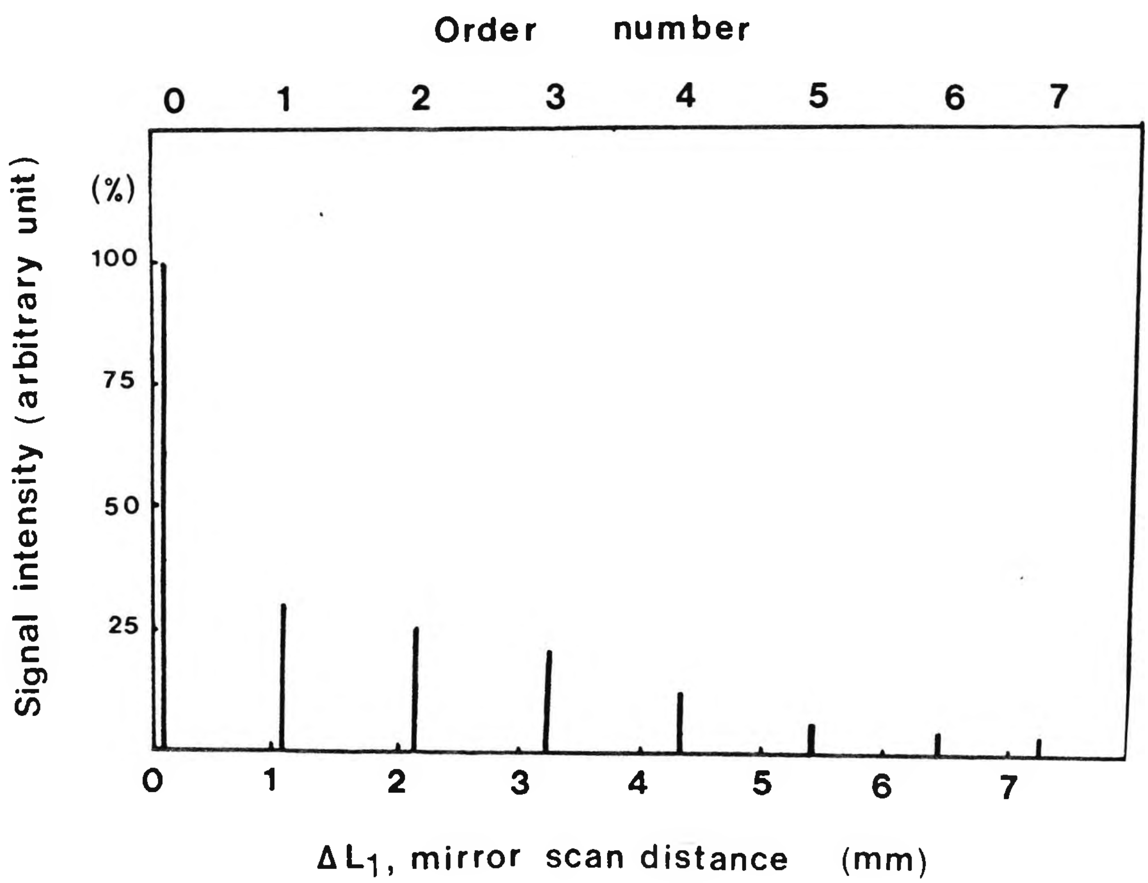

Figure 6.5. *Experimental results of the peak value of signal intensity (arbitrary unit) v ΔL_1 (mm) with no Fabry - Perot interferometer in operation, showing several orders of the original interference regions.*

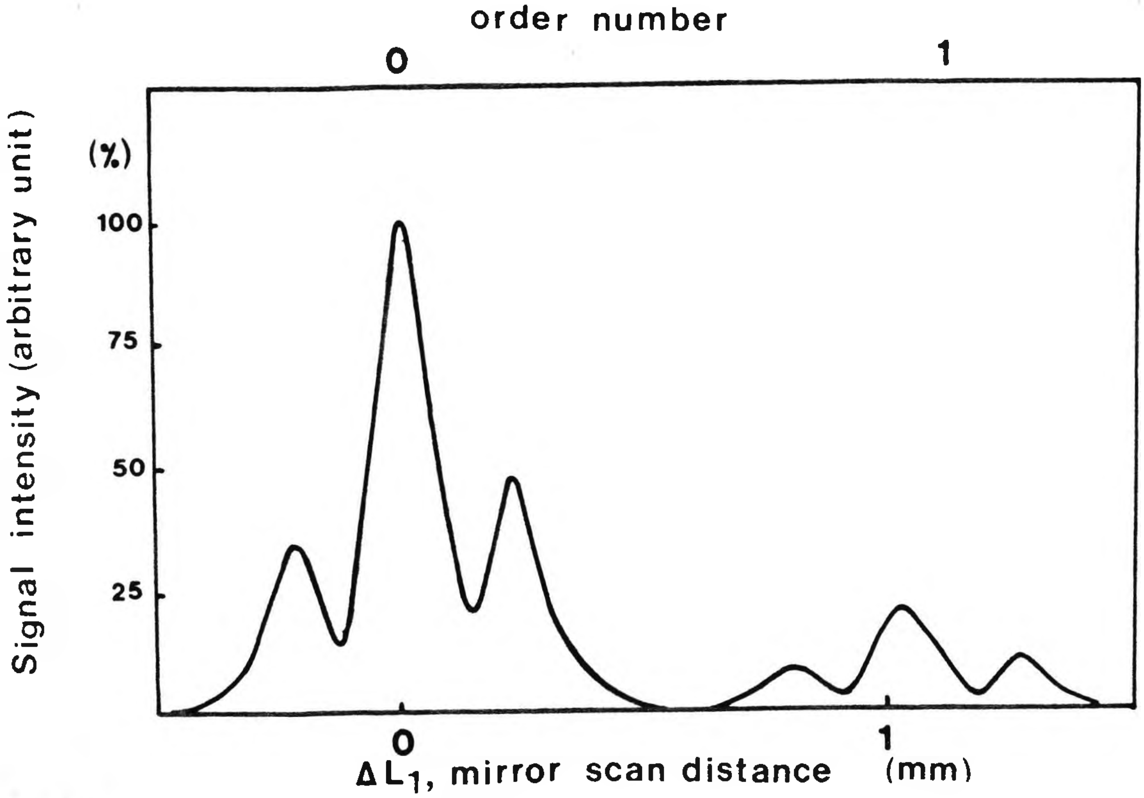

Figure 6.6. *Experimental results of the peak value of signal intensity (arbitrary unit) V ΔL_1 (mm) with Fabry-Perot interferometer in operation, showing sideband regions (ΔL_2=0.435 mm).*

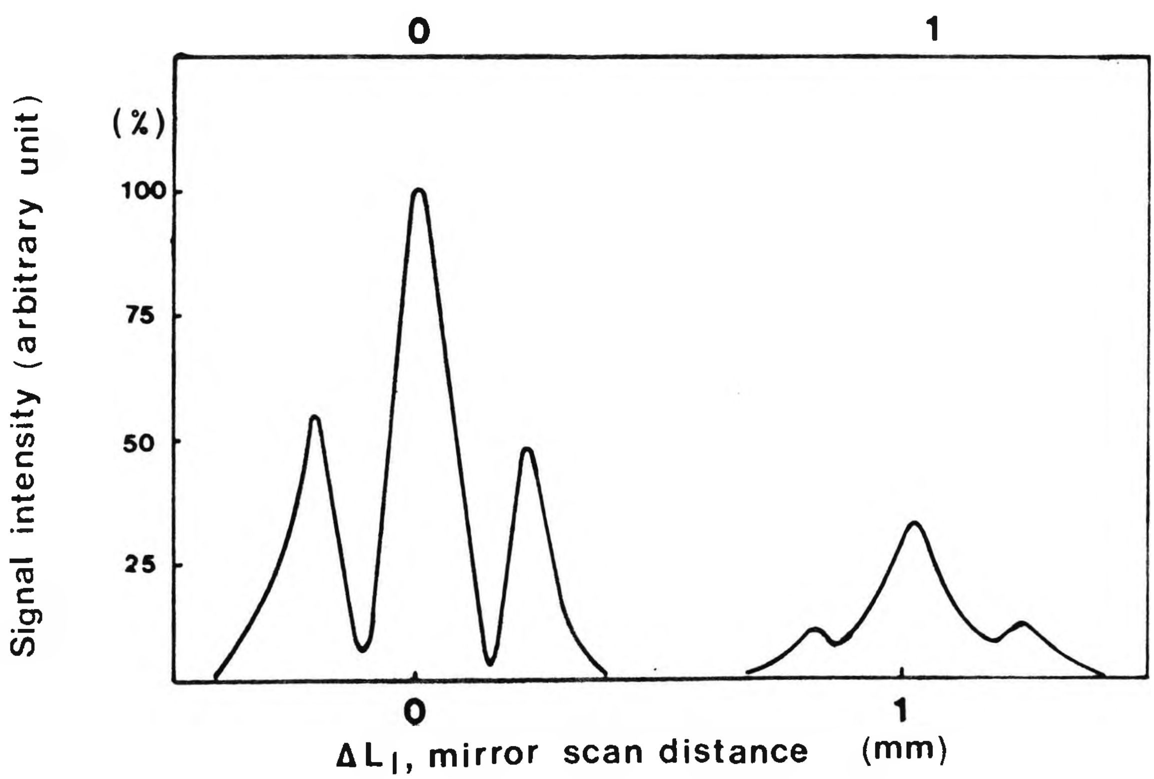

Figure 6.7. *Experimental results of the peak value of signal intensity (arbitrary unit) V ΔL_1 (mm) with Fabry-Perot interferometer in operation, showing sideband regions (ΔL_2 = 0.417mm).*

The phenomenon of the two sideband interference regions can be understood as follows. In the experimental arrangement shown in figure 6.8., the optical path difference (L_2) of the Fabry-Perot cavity is set to be greater than the coherence length (L_c) of the light source. Mirror M_1 in the Michelson interferometer is scanned from the left side of the balance position, O, to the right side. When mirror M_1 is scanned to the position A in figure 6.8., the optical path difference (L_1) is equal to or nearly equal to that of the Fabry-Perot cavity on the left side of its balanced position, i.e., $AO = L_1 \approx L_2$, the two conditions of generating superposed fringes, which are described in section 6.2., are met. Hence the two interferometers are both in operation and the fringes of superposition appear in the left sideband region.

If mirror M_1 is scanned to the position O, as shown in figure 6.8., where the optical path difference (L_1) of the Michelson interferometer is equal to zero or near zero, i.e., $L_1<L_c$, only the first interferometer is now in operation whilst the Fabry-Perot cavity is not because its optical path difference is larger than the coherence length, i.e., $L_2>L_c$. Therefore, the output interference fringes are generated by the Michelson interferometer only and, appear in the original central interference region.

As the mirror M_1 is scanned on the right side of the balanced point to reach the position B, where the two optical path differences are the same or nearly the same, i.e., $OB = L_1 \approx L_2$, the superposed fringes generated by both interferometers appear in the right sideband region.

Therefore, all the central interference regions are generated by the Michelson interferometer only, while all the sideband regions are generated by both the Michelson interferometer and Fabry-Perot cavity.

In a simulation of a real sensing application, a proposed interferometric optical fibre sensor is shown in figure 6.9c. By linking a cavity with a optical fibre interferometric sensor, the interference region can be effectively "shifted" from the zero order region which is around the end of the fibre to a position away from the fibre end, and the position of the shifted region is controlled by the value of the cavity thickness.

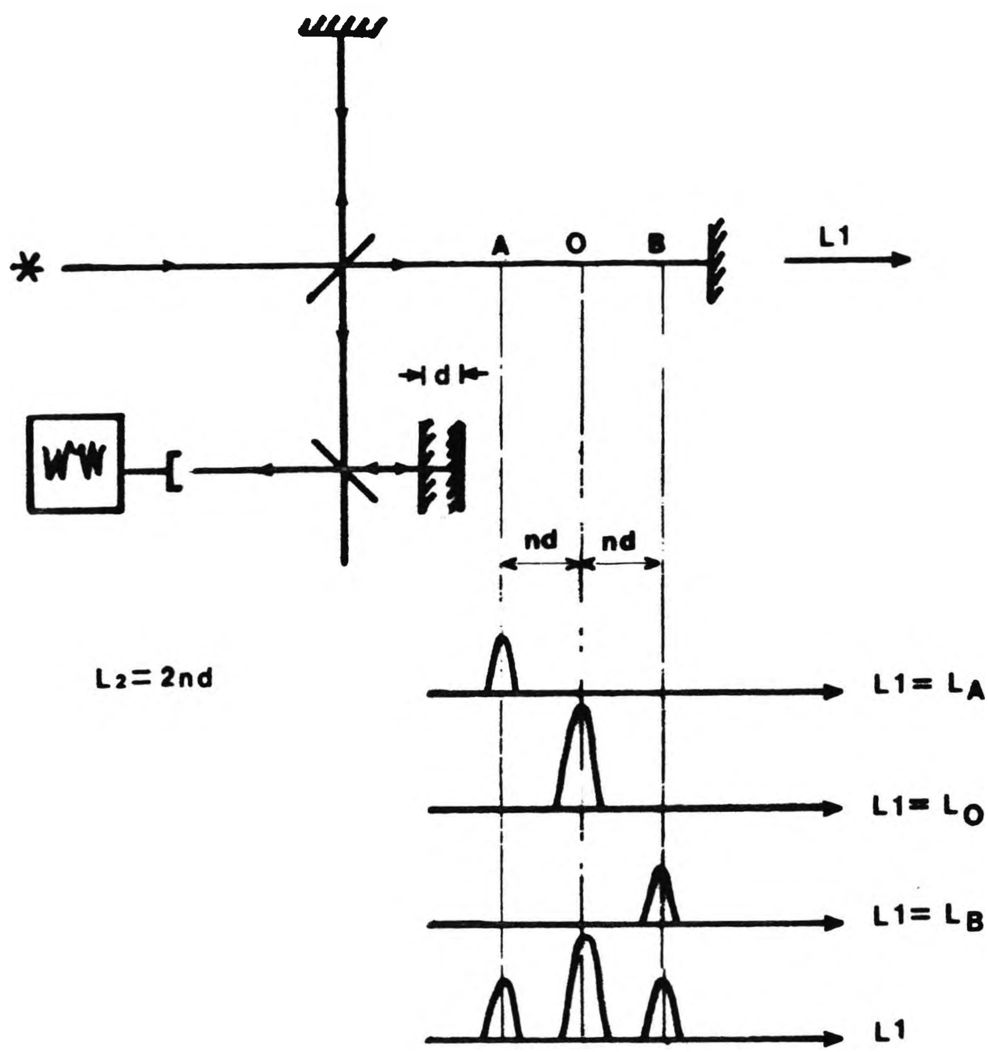

Figure 6.8. *Illustration of the positions of the interference regions when L_1 is scanned from positions A to B (L_2=2nd).*

Figure 6.9. shows comparative results of three different types of interferometers. Figure 6.9a shows an interferometer with a single mode laser light source, and the interference region of this interferometer cannot be defined. Figure 6.9b. shows the same interferometer but with a multimode laser diode light source, where the interference region may be defined by determining the order of the interfered region. For an interferometer as shown in figure 6.9c, which is a fibre version of the coupled interferometer shown in figure 6.1., apart from the original interference regions, some shifted regions can be seen. The position of these shifted regions can be controlled by the thickness of the linked cavity.

Utilising the theoretical model discussed earlier, the results shown experimentally as figures 6.6 and 6.7 were simulated. Two instances of this

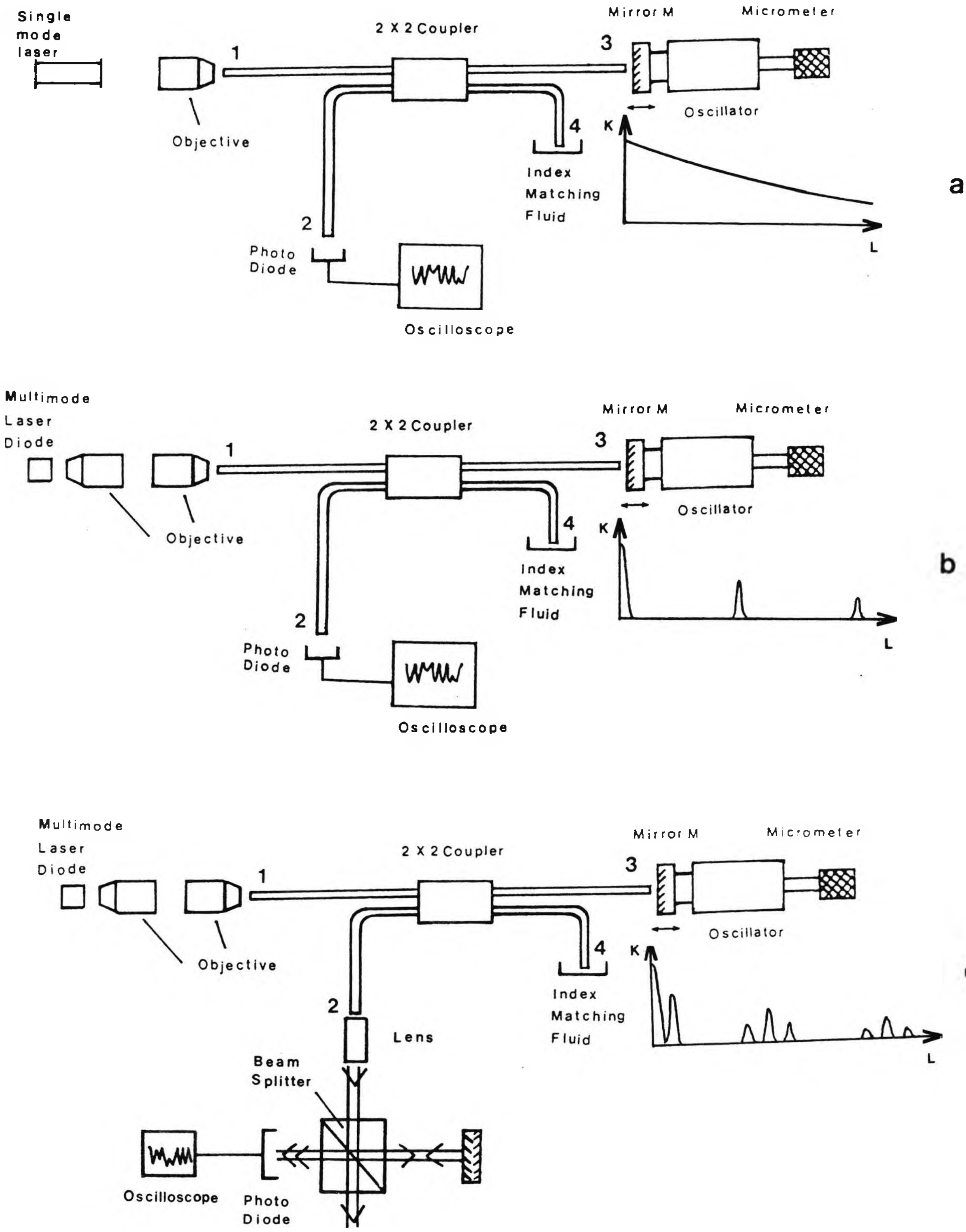

Figure 6.9. *The comparison of the output from different types of interferometers:*
(a) a single mode laser light source
(b) a multimode laser light source
(c) a multimode laser light source with a coupled cavity in operation.

are where L_1 is scanned from 0 to 2.75 mm and L_2 is set to 0.435 mm and 0.417 mm to reproduce the experimental conditions discussed earlier. In both cases agreement is seen in which the separation of the sideband from the centre band is given by the numerical value of L_2. The results are summarised in table 6.1 and illustrated, for the first case, in figure 6.10.

6.6. Discussion

As shown in Table 6.1, excellent agreement is seen between the experimental and theoretical results obtained. These results indicate that by changing the thickness of the Fabry-Perot cavity, the position of the sideband interference regions can be adjusted in a controlled and reproducible way. One of the purposes of the coherence length modulation

Table 6.1 *Comparison of theoretical & experimental results for separation of sideband from centreband*

Cavity Thickness (mm)	Optical Path Differences, L_2 (mm)	Average Separation of Sidebands from Centrebands (mm)	Implied Optical Path Difference (mm)	Average Separation of Sidebands from Centrebands (mm)
0.145	0.435	0.220	0.440	0.435
0.139	0.417	0.213	0.426	0.417

is to shift the interference region (sensing interferometer operating region) into the measurement volume, and the results reported here show a good agreement both theoretically and experimentally on the position of the shifted regions.

In spite of the close agreement on the position of the sidebands when the theoretical and experimental results are compared, the theoretical results do not explain the comparative intensities of the central peak and the sidebands. These figures, normalised to the peak value of the central band of the zero - order region, are shown in Table 6.2.

Table 6.2 *Theoretical & experimental results showing normalized intensities of central peaks & sideband.*

	Zero Order	First Order
Experiment (intensity)		
Central band	100	32
sideband (left)	54	10
sideband (right)	46	11
Theory (intensity)		
Central band	100	98
sideband (left)	50	49
sideband (right)	50	49

This discrepancy may partially be explained by the fact that the shape of the lasing mode itself is not fully taken into account in the theoretical model. If this is included, the peak values of the interference regions will drop, with an exponential envelope profile, which means that the peak value of the first order interference region in figure 6.10 will be less than that which would be shown by using a more accurate theoretical model.

Further, from an experimental point of view, any misalignment of the mirrors will reduce the peak intensities of the shifted interference regions and even a small misalignment can cause them to shrink to zero. This illustrates the importance of the parallelism of the two faces.

Finally, the reflectivity, R, of the Fabry-Perot cavity is also an important factor. Figure 6.11. shows a calculation of the relative intensities of the first sideband to the zero-order region as a function of the cavity reflectivity, R.

Thus good agreement between theory and experiment is observed and useful interference regions with the optical configuration employed are seen. The experimental results obtained in this work using a multimode laser diode as the light source device are not similar to those obtained previously using a narrow-band continuous spectral light source such as an LED. Both types of sources have their spectra contained under a Gaussian-type envelope, but the LED shows a spectral continuum. It is this spectrum

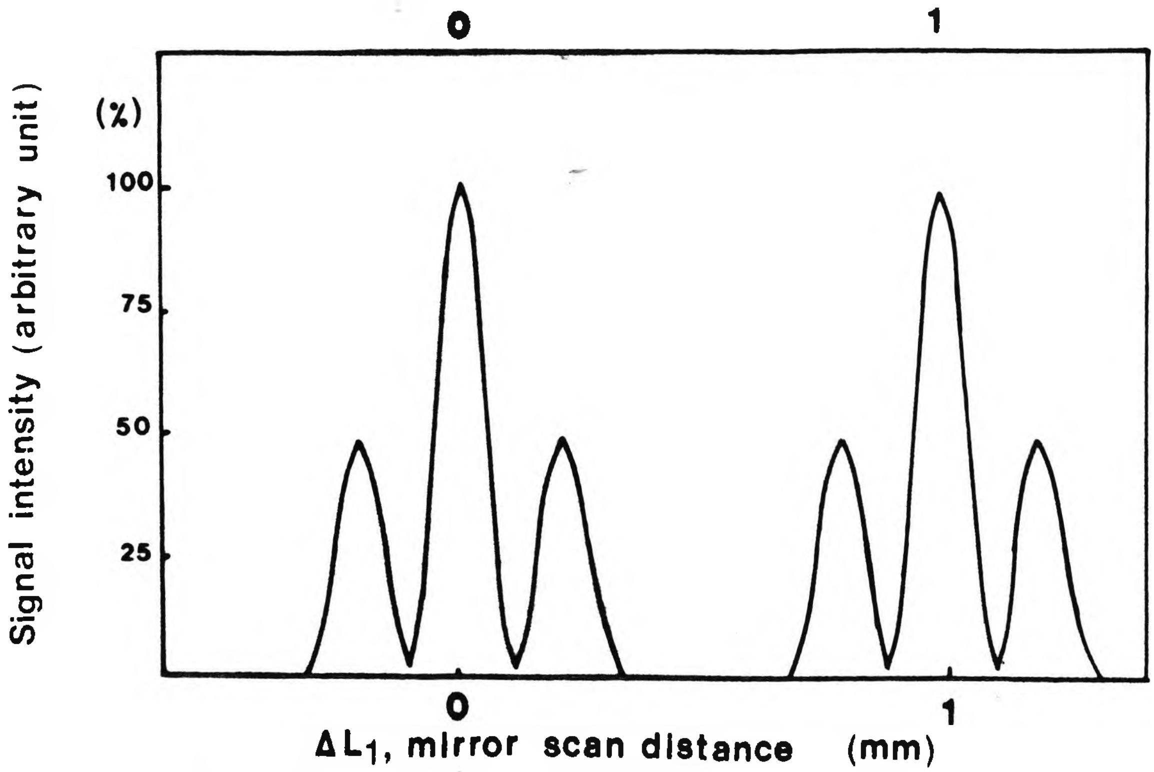

Figure 6.10. *Theoretical results of the peak value of signal intensity (arbitrary unit) v ΔL_1 (mm) with the Fabry - Perot cavity operational (the zero and first order interference regions), showing sideband regions (ΔL_2 = 0.435 mm).*

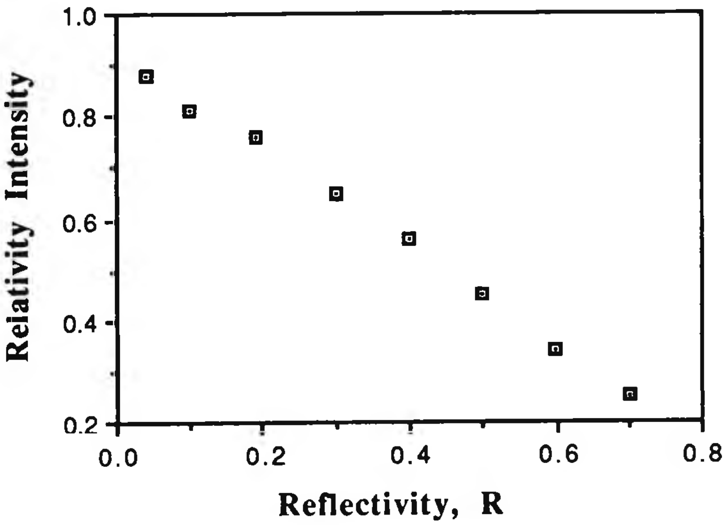

Figure 6.11. *The simulated relative intensities of the first sideband to the zero-order region as a function of the cavity reflectivity, R*

that limits the interference region. Only one interference region can be generated by the LED, while the spectrum of the multimode laser diode consists of a set of discrete spectral lines (~20), each having a Lorentzian line shape. The interference pattern of this light source is a comb shaped one, forming a set of interference regions. Because the spectral structures of two light sources are not the same, the outputs from the coupled interferometer are different. It is the spectral envelope shape that determines the profile of the interference region, while the fine spectral structures within this envelope modifies the spatial distribution of the interference pattern and the peak value. This is the consequence of one being the Fourier transform of the other. Therefore, the principal difference between the use of the two sources is that the multimode laser diode gives an output pattern with periodic interference regions and each region is companioned with two sideband regions on either side, whilst the interference pattern generated by an LED is a single original interference region accompanying with two sideband regions [9].

References:

[1] R.B. Dyott, "The fibre optic Doppler anenometer", IEE J. Microwaves Opt., Accurst 2 13, 1978

[2] T. Bosselmann "Multimode-Fibre Coupled White-light Interferometric position sensor" Optical Fibre Sensors NATO ASI Series, Series E: Applied Sciences No.132 pp.429-32, 1989

[3] R.Jones, M.Hazell and R.Welford "A genric Sensing System Based on Short Coherence Interferometry" pp.17-21, 1990

[4] M.Born and E.Wolf "Principles of Optics" Oxford University Press, pp.360-7, 1980

[5] S.A.Al-chalabi, B.Culshaw and D.E.N.Davies "Partially coherent sources in interferometric sensors" Proc. 1th Int. Conf. on Optical Fibre Sensors (London: IEE) pp.132-5, 1983.

[6] G.Beheim, K.Fritsch and N.R.Poorman "Fibre-linked Interferometric pressure sensor" Rev. Sci. Instrum. 58(9), pp.1655-9, 1987

[7] A.S.Gerges, F.Farahi, T.P.Newson, J.D.C.Jones, D.A.Jackson "Interferometric Fibre-optic Sensor using a short coherence-length source" Electron. Lett. Vol.23 No.21, pp.1110-1, 1987

[8] Y.N. Ning, K.T.V. Grattan, A.W. Palmer and B.T. Meggitt "Characteristics of multimode laser diode in a dual interferometer configuration", IEEE J. Lightwave Technology, 1773-8, 1990.

[9] D.A.Jackson "Monomode fibre optic interferometers and their application in sensing system" Optical Fibre Sensors, NATO ASI series, series E: Applied Sciences, 1-33, 1987.

Chapter 7

Coherence length modulation scheme based on a dual Michelson interferometer using a multimode laser diode

Abstract:

The use of a multimode laser diode in a dual Michelson interferometer arrangement is investigated, both theoretically and experimentally, using "coherence length modulation". A reproducible way of "shifting" interference regions is considered for the potential use of the scheme in optical sensors. The measurement volume of the sensor can be determined and shifted along the optical axis of the optical system. Since the second interferometer can be used to induce a carrier frequency signal, a heterodyne signal processing scheme can be employed to recover the sensing signal, and therefore, in the case of a dynamically changing measurand, the direction of the movement can be determined.

7.1. Introduction

In Chapter 6, the "coherence length modulation" scheme based on a coupled Michelson-Fabry Perot interferometer was introduced, and the characteristics of a multimode laser diode in this dual interferometer were described. It can be seen that by introducing the second interferometer, the working region of the first interferometer can be effectively shifted over a designed distance along the optical axis [1], and thus the measurement volume of the first interferometer can be shifted.

However, there are still two problems needed to be solved. The first is that the shifted distance, which is equal to half of the optical path difference of the second Fabry-Perot cavity [1], is fixed when the cavity is selected. The second is that the direction of the moving body or flow cannot be determined.

There are two possible methods to solve the first problem: one is by using a scannable Fabry-Perot cavity to change the optical path difference, and therefore, the position of the measurement volume. Another is to use a Michelson interferometer with one arm being scanned. This will introduce the variation of the optical path difference. The second problem can be solved by means of introducing a carrier frequency into the light beam as a reference frequency. This is the well-known heterodyne signal recovery scheme.

In order to change the shifted distance of the interference regions and to introduce the heterodyne signal recovery scheme, a coupled Michelson : Michelson interferometer experimental arrangement, shown in figure 7.1, was used to investigate the characteristics of a multimode laser diode in a dual Michelson interferometer. The theoretical and experimental results are described in this chapter. It can be seen that a more detailed study is obtained from this arrangement than was from the Michelson : Fabry-Perot interferometer discussed in Chapter 6. This is due to the fact that the optical path differences in the coupled Michelson : Michelson interferometers can be easily adjusted. Also, because the second interferometer can be modulated by an induced frequency signal, a heterodyne signal processing technique can be introduced to recover the sensing signal.

In section 7.2., the experimental arrangement employed in this work is described. A theoretical simulation of the dual interferometer shown in figure 7.1 is detailed in section 7.3. The experimental results are presented and discussed in section 7.4. Possible applications are suggested in the conclusion, section 7.5.

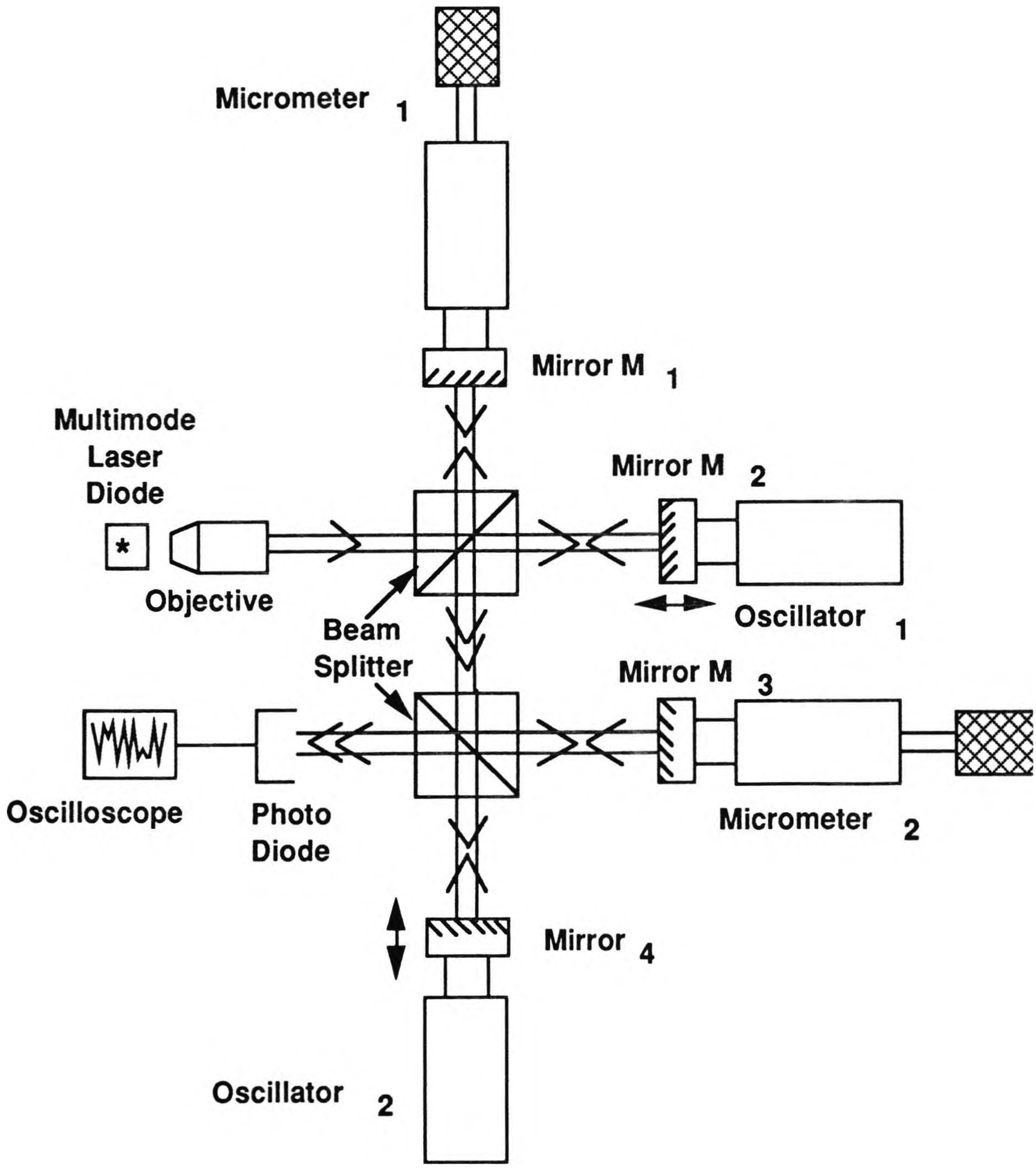

Figure 7.1. *Schematic optical arrangement of the dual coupled Michelson interferometer used in this work.*

7.2. Experimental arrangement

In figure 7.1., which shows the optical configuration employed in this work, the micrometers 1 and 2 were used to vary the optical path differences in the two Michelson interferometers. The oscillator 1 provides an input signal by vibrating the mirror M_2 which was attached to it. The second oscillator 2, associated with the second interferometer, was used to introduce a different frequency signal which can be considered as a carrier in the heterodyne demodulation technique. The light source employed in the arrangement is a multimode laser diode (SONY LT023) with a central wavelength of 780 nm. The driving current of the laser diode is 43.4 mA. The detector used in the experiment arrangement is a high sensitivity photodiode (HUV-1100BQ), manufactured by EG&G.

7.3. Theoretical considerations

In order to simulate the optical output of the dual coupled Michelson interferometer configuration, which is shown in figure 7.1, a mathematical model was developed, based on the assumptions used in section 5.3.2.

For light beams normal to the mirrors of the first Michelson interferometer, the optical path difference, ϕ_1, between the beams reflected from mirrors M_1 and M_2 is given by

$$\phi_1 = 2\pi \frac{2\Delta L_1}{\lambda_j} = 2\pi\sigma_j L_1 \tag{7.1}$$

where $\sigma_j = 1/\lambda_j$ (the wave number of the jth lasing mode) and ΔL_1 is the mirror scan distance, L_1 is the optical path difference introduced by the first interferometer. When the oscillator 2 is driven at the frequency of ω_s, L_1 can be written as:

$$L_1 = L_{10} + L_{1s} \sin(\omega_s t) \tag{7.2}$$

where L_{10} is the "static" optical path difference, and L_{1s} is twice the amplitude of the vibration of the mirror M_2. In the experiments, some part of the light energy, assumed for ease of calculation to be about 50%, emitted from the light source is reflected back to the light source which is due to the use of the beam splitter. This part of light energy can be omitted because it does not contribute to the detected signal. The amplitudes of the radiation electric fields are $A_o/2$, where Ao is the half of the amplitude of the electric field emitted from the light source. The corresponding radiation electric fields E_{j1} and E_{j2} from the two light beams in the first Michelson interferometer are given by:

$$E_{j1} = \left(\frac{A_o}{2}\right)\exp\left[-\pi\left(j\,\frac{\Delta\sigma}{\delta\sigma}\right)^2\right]\exp(i\omega t) \tag{7.3}$$

and

$$E_{j2} = \left(\frac{A_o}{2}\right)\exp\left[-\pi\left(j\,\frac{\Delta\sigma}{\delta\sigma}\right)^2\right]\exp(i\omega t + i\phi_1) \tag{7.4}$$

where $\Delta\sigma$ is the difference between adjacent model wave numbers of full width $\delta'\sigma$.

$\delta\sigma$ is the envelope full width of all the modes.

σ_j is the wave number of the jth lasing mode.

These laser modes are illustrated schematically in figure 5.2.

These radiation fields enter the second Michelson interferometer and are divided into two beams, with one yielding an optical phase difference, ϕ_2, introduced by the second interferometer, and given by

$$\phi_2 = 2\pi\,\frac{2\Delta L_2}{\lambda_j} = 2\pi\sigma_j L_2 \tag{7.5}$$

where ΔL_2 is the mirror scan distance, and $L_2 = 2\Delta L_2$ is the optical path difference of the second interferometer. When the oscillator 2 is driven at the frequency ω_r, L_2 can be written as:

$$L_2 = L_{20} + L_{2r}\sin(\omega_r t) \tag{7.6}$$

where L_{20} is the "static" optical path difference, and L_{2r} is twice the amplitude of the vibration on the mirror M_4. For the case when there is no light reflected from the second interferometer back to the first one, the electric fields received by the detector consist of four terms, which are:

$$E_{j1} = \left(\frac{A_o}{4}\right)\exp\left[-\pi\left(j\,\frac{\Delta\sigma}{\delta\sigma}\right)^2\right]\exp(i\omega t) \tag{7.7}$$

$$E_{j2} = \left(\frac{A_o}{4}\right)\exp\left[-\pi\left(j\,\frac{\Delta\sigma}{\delta\sigma}\right)^2\right]\exp(i\omega t + i\phi_1) \tag{7.8}$$

$$E_{j3} = \left(\frac{A_o}{4}\right)\exp\left[-\pi\left(j\,\frac{\Delta\sigma}{\delta\sigma}\right)^2\right]\exp(i\omega t + i\phi_2) \tag{7.9}$$

$$E_{j4} = \left(\frac{A_o}{4}\right)\exp\left[-\pi\left(j\,\frac{\Delta\sigma}{\delta\sigma}\right)^2\right]\exp[i(\omega t + \phi_1 + \phi_2)] \tag{7.10}$$

Hence the total radiation electric field for the jth lasing mode of the diode is given by

$$E_j = E_{j1} + E_{j2} + E_{j3} + E_{j4} \tag{7.11}$$

and the intensity is given by the product shown below

$$I_j = (E_{j1} + E_{j2} + E_{j3} + E_{j4})\,(E_{j1}^* + E_{j2}^* + E_{j3}^* + E_{j4}^*) \tag{7.12}$$

Substitution of equations 7.7. to 7.10. into the above 7.12. yields an expression for I_j as

$$I_j = I_o + I_1 + I_2 + I_3 + I_4 \tag{7.13}$$

where

$$I_o = \frac{A_o^2}{4}\exp\left[-2\pi\left(j\frac{\Delta\sigma}{\delta\sigma}\right)^2\right] \tag{7.14}$$

$$I_1 = \left(\frac{A_o^2}{4}\right)\cos(\phi_1)\exp\left[-2\pi\left(j\frac{\Delta\sigma}{\delta\sigma}\right)^2\right] \tag{7.15}$$

$$I_2 = \left(\frac{A_o^2}{4}\right)\cos(\phi_2)\exp\left[-2\pi\left(j\frac{\Delta\sigma}{\delta\sigma}\right)^2\right] \tag{7.16}$$

$$I_3 = \left(\frac{A_o^2}{8}\right)\cos(\phi_1 + \phi_2)\exp\left[-2\pi\left(j\frac{\Delta\sigma}{\delta\sigma}\right)^2\right] \tag{7.17}$$

and

$$I_4 = \left(\frac{A_o^2}{8}\right)\cos(\phi_1 - \phi_2)\exp\left[-2\pi\left(j\frac{\Delta\sigma}{\delta\sigma}\right)^2\right] \tag{7.18}$$

For all the 2m+1 modes, the total output of the detector is proportional to the total intensity, I, given by

$$I = \sum_{j=-m}^{+m} I_j \tag{7.19}$$

or

$$I = \sum_{j=-m}^{+m} I_o + \sum_{j=-m}^{+m} I_1 + \sum_{j=-m}^{+m} I_2 + \sum_{j=-m}^{+m} I_3 + \sum_{j=-m}^{+m} I_4 \tag{7.20}$$

The total intensity is given by the above five terms, representing the superposition of fringes. The first one gives only a DC term, while the others, under the different conditions, will give a different type of contribution to the interference patterns. For example, under the condition of L_2 being fixed and L_1 being scanned, the third summation in equation 7.20, $\sum_{j=-m}^{+m} I_2$, which is generated by the second interferometer only, will become a DC term, and the 2nd summation, $\sum_{j=-m}^{+m} I_1$, which represents the superposition fringes generated by the first interferometer only, gives the so-called original interference regions. The 4th and the 5th summations, $\sum_{j=-m}^{+m} I_3$ and $\sum_{j=-m}^{+m} I_4$, which represent the superposed fringes generated by both interferometers, give the shifted interference regions on both the left side and the right side of the original interference regions generated by the first interferometer.

It is these shifted reference regions that play the main roles in the coherence length modulation. Experiments were carried out and results are shown illustrating the performance of coherence length modulation using this dual coupled Michelson interferometer.

7.4. Experimental results and discussion

A number of experiments were carried out to study the performance of the coherence length modulation of the multimode laser diode under different conditions. In the experiments, the mirror M_2 in the first interferometer is driven at a frequency of 150 Hz by the oscillator 1, inducing a simulated input signal. The amplitude of the output signal, shown in figure 7.2, varies as the change of the mirror scan distance ΔL_1 or the optical path difference L_1, when the dual interferometer is set within the interference regions.

The conditions to generate the superposed fringes, described in chapter 6, are that the optical path differences (L_1, L_2) of the two interferometers are larger than the coherence length (L_c) of the light source used, i.e., $L_1 >> L_c$, $L_2 >> L_c$, and the difference between these two optical path differences is less than the coherence length, i.e., $|L_1 - L_2| < L_c$. Therefore, when the optical path difference of the first interferometer is changed by the scanning mirror M_2, the superposed fringes appear when the dual interferometer is working under these conditions (i.e. $L_1 >> L_c$, $L_2 >> L_c$ and $|L_1 - L_2| < L_c$) and do not appear when the dual interferometer does not meet these conditions. The output signal detected against the change of the optical path difference of the interferometer is recorded and plotted in figures 7.4 to 7.8.

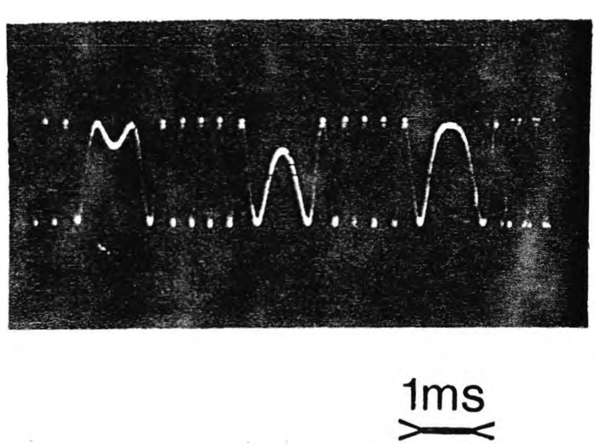

Figure 7.2. *Output signal generated by vibration of mirror M_2. (vertical scale: arbitrary unit).*

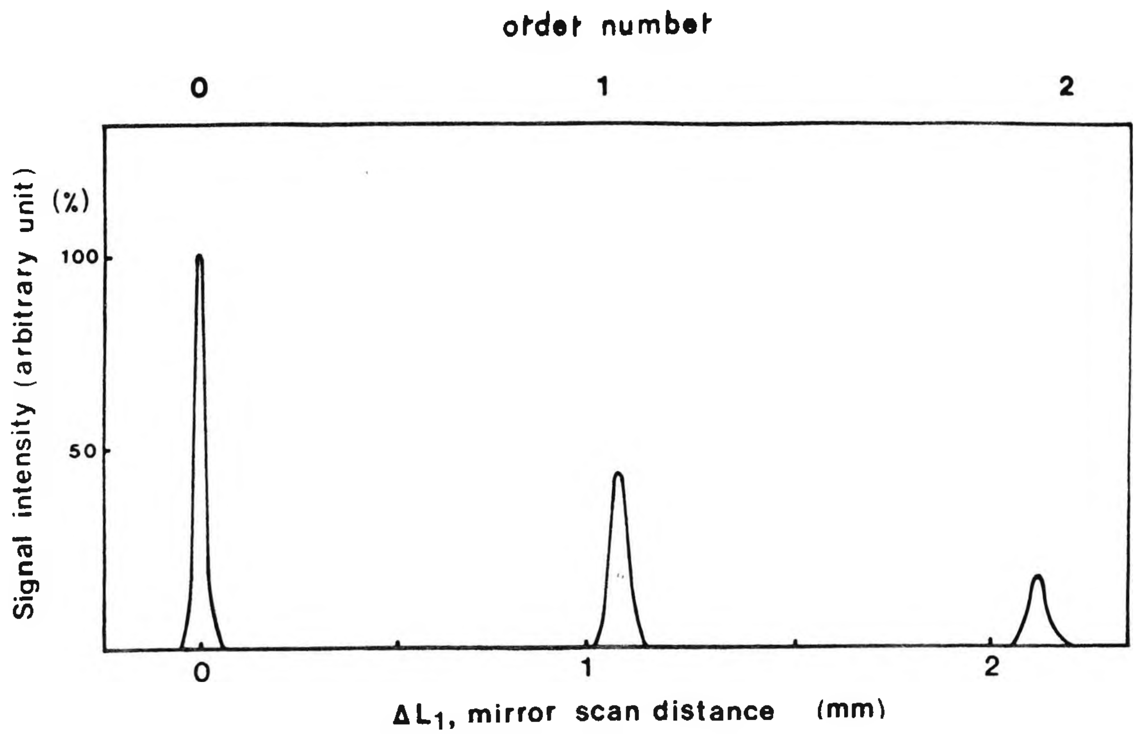

Figure 7.3. *Experimental results of the peak value of signal intensity (arbitrary unit) v ΔL_1 (mm) with ΔL_2 set to zero.*

Initially, ΔL_2 was set equal to zero, i.e., ϕ_2=0. The 3rd summation in equation 7.20 becomes a DC term, and the 2nd, 4th and 5th summations represent the superposed intensity generated by the first interferometer. Therefore the output signal amplitude varies as the change of ΔL_1, achieved by scanning with micrometer 1. Figure 7.3 shows detailed plots of optical output intensities when the mirror M_1 scans a distance ΔL_1 covered the zero, first and second original interference regions, which corresponds to the second, fourth and fifth summations in equation 7.20.

The optical path difference, L_2, of the second interferometer was then set equal to 0.3 mm. The mirror scan distance ΔL_1 is varied by adjusting the micrometer 1. Two "sideband" interference regions appearing about the original regions can be seen (figure 7.4), which illustrates the same phenomenon discussed in the chapter 6. In this case, both interferometers are in operation, and the intensity of the optical output is represented by the 2nd, 4th and 5th summations in equation 7.20. Figure 7.5 illustrates the details of the contributions from each summation. As shown in figure 7.5 the second interferometer is set at ΔL_2 = 2d, while the first interferometer is scanned from the left side of the balanced point, O, to the right side. The summation $\sum I_1$ gives the original interference regions; $\sum I_3$

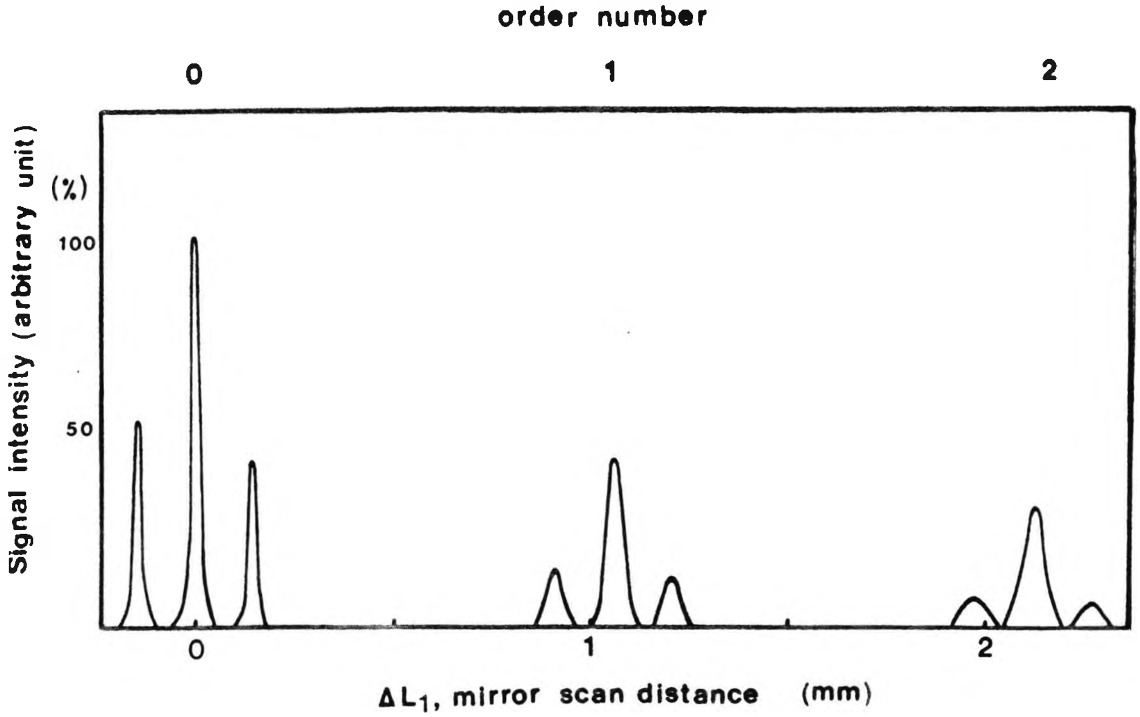

Figure 7.4. *Experimental results of the peak value of signal intensity (arbitrary unit) v ΔL_1 (mm) with ΔL_2 set to 0.3 mm.*

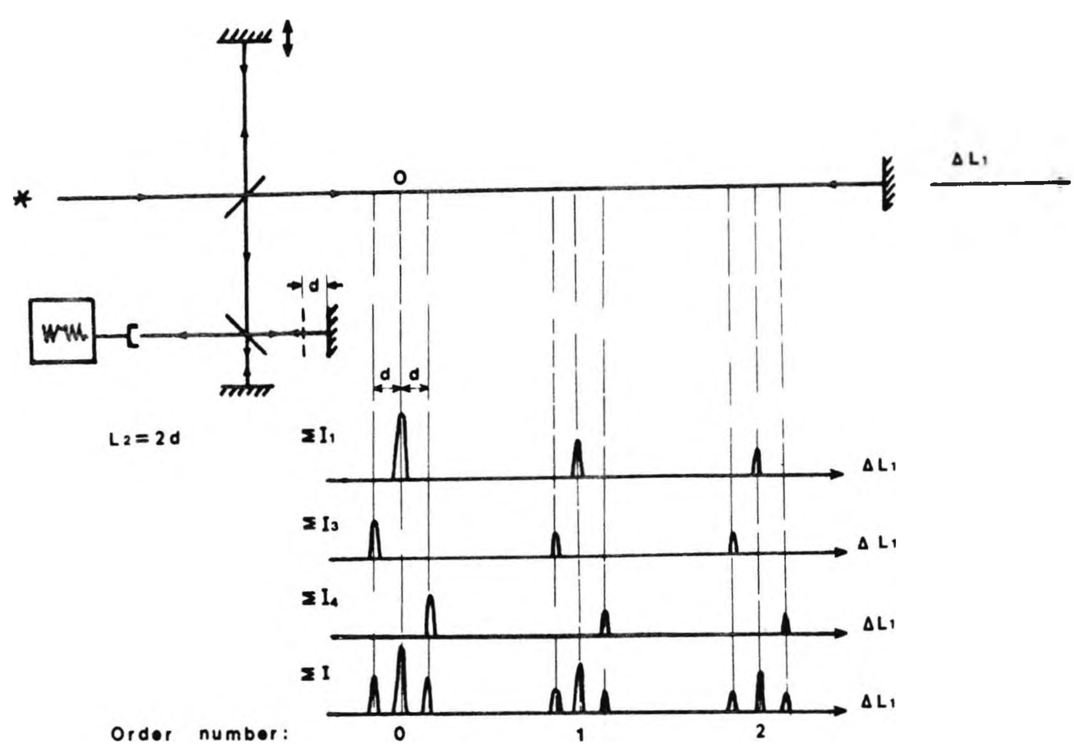

Figure 7.5. *The illustration of the interference regions with ΔL_2 = 2d and ΔL_1 is scanned. t*

and $\sum I_4$ give the left and right shifted regions respectively. The total intensity pattern is the one that each original interference region is accompanied by two shifted regions. This is the same result described in the section 6.5.

However, when ΔL_1 was fixed while ΔL_2 was changed by the micrometer 2, the signal induced by the vibrating mirror in the first interferometer cannot be detected in the original interference regions. It can however be detected in the two sideband or shifted interference regions, which are responding to the 4th and 5th summations in equation 7.20., i.e. $\sum I_3$ and $\sum I_4$, as shown in figure 7.6. The separation between each pair of the shifted interference regions was equal to ΔL_1. figures 7.6 and 7.7 show the output intensities obtained when ΔL_1 was set equal to 0.2 mm and 0.4 mm respectively. Figure 7.8 shows the intensity contributions of the 4th and 5th summations in equation 7.20. In this case, the 2nd summation becomes a DC term due to $L_1=d>L_c$, while the 3rd summation becomes a DC term as well, as` there is no induced vibrating signal in the second interferometer. These results illustrate the fact that the superposed fringes inside the original interference regions were generated by the first

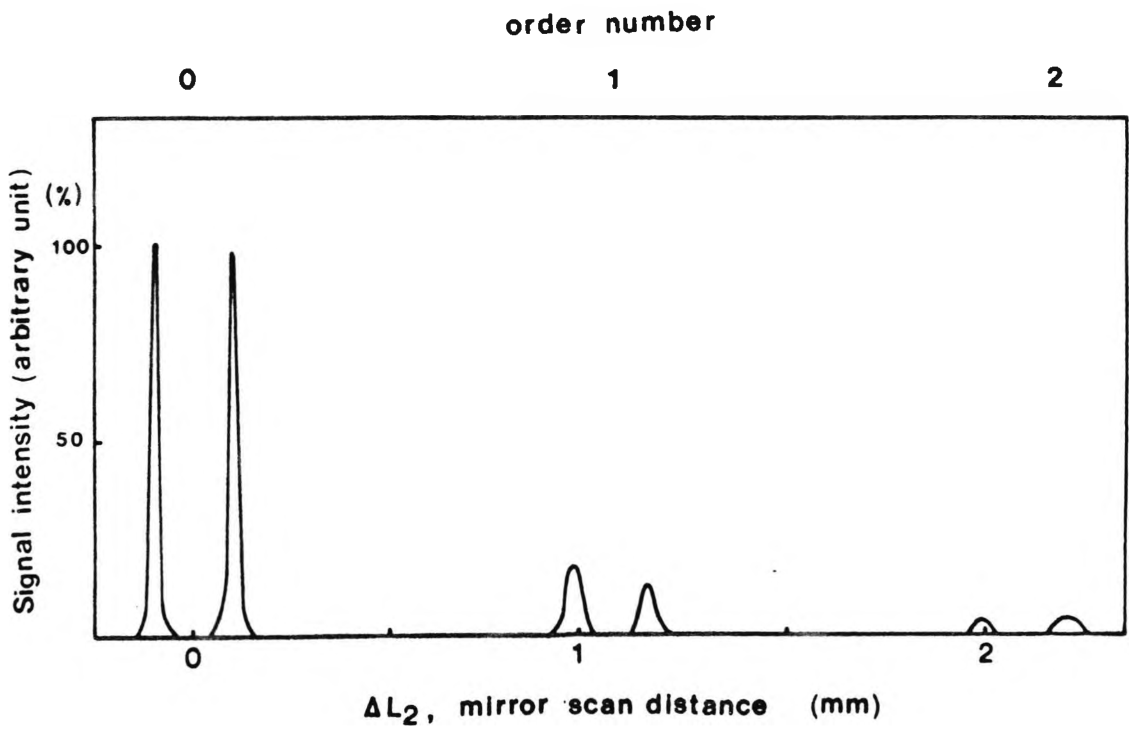

Figure 7.6. *Experimental results of the peak value of signal intensity (arbitrary unit) v ΔL_2 (mm) with ΔL_1 set to 0.2 mm.*

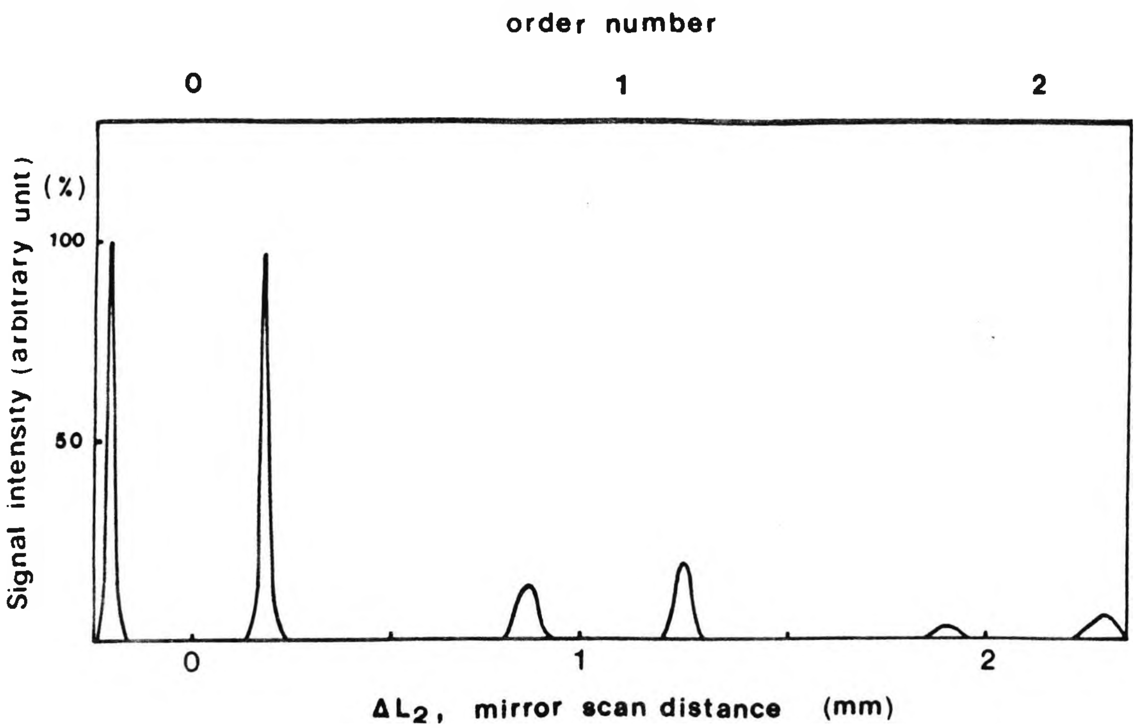

Figure 7.7. *Experimental results of the peak value of signal intensity (arbitrary unit) v ΔL_1 (mm) with ΔL_2 set to 0.4 mm.*

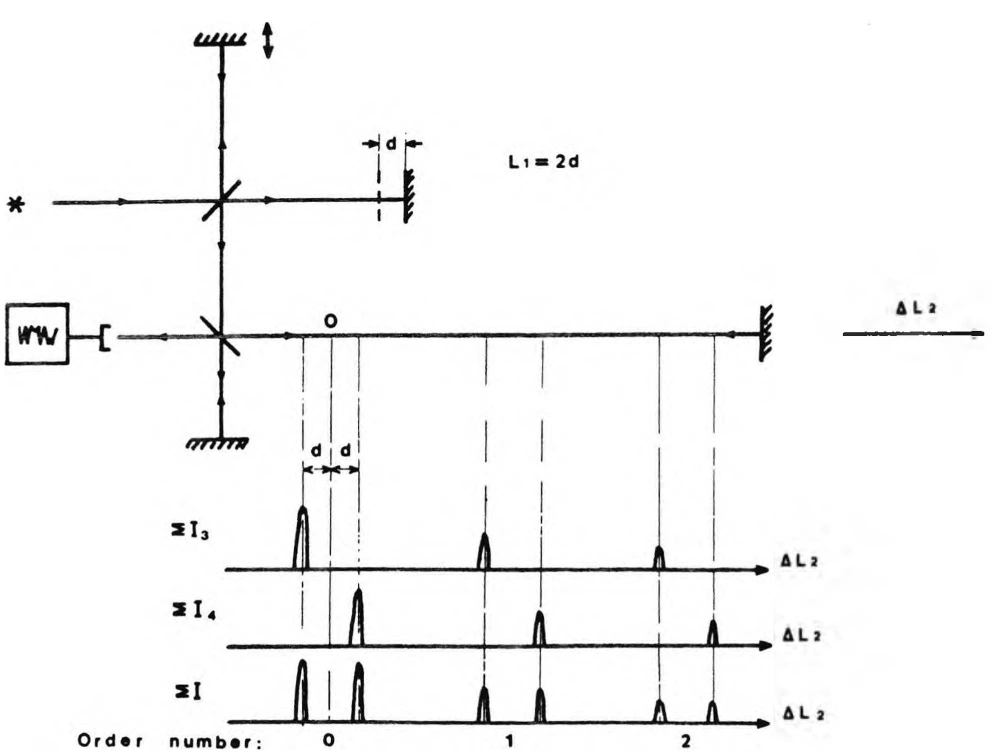

Figure 7.5. *The illustration of the interference regions with ΔL_1 = 2d and ΔL_2 is scanned. t*

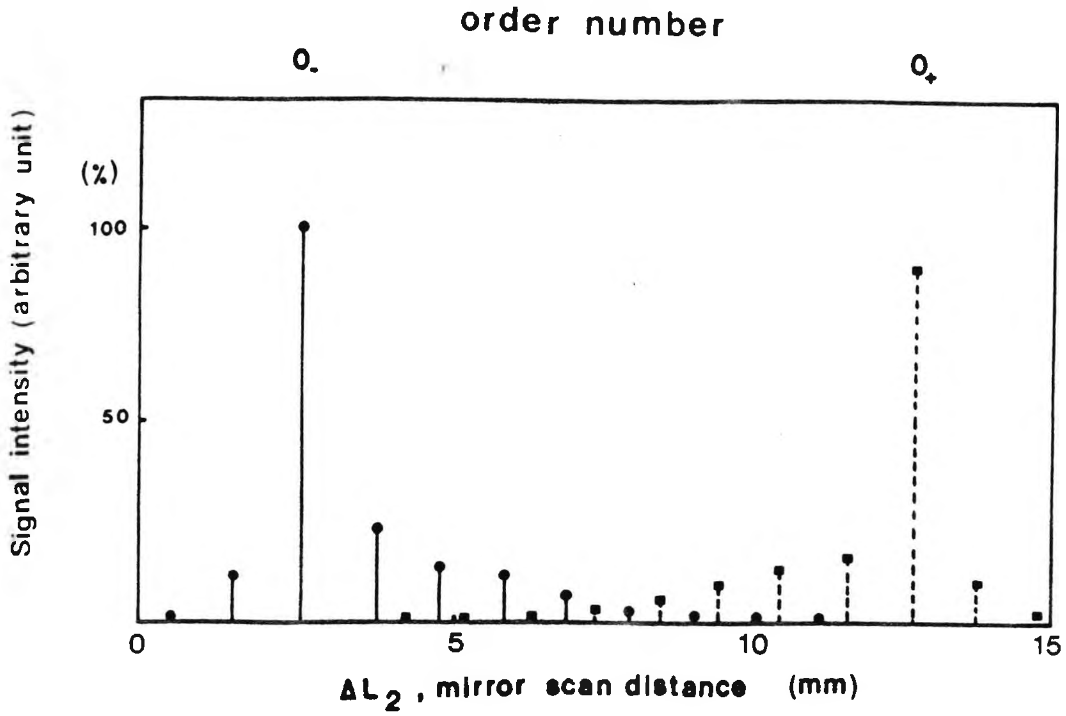

Figure 7.9. *Experimental results of two sets of the peak value of the interference regions (arbitrary unit) v ΔL_2 (mm), with ΔL_1 set equal to 10 mm.*

interferometer only, and the two sideband regions were the result of the interaction between coupled interferometers. It is clear that the positions of the shifted interference regions can be easily designed by setting the "offset" optical path difference in one of the two interferometers. Figure 7.9 shows a plot of two sets of peak amplitudes of the shifted interference regions with L_1 set to 10 mm. It should be noted that the greatest intensity is concentrated on the two central regions, and this means that the dominant measurement region can be easily defined.

Figure 7.10 shows the peak value of the interference region shifted from the zero order region changes as a function of the "offset" optical path difference or the shifted distance, which illustrates that this shifted distance can be as large as a few millimetres.

In order to investigate the possibility of using a heterodyne signal recovery technique, oscillator 2 is used to drive mirror M_4 at an arbitrary frequency, chosen to be 200 Hz, while L_1 is set to 0.2 mm and M_2 is vibrating at a frequency of 125 Hz. Figures 7.11 and 7.12 show the output signals when the first and the second interferometer are operating separately.

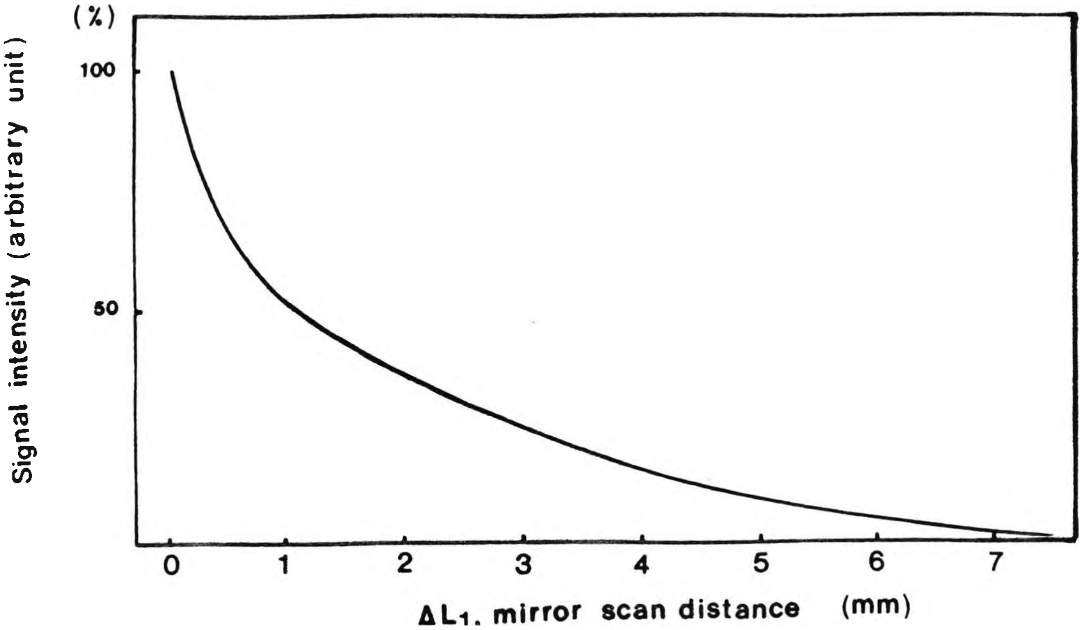

Figure 7.10. *Experimental results of the peak value of the interference regions (arbitrary unit) shifted from the zero order v the optical path difference induced by the interferometer.*

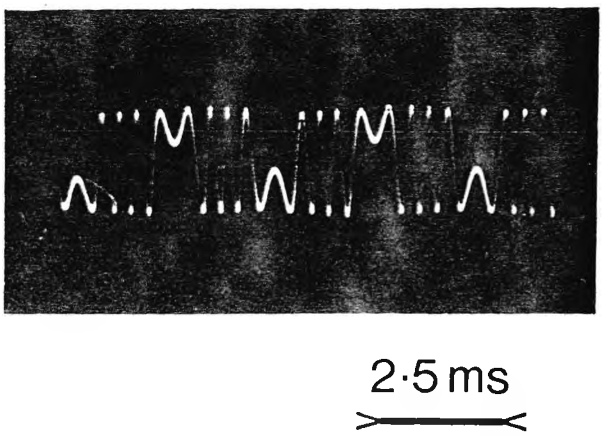

Figure 7.11. *Optical interference signal recorded on the photodiode in the first interferometer (Vertical scale: arbitrary unit).*

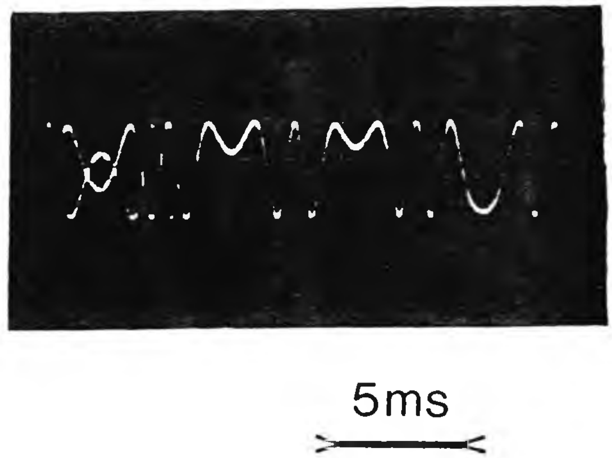

Figure 7.12. *Optical interference signal recorded on the photodiode in the second interferometer (Vertical scale: arbitrary unit).*

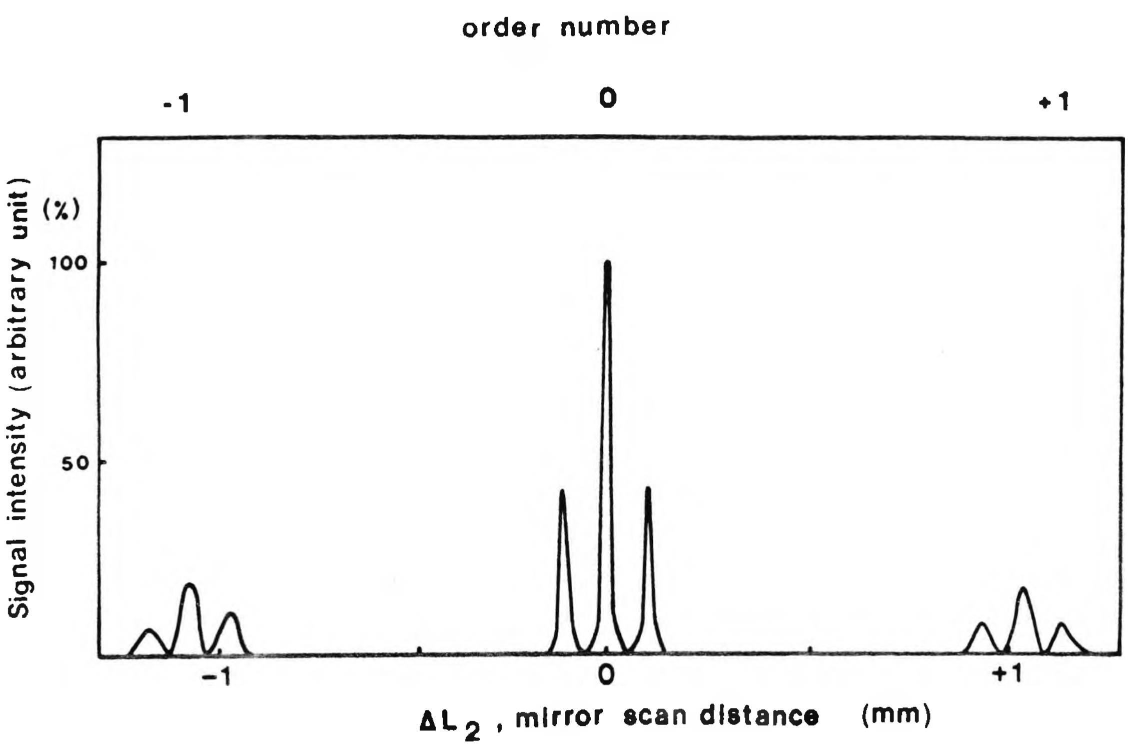

Figure 7.13. *Experimental results of the peak value of signal intensity (arbitrary unit) v ΔL_2 (mm) with ΔL_1 set to 0.2 mm, and the first oscillator working at a frequency of 125 Hz, the second one at 200 Hz.*

Figure 7.13 illustrates the details of the zero and first order interference regions (both negative and positive, lying on either side of the zero order region). The difference between the results shown in figure 7.4 and in figure 7.13 is that the former illustrates the same output signal (figure 7.2) for all the original and the shifted interference regions, i.e., the output signal received in all the interferometer regions is generated by the vibration of M_2 only; whilst in the second one, the output signal caused by the vibration of M_2 only appears in the original interference regions, and in the shifted regions, the signal shows a phase modulation (figure 7.14) which is generated by the vibrations of M_2 and M_4.

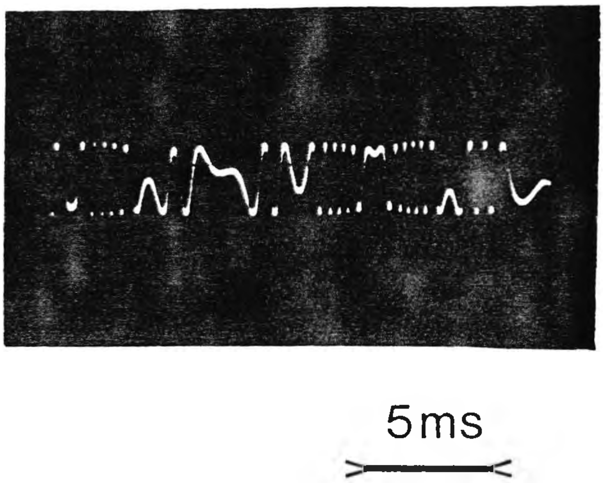

Figure 7.14. *Optical interference signal recorded on the photodiode in the shifted regions (Vertical scale: arbitrary unit).*

7.5. Conclusion

From the experiment results shown above, it can be seen that:

(a) the superposed fringes in the original interference regions are generated by the first interferometer only, which respond to the second summation in equation 7.20.

(b) the superposed fringes in the shifted interference regions are the results of the interaction between the two coupled interferometers, and therefore, those fringes carry information on the optical path differences in both interferometers.

(c) a heterodyne signal can be achieved in the shifted interference regions by introducing a high carrier frequency signal in the second interferometer.

(d) the characteristics of the multimode laser diode in the coupled Michelson interferometers may be exploited to develop a different kind of sensors for flow speed or distance measurement. However, care must be taken to avoid using the original interference region as a shifted region, where the heterodyne signal will become unstable. This can be explained by the fact that if a shifted region is overlapped with an original region, the coherence lengths of the both two interferometers are less than the that of the multimode diode, i.e., $L_1 < L_c$ and $L_2 < L_c$, thus both interferometers are in the operating region, the sensitivity of the whole system will be double of that of a single interferometer. A slight disturbance from outside will cause a signal change.

The performance of coherence length modulation of a multimode laser diode in a dual Michelson interferometer configuration was presented, both experimentally and in terms of a theoretical analysis. A repeatable and controllable way of "shifting" interference regions to a designated region can be achieved through the use of the coherence length modulation technique [2]. The possibility of employing an ordinary heterodyne demodulation method was shown, and the further application of this scheme are described in the chapter 8 and 9.

References

[1] Y.N. Ning, K.T.V. Grattan, A.W. Palmer and B.T. Meggitt "Characteristics of multimode laser diode in a dual interferometer configuration", IEEE J. Lightwave Technology, 8, 1773-8, 1990.

[2] Y.N. Ning, K.T.V. Grattan, A.W. Palmer and B.T. Meggitt "Coherence length modulation of a multimode laser diode in a dual Michelson interferometer configuration", Appl. Opt. 31, 1332-7, 1992.

Chapter 8

Proposes for an optical fibre sensor for velocity and vibration measurement

Abstract

In this chapter, an arrangement for a new sensing scheme using the coherence length modulation of a multimode laser diode is proposed and described. The optical fibre sensor based upon this scheme can be used for velocity and vibration measurement. The basic optical configuration used in this scheme is a dual Michelson interferometer which has already been described in the chapter 7. By the use of a Bragg cell in the second interferometer, a carrier frequency was induced into one light beam. Therefore, a heterodyne output signal from this dual interferometer can be generated. The measurement of flow movement or mechanical vibration can then be determined through the use of conventional electronic techniques.

8.1. Introduction

Based upon the results obtained on the dual Michelson interferometer, a new sensing scheme can be developed to built an optical fibre sensor which may be used in flow or vibration measurements. In Section 8.2, the basic configuration and the theoretical analysis of this optical fibre sensor proposed are described. The "proof-of-principle" studies on using this sensor in flow and vibration measurements are presented in Sections 8.3 and 8.4. This chapter ends with the conclusion section 8.5.

8.2. The basic configuration of the proposed OFS and its theoretical background

8.2.1. The basic configuration of the proposed OFS

Figure 8.1. shows the optical configuration of the proposed optical fibre sensor, which is actually a coupled dual Michelson interferometer. In the first fibre interferometer, light reflected from the fibre end interferes with that reflected from moving objects which can be either scattering particles in flow measurement or a vibrating surface in a vibration measurement. Because the reflectivity of the fibre end is very small, about 4% of the injected optical intensity, the multiple reflections between the fibre end and moving object are very weak, and thus, this element may be considered as a Michelson interferometer.

Since a common mode design was employed in this configuration, i.e., both reference and signal beams travel the same optical path, the problem of phase perturbation induced by environmental effects such as temperature and pressure changes can be considerably minimised. In order to obtain directional information on the moving target, a Bragg cell is employed to induce a carrier frequency or a reference frequency into one of the light beams in the second interferometer, forming a heterodyne signal at the output of the sensor. Another function of the Bragg cell is to serve as a beam splitter.

In order to verify the basic operating concepts of the proposed optical fibre sensor, an optical experimental system was constructed and shown in figure 8.2. This is a bulk-optic-component version of the proposed optical fibre sensor shown in figure 8.1.

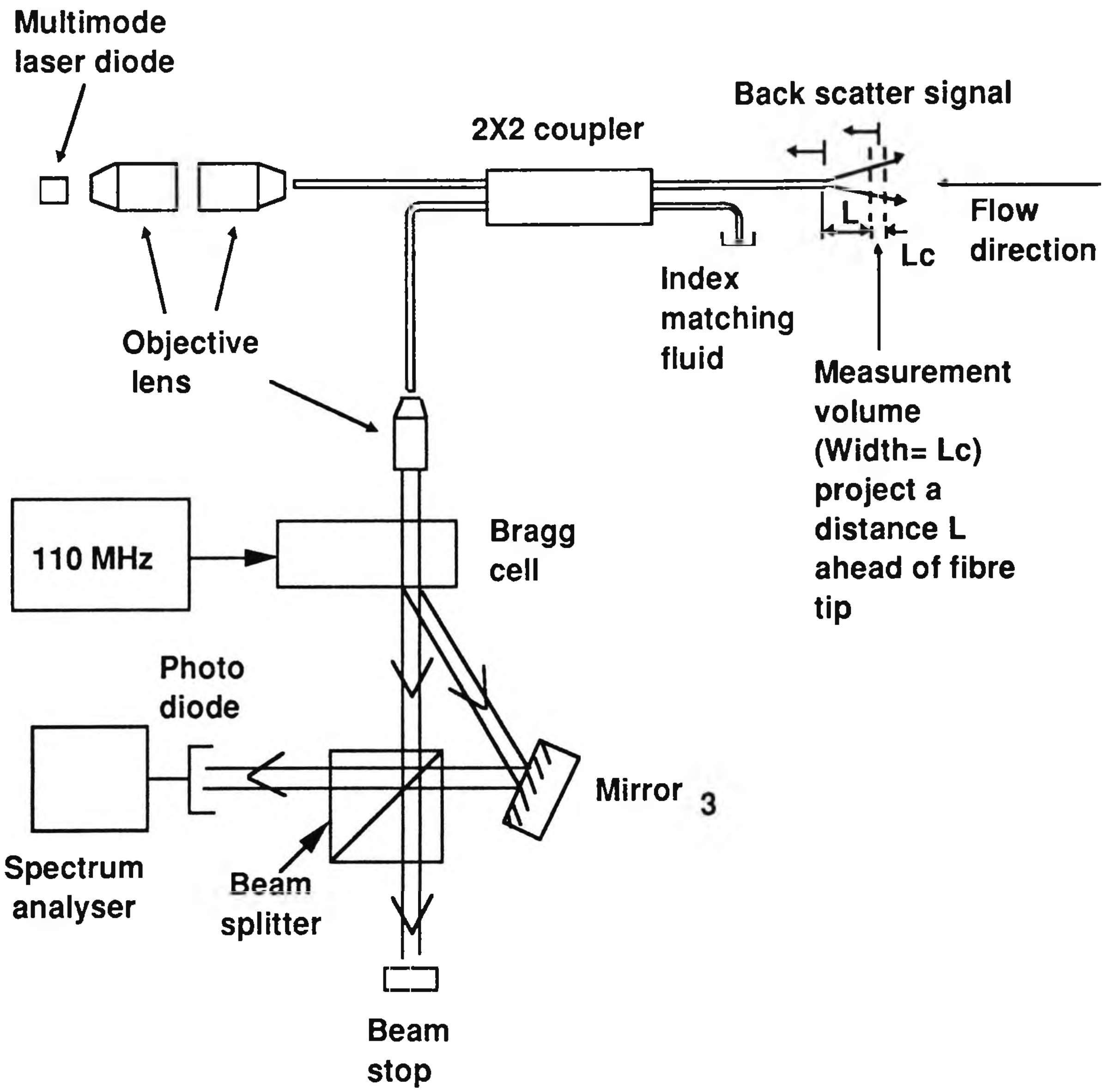

Figure 8.1. *Schematic optical arrangement, using optical fibres, proposed in this work.*

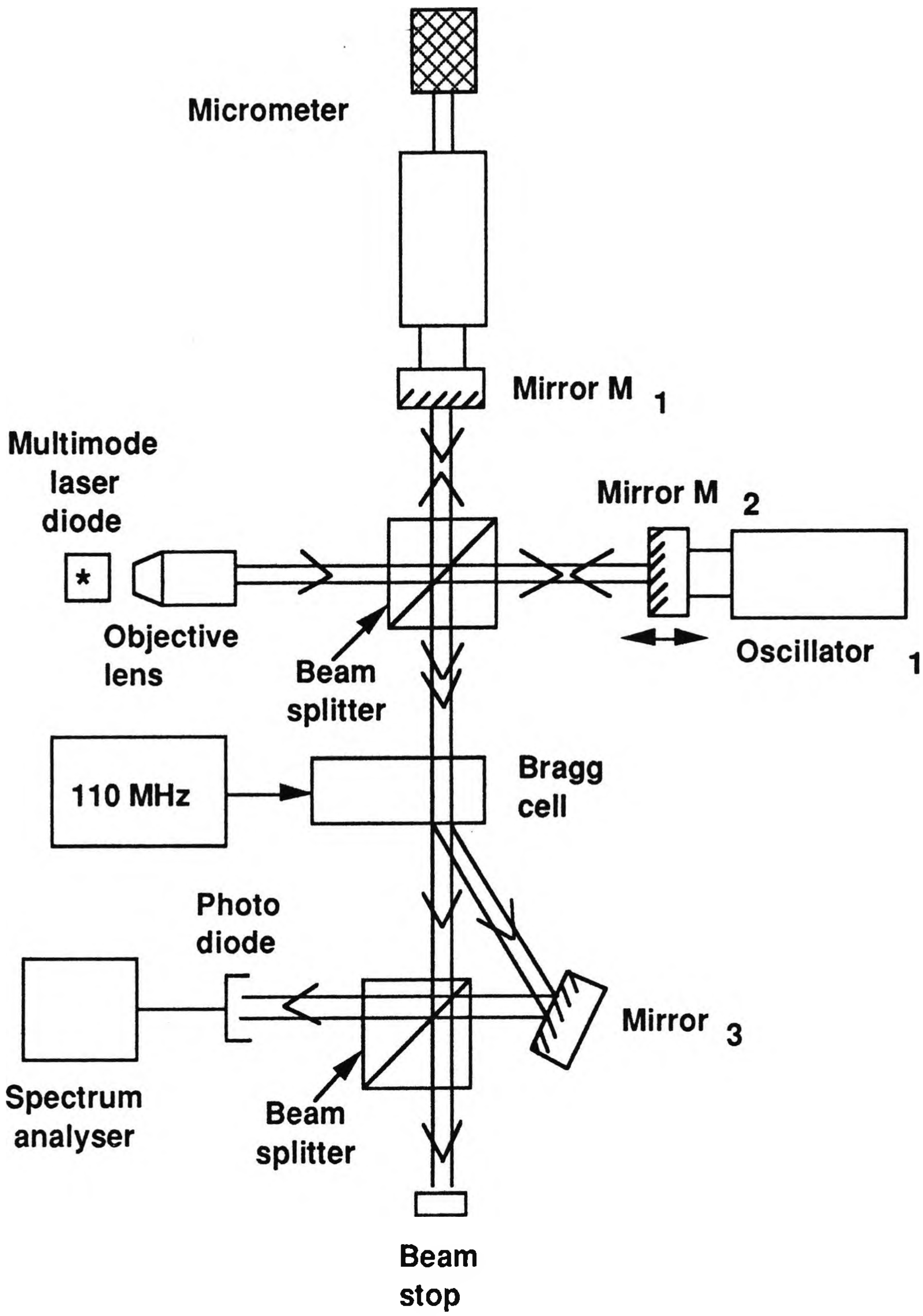

Figure 8.2 *Schematic optical arrangement of the coupled Michelson : Bragg cell interferometer used in this work.*

As shown in figure 8.2, the first interferometer, the Michelson sensing interferometer, is used to introduce the signal simulating the sensing effect, and the second interferometer, consisting of a Bragg cell, a beam splitter and a mirror, is employed as a recovery interferometer to introduce an off-set imbalance (4.25 mm) and a modulation at the frequency of 110 MHz in one arm. The mirror, M_1 in the first interferometer can be scanned by a micrometer, while the mirror M_2 attached to a loud speaker is driven by an oscillator with a sawtooth waveform at the frequency of 400 Hz, which is shown in figure 8.3. A multimode laser diode (SONY LT023, the central wavelength is 780 nm) was used as the light source, having a coherence length of about 200 μm in the zero order of the interference region. The optical output of the Michelson interferometer was coupled to the Bragg cell interferometer. The output signal is then detected by a high speed avalanche photo diode (APD) detector (Antel). The electronic signal from the detector was analysed with a spectrum analyser.

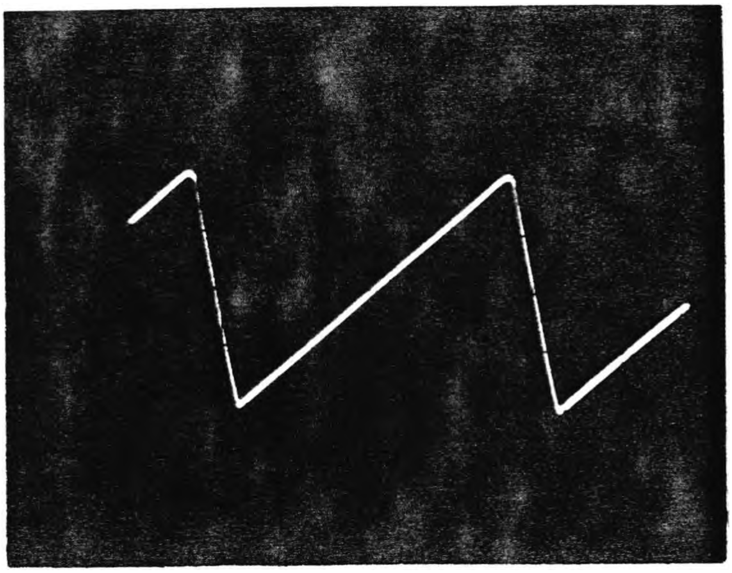

Figure 8.3. *Electrical input signal to the oscillator driving mirror M_2 (Period of waveform is 2.5 ms).*

8.2.2. The theoretical analysis

A simulation of the optical output characteristics of the configuration shown in figure 8.2. was made by constructing a mathematical model which is based on the assumptions discussed earlier in section 5.3.2.

For the beams normal to the mirrors of the first interferometer, the phase difference, ϕ_1, between the beams reflected from mirror M_1 and M_2 is given by:

$$\phi_1 = 2\pi\,(2\Delta L_1)/\lambda_j = 2\pi\,\sigma_j\,L_1 \qquad (8.3)$$

where σ_j, is the wave number of the jth lasing mode, i.e., $\sigma_j = 1/\lambda_j$ and $2\Delta L_1$ is the optical path difference introduced by the first interferometer, given by L_1.

When a signal from or simulating a sensor input is applied to mirror M_2, inducing a vibration at a frequency of ω_s, L_1 can be written as:

$$L_1 = L_{10} + L_{1s} \sin(\omega_s t) \tag{8.4}$$

where L_{10} is the "static" optical path difference, and L_{1s} is twice the amplitude of the vibration of the mirror M_2. The electric fields, E_{j1} and E_{j2}, generated by the jth lasing mode are reflected by mirrors 1 and 2, and given by

$$E_{j1} = \frac{A_o}{2} \exp\left[- \pi \left(j \frac{\Delta\sigma}{\delta\sigma} \right)^2 \right] \exp(i\omega t) \tag{8.5}$$

$$E_{j2} = \frac{A_o}{2} \exp\left[- \pi \left(j \frac{\Delta\sigma}{\delta\sigma} \right)^2 \right] \exp[\, i(\omega t + 2\pi \, \sigma_j \, L_1) \,] \tag{8.6}$$

where $A_o/2$ is the half amplitude of the incident radiation.

$\Delta\sigma$ is the difference between adjacent modal wave numbers of full width $\delta'\sigma$.

$\delta\sigma$ is the envelope full width of all the modes.

σ_j is the wave number of the jth lasing mode.

This was illustrated schematically earlier in figure 5.3.

These radiation fields enter the Bragg cell and two beams emerge, one at the fundamental optical frequency and the other having a frequency change due to the effect of the Bragg cell. Hence the optical electric fields received by the detector consist of four components which are:

$$E_{j1} = \frac{A_o}{4} \exp\left[- \pi \left(j \frac{\Delta\sigma}{\delta\sigma} \right)^2 \right] \exp(i\omega t) \tag{8.7}$$

$$E_{j2} = \frac{A_o}{4} \exp\left[- \pi \left(j \frac{\Delta\sigma}{\delta\sigma} \right)^2 \right] \exp[\, i(\omega t + \phi_1) \,] \tag{8.8}$$

$$E_{j3} = \frac{A_o}{4} \exp\left[- \pi \left(j \frac{\Delta\sigma}{\delta\sigma} \right)^2 \right] \exp[\, i(\omega t + \phi_2 + \omega_b t) \,] \tag{8.9}$$

$$E_{j4} = \frac{A_o}{4} \exp\left[- \pi \left(j \frac{\Delta\sigma}{\delta\sigma} \right)^2 \right] \exp[\, i(\omega t + \phi_1 + \phi_2 + \omega_b t) \,] \tag{8.10}$$

where ω_b is the Bragg cell frequency, ϕ_2 is the phase difference caused by the second interferometer and given by

$$\phi_2 = 2\pi \, (2\Delta L_2)/\lambda_j = 2\pi \, \sigma_j \, L_2 \tag{8.11}$$

L_2 is the OPD of the second interferometer. Hence the total radiation electric field for the jth lasing mode of the laser diode is composed of a series of components i.e.:

$$E_j = E_{j1} + E_{j2} + E_{j3} + E_{j4} \tag{8.12}$$

and the intensity so represented is given by the product shown below in equation 8.13., i.e.

$$I_j = (E_{j1} + E_{j2} + E_{j3} + E_{j4})\,(E_{j1}^* + E_{j2}^* + E_{j3}^* + E_{j4}^*) \tag{8.13}$$

Substitution of equations from 8.7 to 8.10 into the equation 8.13 yields an expression for I_j, which is:

$$I_j = I_o + I_1 + I_2 + I_3 + I_4 \tag{8.14}$$

where

$$I_o = \frac{A_o^2}{4} \exp\left[-2\pi \left(j \frac{\Delta\sigma}{\delta\sigma} \right)^2 \right] \tag{8.15}$$

$$I_1 = \frac{A_o^2}{4} \cos(\phi_1) \exp\left[-2\pi \left(j \frac{\Delta\sigma}{\delta\sigma} \right)^2 \right] \tag{8.16}$$

$$I_2 = \frac{A_o^2}{4}\cos(\omega_b t + \phi_2)\exp\left[-2\pi\left(j\frac{\Delta\sigma}{\delta\sigma}\right)^2\right] \tag{8.17}$$

$$I_3 = \frac{A_o^2}{8}\cos(\omega_b t + \phi_2 + \phi_1)\exp\left[-2\pi\left(j\frac{\Delta\sigma}{\delta\sigma}\right)^2\right] \tag{8.18}$$

$$I_4 = \frac{A_o^2}{8}\cos(\omega_b t + \phi_2 - \phi_1)\exp\left[-2\pi\left(j\frac{\Delta\sigma}{\delta\sigma}\right)^2\right] \tag{8.19}$$

For the total output intensity of the all modes of the multimode laser diode, I, is given by:

$$I = \sum_{j=-m}^{+m} I_j \tag{8.20}$$

or

$$I = \sum_{j=-m}^{+m} I_o + \sum_{j=-m}^{+m} I_1 + \sum_{j=-m}^{+m} I_2 + \sum_{j=-m}^{+m} I_3 + \sum_{j=-m}^{+m} I_4 \tag{8.21}$$

8.3. An optical fibre sensor used for flow measurement

From the results described in the chapters 6 and 7, it can be seen that the measurement volume of a dual coupled interferometer with a multimode laser diode light source can be shifted away from the zero-order interference region to a specifically designed region. Thus if the fibre version is used in flow measurement in the liquids, the measurement volume can be shifted out of the stagnant region caused by the present of the fibre end. Therefore, optical scattering signals unaffected by this low velocity region can be detected [1].

By using the experimental arrangement shown in figure 8.2., the "proof-of-principle" studies on using this sensor in flow measurements can be carried out.

Equation 8.21 shows that the optical output of the dual interferometer consists of five summations, i.e., five groups of superposition fringes. Under the conditions that ΔL_2 is fixed at the value of $\Delta L_2 >> L_c$, and ΔL_1 is scanned, the first summation, $\sum I_o$, in the equation 8.21 only gives a DC signal. As shown in figure 8.4, the second summation $\sum I_1$, which has

Doppler frequency information in its phase, represents the superposed fringes generated by the first interferometer in its original interference regions. When $\Delta L_2 >> L_c$, it will become a DC signal at the output of the system. The third summation $\sum I_2$, which only has a Bragg cell frequency, does not give any superposed fringes because ΔL_2 is fixed. The 4th and the 5th summations, $\sum I_3$ and $\sum I_4$, which have both the Bragg cell frequency and the Doppler frequency, give the superposed fringes which are generated by the two interferometers in the shifted interference regions. It should be noted that the difference between the 4th and 5th summations implies the different positions of the shifted interference regions. This difference is shown in figure 8.4.

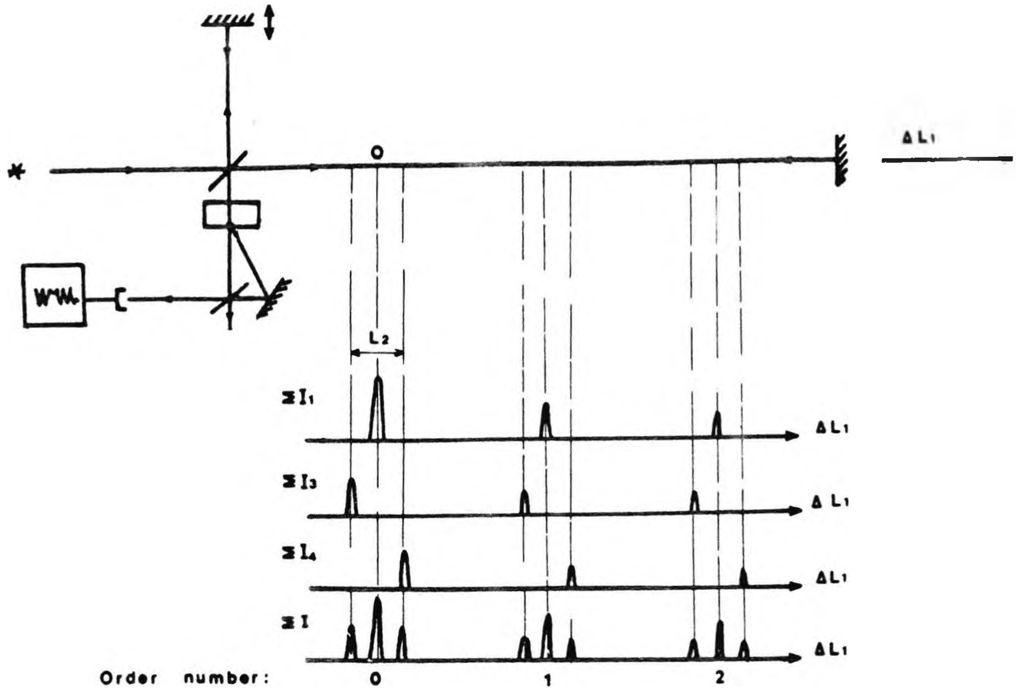

Figure 8.4. *The illustration of the interference regions with ΔL_2 being fixed and ΔL_1 is scanned.*

In a practical case, the intensity of the light beam emerging from the fibre end will reduce as ΔL_1 increases, and therefore, the intensities of the interference fringes in the higher order regions are very low compared with those in the zero order region. As for the superposed fringes in the shifted interference regions, only those in the interference region shifted from the zero order region have a comparable higher intensity. The intensities of the fringes in the regions shifted from the higher order interference regions will become even lower. This means, in the practical case, only two groups of light beams are collected from two interference regions, as shown in figure 8.5. The first one, with the Doppler frequency in its phase, is scattered from the original zero order region and the other one, with both the Bragg cell frequency and the Doppler frequency in its phase, is scattered from the region shifted from the original zero order region. Therefore, by using spectral analysis techniques, these two groups of scattered light beams can be separated easily.

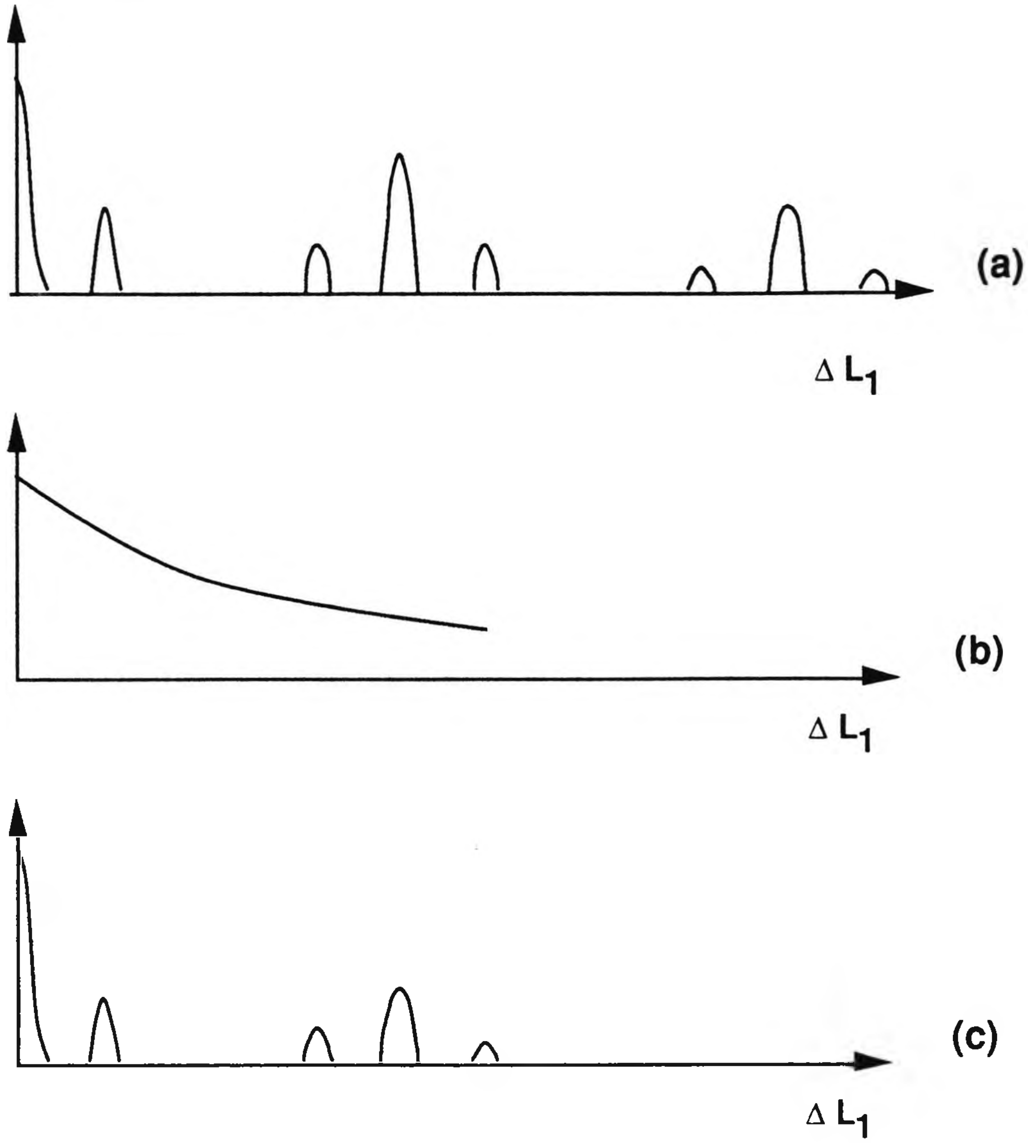

Figure 8.5. *The schematic diagram showing the variation of the detected optical intensities in the different cases:*

(a) Peak values of the output intensity via the variation of ΔL_1 *in the open path.*

(b) Light intensity emerging from the fibre end drops as ΔL_1 *increase.*

(c) Peak values of the output intensity via the variation of ΔL_1 *from the fibre end, showing that light intensity from the original zero region and that shifted from the zero region is the main part of the output signal.*

As mentioned in chapter 7, the position of the shifted region is determined by the off-set optical path difference in the second interferometer, and thus the measurement volume of the first interferometer can be moved into the zero-order shifted interference region. The position of this region can be scanned by changing the OPD of the second interferometer.

When the optical path difference of the Michelson interferometer is set to match that of the Bragg interferometer, the dual interferometer is now working inside the interference region shifted from the original zero-order region. When both ΔL_1 and ΔL_2 are fixed, ϕ_1 and ϕ_2 in the equations from 8.15 to 8.19 are not changed, thus the optical output only contains a carrier at the Bragg frequency (110 MHz). When ΔL_2 is fixed and ΔL_1 is scanned away from the balance point where $\Delta L_1 = \Delta L_2$ or $L_1 = L_2$, the output signal drops to zero as the difference of the two path length differences exceeded the value of the light source coherence length, i.e., $|L_1 - L_2| > L_c$. Displacement of one mirror in the Michelson interferometer, through the use of the micrometer adjustment, produced a change in phase of the carrier signal (as shown in figure 8.6) relative to the Bragg drive oscillator signal.

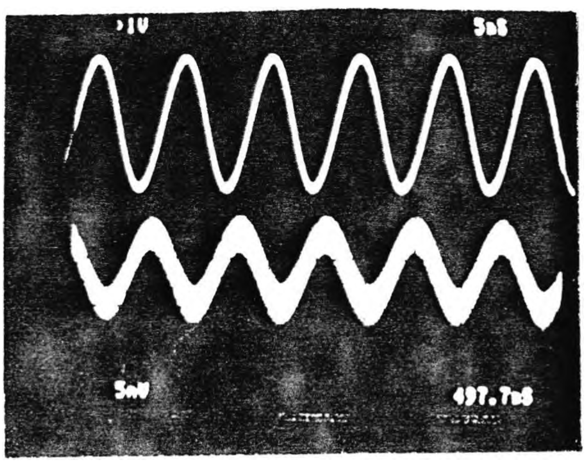

Figure 8.6. *Interferometer output signal (low trace) against 100 MHz Bragg cell drive waveform.*

In the experiment studies, both sinusoidal and serrodyne displacement modulations were applied to one mirror in the Michelson interferometer shown in figure 8.2. In the former case, a frequency spectrum symmetrical about the carrier frequency (Bragg frequency: 110 MHz) was observed. This result, as shown in figure 8.7, is typical of the sinusoidal modulation and corresponds to the 5th summation of the equation 8.20. In the latter case, two predominant Doppler frequency components were observed, placed asymmetically about the carrier, since the sawtooth displacement ramp has a fast, but finite flyback period as is shown in figure 8.8. It is clear that by comparing the frequency of the output with the carrier frequency, the direction of the movement is ready determined.

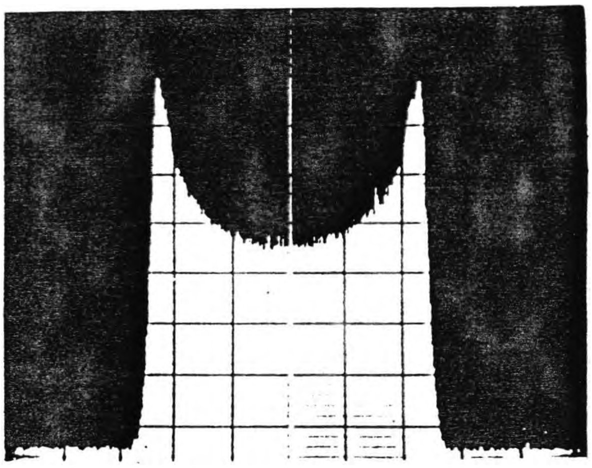

Figure 8.7. *Interferometer output frequency spectra produced by a sinusoidal modulation applied to one Michelson interferometer mirror (100 MHz marker at Bragg cell carrier frequency).*

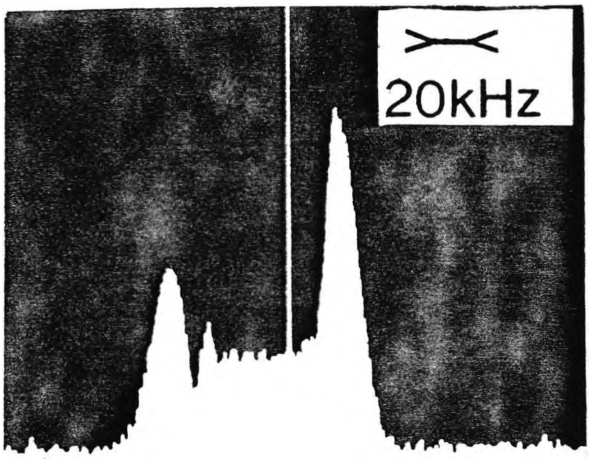

Figure 8.8. *Interferometer output frequency spectra produced by a sawtooth waveform modulation applied to one Michelson interferometer mirror (100 MHz marker at Bragg cell carrier frequency).*

8.4. An optical fibre sensor used for vibration measurement

In this section a heterodyne vibration sensor using a coherence length modulation technique is proposed and described. In this scheme, the difficult of coupling light from a Bragg cell into a fibre, which occurs in an ordinary heterodyne interferometric system, is relieved by changing the position of Bragg cell from one arm of the interferometer to the front of detector. A theoretical analysis and experimental results, both for the single mode light source and the multimode light source, are presented.

8.4.1. The early work

Based on classical optical fibre interferometer configurations, the heterodyne signal recovery technique employed in remote vibration measurement has been reported in a number of papers [2,3,4]. One of the attractive advantages of this technique is that by using it, the direction of movement can be determined directly. Unfortunately, the conventional Bragg cell, used to shift the frequency in one of the arms in an interferometer, is not a component easily integrated to suit a fibre optic interferometer. Coupling light from Bragg cell into fibres will give a problem of optical intensity loss in the coupling.

One of the first approaches of improving the arrangement was used by Kyuma et al. (as shown in figure 8.9.) [4]. In their experimental arrangement, the light beam in one arm passes through two beam splitters and then is coupled into the fibre, while the light beam in another arm is modulated by the Bragg cell, and then combined with the received signal light to form the heterodyne signal at the detector. This arrangement can ease the coupling problems and thus enable a reduction in the probe size. However, there still exist another problem, i.e., the problem of the phase perturbation, which is introduced from the environmental changes, such as temperature, pressure and vibration. This problem is largely due to the separation of the reference arm and the signal arm in the interferometer.

From the results of the study shown above, it can be seen if a heterodyne vibration sensor is constructed based upon the coherence length modulation scheme [5], the coupling difficult can be relieved by changing the position of the Bragg cell from one arm of the interferometer to the front of detector, as shown in figure 8.2. In this case, instead of coupling the light beam from the Bragg cell into fibres, the light beam is coupled from fibres into the Bragg cell.

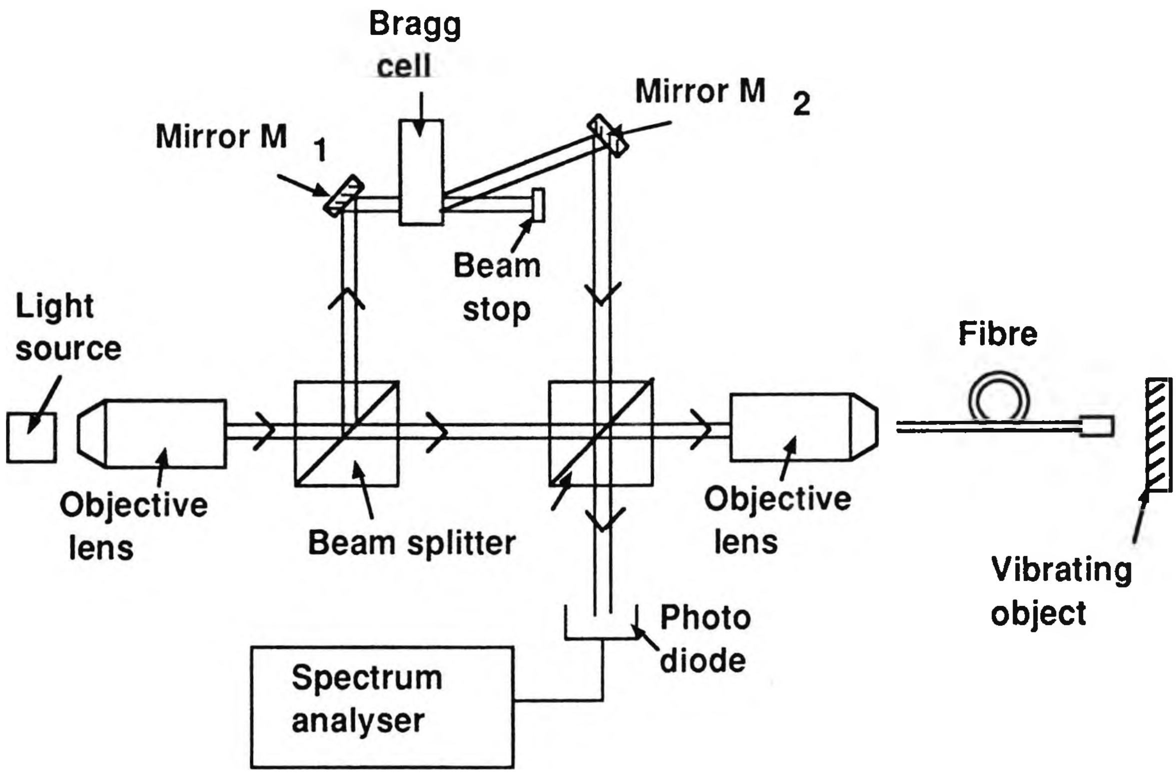

Figure 8.9. *Schematic optical arrangement (similar to that of Nokes et al [3] and Kyuma et al [4]).*

Since the position of Bragg cell is changed, another problem appears for the ordinary single mode laser heterodyne interferometer arrangement, i.e., there are two side-band shifted frequencies around the carrier frequency. Therefore, the direction of movement cannot be determined. This was confirmed in the experimental result shown below.

8.4.2. The experimental results

By using the experimental arrangement shown in figure 8.2., a study on the performance of the sensing system using both single mode and multimode laser sources was carried out.

According to the theoretical analysis in section 8.2.1., when a single mode laser is employed in the sensing system, i.e., j=1, there are four optical intensity components received by the photodiode which can be represented by the equations 8.15 to 8.19 for the case of j=1. The intensity components represented by equations 8.15 and 8.16 describe a DC signal and a phase modulation signal with a zero carrier frequency respectively, another three components, shown in equations 8.17 to 8.19, are AC signals with different frequencies. In the experiment, the performance of a signal mode HeNe laser in the experimental arrangement was studied. The output from the spectrum analyser is illustrated by figure 8.10 and shows three frequency domains around the Bragg cell frequency. The central frequency is due to the Bragg cell shifting at 110MHz, which corresponds in intensity terms to the output of equation 8.17; while two sideband signals are generated at Doppler frequencies introduced by the vibration induced in the mirror M_2. These two frequencies similarly respond to the output of equations 8.18 and 8.19. It is clearly that using the single mode laser in this experimental arrangement cannot give the direction of vibration.

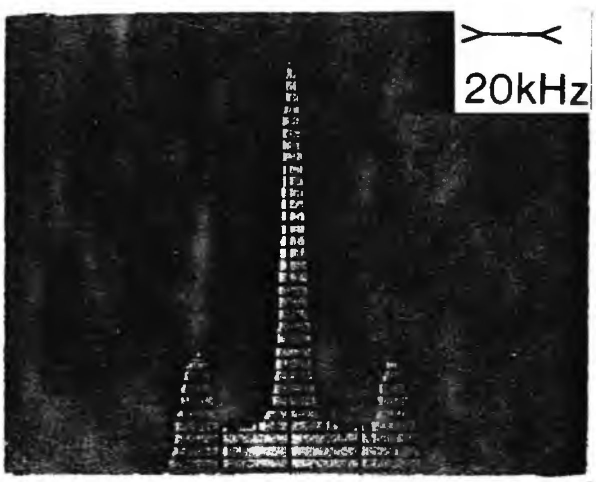

Figure 8.10. *Spectral output of the arrangement, obtained using single mode He-Ne laser source, showing the central peak frequency and tow sideband frequencies.*
Horizontal scale: 20 kHz per division
Vertical scale: arbitrary unit.

In the case of using a multimode laser diode as the light source in the same arrangement, i.e., j=m, only one of the four groups of superposition fringes can be obtained as described in equation 8.20. In the experiment, the micrometer in the first interferometer was used to adjust the value of the OPD, L_1, of the first interferometer to match that of the second interferometer, L_2 at the value of 4.25 mm. When the M_2 was driven with a sawtooth waveform illustrated at a frequency of 400 Hz, its movement showed velocities in different directions, introducing different Doppler frequencies. If the mirror movement is towards the beam splitter, the Doppler frequency shift adds to the Bragg cell frequency and if the mirror is moving away from the beam splitter, the total frequency shift is reduced to less than the value of the Bragg frequency. Figure 8.8 shows the spectrum of the output signal obtained. This contrasts with the output achieved with the other source where now a range of frequencies is obtained, asymmetric about the central frequency, whose presence is indicted by the white line on the photograph. This shows the effect of the sawtooth ramping signal applied to the moving mirror, and confirms that directional and thus velocity information can now be obtained by using the arrangement shown in figure 8.2.

Another significant characteristic of this arrangement is that the carrier frequency does not come through to the detector, as shown in figure 8.10, and this makes the electronic demodulation much simpler. Thus a conventional demodulation techniques, such as the use of an inexpensive integrated circuit device like a phase-locked-loop (PLL) can be used directly [6].

8.5. Conclusions

In this chapter, a new type of optical fibre sensor based on coherence length modulation is proposed. The performance of the bulk-optical component version has shown the possibility of using this new sensor to measure the flow velocity. The problem in conventional techniques where the presence of a fibre disturbs the patterns of the fluid may be overcome by shifting the measurement volume from near the fibre end to a distance ahead of the fibre end and into the unperturbed flow region. By introducing a carrier frequency into one light beam of the second interferometer, a heterodyne output signal may be demodulated by conventional techniques. This has already been verified in the chapter 7.

A comparison of the performances of a single mode laser and multimode laser diode in the configuration shown has been demonstrated both in a simple theoretical analysis and by experiment. By using the coherence length modulation technique discussed, the problem mentioned in chapter 4 where the directional information of a movement is lost can be solved, and the heterodyne signal can be obtained directly from this vibration sensing scheme which shows the advantages both of ease of adjustment and the facility for the direct measurement of vibration. Additionally the use of a multimode laser diode is both convenient and inexpensive, by comparison to the employment of a gas laser.

References

[1] B.T. Meggitt, W.J.O. Boyle, K.T.V. Grattan, A.W. Palmer and Y.N. Ning "Fibre Optic Anemometry Using an Optical Delay Cavity Technique" Eight International conference - Fibre Optics and Poto-Electronics, London, April, 1990.

[2] Takashi Nakayama "Fibre LDA System" Optical Fibre Sensors, NATO ASI series E: Applied Sciences- No.132 pp.217-226 1987.

[3] Mark A. Nokes, Bruce C. Hill, Anthony E. Barelli "Fibre optic heterodyne interferometer for vibration measurement in biological systems" Rev. Sci. Instrum. 49(6), Jan pp.722-728 1978.

[4] Kazuo Kyuma, Shuichi Tai, Koichi Hamanaka, & Masahiro Nunoshita "Laser Doppler velocimeter with a novel optical fibre probe" Appl. Opt. Vol.20, No.14, 15 July 1981.

[5] Y.N. Ning, K.T.V. Grattan, A.W. Palmer, B.T. Meggitt "Characteristics of a multimode laser diode in a dual interferometer configuration" IEEE J. Lightwave Technology, 1773-8, 1990.

[6] Y.N. Ning, K.T.V. Grattan, A.W. Palmer, B.T. Meggitt "An all fibre laser low cost" rangefinder "for small vibration measurement" Conf. on Laser Diode Tech. and Appl. 18-20 Jan.1989 Los Angeles California USA, SPIE Proc. Vol.1043 pp.284-290, 1989

Chapter 9

General Conclusion and Summary

By analysing the basic characteristics and function of optical fibre sensor techniques, a new systematic classification of optical fibre sensor techniques has been introduced. They may be classified according to the types of fibre, the light sources and the modulation schemes on which they are based. Taking sensor devices into account, such a general review of and novel classification for the optical fibre sensors is presented in chapter 2. From this review, it can be seen that the field of optical fibre interferometric systems using low coherence light sources has become one of the most active and important areas. In order to summarise the main characteristics of these, a detailed review of fibre-optic interferometric systems using low coherence light sources was shown in chapter 3. It can be seen that by using these systems, it is possible to achieve a number of advantages in sensor systems which cannot be obtained using only conventional high coherence laser sources.

Although the effort has been made to replace the optical bulk components through employing an electronic processing scheme (chapter 4), the problem of the lack of directional information in interferometric measurement schemes still occurs. Since a common-mode interferometer configuration is employed in the electronic processing scheme which was discussed, the measurement system shows extreme simplicity in the configuration by virtue of the all fibre interferometer and direct electronic processing, when comparing it to the interferometric system using optical bulk components.

When a multimode laser diode is used as an low coherence light source in an interferometric system, the output intensity of the interferometer gives the characteristics of a series of constructive interference regions which cannot be replicated when using other types of low coherence light sources, such as a LED or a white light lamp (chapter 5). From the application point of view, it can be seen that this high output power, low cost, low coherence source with a small emitting area, available in commercial quantities may be used in the important field of coherence multiplexing in optical fibre systems.

The optical output from a dual coupled interferometer consists of the original interference regions, which are generated by the first interferometer, and the "side-band" interference regions which, when generated by both interferometers, may be considered as "shifted regions".

The position of these shifted interference regions can be effectively controlled by changing the optical path difference of the second interferometer. The theoretical and experimental results obtained in this work show that if the shifted interference region is used as a working region in the measurement, the geometry of the measurement volume may be defined and designed (chapters 6 and 7).

If an interferometric velocity measurement system consists of a coupled Michelson : Bragg cell interferometer, a heterodyne signal may be obtained directly from the output of this interferometric system, and thus the velocity of a moving object may be detected. The feasibilities of the two possible applications of this scheme are demonstrated in chapter 8

To summarise, through the theoretical and experimental studies of the "CD-type" multimode laser diodes discussed in an interferometer or in several types of coupled dual interferometers, the coherence characteristics of such a low coherence light source were demonstrated. Through the use of the "white-light interferometer" or the coherence length modulation scheme, the possibility of defining the geometry of the measurement volume in a coupled dual interferometric system was shown. It was also shown that by using a heterodyne signal recovery scheme in the coherence length modulation scheme, directional information of a vibration body can be determined. Although the results presented in this thesis show that there are some advantages of using a multimode laser diode as a low coherence light source, the following work still needs to be done in order for these schemes to be used more efficiently:

(a) Investigation of the characteristics of a multimode light beam inside a multimode fibre, and therefore, the feasibility of using a multimode fibre to deliver this low coherence light could be shown.

(b) Calculation and verification of the noise level which may be caused by noise due to longitude modes and temperature perturbations.

(c) Estimation of the energy budget of the experimental arrangement in order to optimise the sensor system.

Appendix:

Publications:

[1] Y.N. Ning, K.T.V. Grattan, W.M. Wang and A.W. Palmer, "A systematic classification and identification of optical fibre sensors", Sensors and Actuators, 29, 21-36, 1991.

[2] K.T.V. Grattan, Y.N. Ning, W.M. Wang and A.W. Palmer, "A review and classification of optical fibre sensors", Paper accepted for IMEKO XII World Congress, September 1991, Beijing, P. R. China. Pub: Acta IMEKO, 1991.

[3] Y.N. Ning, K.T.V. Grattan and A.W. Palmer, "Fibre-optic interferometric systems using low coherence light sources", Sensors and Actuators, 30, 181-192, 1991.

[4] Y.N. Ning, K.T.V. Grattan and A.W. Palmer, "The use of low coherence light sources in fibre-optic interferometric systems" Chapter 21 in book "Optical sensors" Ed. E. Wagner, R. Dandliker, R. Spenner. Pub: VCH Verlagsgesellschift mbH, Weinheim, Germany, 530-550, 1992.

[5] Y.N. Ning, B.T. Meggitt, K.T.V. Grattan, and A.W. Palmer "An all fibre laser low cost 'rangefinder' for small detection measurements", Proceedings, SPIE 1043, 284-90, 1989.

[6] K.T.V. Grattan, A.W. Palmer, B.T. Meggitt and Y.N. Ning "Optical fibre approach to shaft monitoring - vibration and rotation measurement", Paper presented at Australian Conference on Instrumentation and Measurement, 1989 (AIM'89) Adelaide, Australia. (National Conference Publication No. 89/17), Pub: Australian Institution of Engineers, 305-308, 1990.

[7] Y.N. Ning, K.T.V. Grattan, A.W. Palmer and B.T. Meggitt "A novel detection scheme for vibration monitoring using optical techniques", Optics and lasers in Engineering, 15, 115-126, 1991.

[8] Y.N. Ning, B.T.Meggitt, K.T.V. Grattan and A.W. Palmer, "Characteristics of laser diodes for interferometric use", Appl. Opt. 28, 3656-60, 1989.

[9] K.T.V. Grattan, B.T. Meggitt, Y.N. Ning and A.W. Palmer "Application of multimode semiconductor laser diodes to fibre optic interferometric sensors", Captures 89, Conf. Proc. Pub: CIAME, Paris, 484-91, 1989.

[10] K.T.V. Grattan, A.W. Palmer, Y.N. Ning and B.T. Meggitt "Interferometric sensors - Extension of range using low coherence light from laser diodes" (EFOC/LAN 1989) Conf. Proc. Pub: Information Gatekeepers Inc., Boston, MA, 375-380, 1989.

[11] K.T.V. Grattan, A.W. Palmer, B.T. Meggitt.and Y.N. Ning "Use of laser diode sources in low coherence operation in fibre optic sensors", Paper presented at Australian Conference on Instrumentation and Measurement, 1989 (AIM'89) Adelaide, Australia. (National Conference Publication No. 89/17), Pub: Australian Institution of Engineers, 300-4, 1990.

[12] Y.N. Ning, K.T.V. Grattan, A.W. Palmer and B.T. Meggitt "Characteristics of a multimode laser diode in a dual interferometer configuration", IEEE/OSA J. Lightwave Technology, 8, 1773-8, 1990.

[13] B.T. Meggitt, Y.N. Ning, K.T.V. Grattan, A.W. Palmer and W.J.O. Boyle "Fibre optic anemometer using an optical delay cavity technique", Eighth Int. Conf. on "Fibre optics and opto-electronics", SPIE 1314, 321-9, 1990.

[14] Y.N. Ning, K.T.V. Grattan, A.W. Palmer and B.T. Meggitt "Coherence length modulation of a multimode laser diode in a dual Michelson interferometer configuration", Appl. Opt. 31, 1322-7, 1992.

[15] Y.N. Ning, K.T.V. Grattan, W.J.O. Boyle and B.T. Meggitt "The use of multi-mode laser diodes in low-coherence coupled - cavity interferometry", Paper presented at "The International Congress on "Optical science and Engineering", Proc. on "Fiber Optical Sensors IV", SPIE 1267, 142-52, 1990.

[16] Y.N. Ning, K.T.V. Grattan, A.W. Palmer and B.T. Meggitt "Characteristics of a multimode laser diode source in several types of dual-interferometer configuration", SPIE's Tech. Symposium "OE/FIBRES'90" San Jose, USA 16-21 Sept. 1990. Proc. on "Fiber Optic and Laser Sensors VIII", SPIE 1367, 1991.

[17] Y.N. Ning, K.T.V. Grattan, A.W. Palmer, B.T. Meggitt, and K. Weir, "A novel optical heterodyne vibration sensor scheme, preserving directional information and using a short coherence length source" to be published in "Optics communications", 85, 10-16, 1991.

[18] K.T.V. Grattan, Y.N. Ning, A.W. Palmer and N.D. Fox "A simple endoscopic automatic vision system applied to monitoring of adhesive bonding", Rev. Sci. Instrum. 61(6), 1658-63, 1990.